

# ACL Strain During Single-Leg Jump Landing: An Experimental and Computational Investigation

by

Anna Maria Polak

A thesis

presented to the University of Waterloo

in fulfillment of the

thesis requirement for the degree of

Master of Applied Science

in

Mechanical Engineering

Waterloo, Ontario, Canada, 2018

©Anna Maria Polak 2018

I hereby declare that I am the sole author of this thesis. This is a true copy of the thesis, including any required final revisions, as accepted by my examiners.

I understand that my thesis may be made electronically available to the public.

## Abstract

The anterior cruciate ligament (ACL) is a commonly-injured ligament in the human knee joint. ACL injury repair is a costly procedure; however, left unrepaired, ACL injuries can lead to complications later in life. In order to understand ACL injury, metrics such as strain in the ACL are measured under various loading conditions. A motion which has potential to cause ACL injury, a single leg jump landing, was replicated and ACL strain was recorded. Two common approaches for this purpose are *in-vitro* studies involving cadavers, and finite element (FE) modelling of the knee joint. Once ACL strain during the potentially injurious motion is evaluated, it is easier to work towards potential improvements to protective or rehabilitative equipment, such as knee braces. The objective of the current study was to measure ACL strain during a single leg jump landing using two different methods:

1. *In-vitro* experiments involving cadavers:
  - ACL strain *vs.* time was measured with unbraced and braced cadaver knees.
2. Finite element modelling of the human knee:
  - The finite element model was assessed using the *in-vitro* experiments, and can potentially be used to evaluate braced knee conditions in the future.

The inputs for the experiments and finite element model were taken from motion capture, which was done *in-vivo* on two participants in a previous study. The two participants provided input kinetics and kinematics of a single-leg jump landing. The kinematic and kinetic inputs were then applied to three cadaveric specimens using the dynamic knee simulator (DKS) at the University of Waterloo, and ACL strain relative to the beginning of the trial was measured. The cadaver knees were also tested wearing an Össur CTi Custom knee brace, and the effect of the knee brace on relative ACL strain was measured. A finite element model of the human knee joint was also investigated by extracting the right leg of an existing full human body model, the Global Human Body Model Consortium (GHBMC) average-sized male (M50) model, and updating some of the tissue mechanical properties. The same boundary conditions from the experimental

study were applied to the GHBM right leg model, and relative ACL strain was calculated and compared against the experimental data.

The experimental maximum relative ACL strain for an unbraced full jump landing was 0.032 and 0.057 for participant #1 input and 0.062 for participant #2 input. The computational maximum relative ACL strain was 0.042 for participant #1 input and 0.139 for participant #2 input. The finite element model was able to replicate the experimental ACL strain vs. time curves reasonably well, with a mean squared error of less than 0.01 for all loading scenarios.

The results of the unbraced vs. braced jump landing experiments showed that the knee brace had no effect on ACL strain. The mean squared error between unbraced and braced ACL strain vs. time curves was less than 0.0011 for all loading cases, which is a low error value when compared to strains in the range of 0.015-0.089.

The jump landing finite element model is an important first step in using finite elements to predict relative ACL strain during jump landing. Future research directions include study of factors affecting ACL strain, incorporating the knee brace into the finite element model to investigate possible improvements to the brace, and investigating the benefits of adopting a subject-specific geometry for the model.

## Acknowledgements

First of all, I would like to thank my supervisors Dr. Naveen Chandrashekar and Dr. Duane Cronin for providing me with this opportunity.

To Ryan Bakker, Mayank Kalra, and Harish Rao: Thank you for all the hours of time you sacrificed and all the nuggets of wisdom you provided in the lab in order to help me finish my experiments! Spending many hours in the lab made us all appreciate the world outside of it.

Thank you to my family and friends for all the adventures that kept me smiling and excited. To Kaab Omer and Dr. P, I appreciate your encouragement and support. Thank you for teaching me that red wine pairs well with finite element analysis. I also appreciate that Graeme Milligan and Ryan Barrage have taught me what the equation of a line looks like.

Finally, I would like to thank David Bruneau for keeping me motivated and celebrating my successes with me!

# Table of Contents

Abstract.....	iii
Acknowledgements.....	v
Table of Contents.....	vi
List of Figures.....	viii
List of Tables.....	xii
Chapter 1 Introduction.....	1
1.1 Motivation.....	1
1.2 Research Objectives.....	2
1.3 Thesis Overview.....	2
Chapter 2 Biomechanical Background.....	4
2.1 Anatomical Planes and Directions.....	4
2.2 Knee Anatomy.....	6
2.3 ACL Anatomy.....	11
Chapter 3 Literature Review.....	13
3.1 Jump Landing Experimental Models.....	13
3.1.1 The University of Michigan Simulator.....	13
3.1.2 The Ohio State University Simulator.....	15
3.1.3 The Texas Tech University Simulator.....	16
3.1.4 The University of Waterloo Simulator.....	16
3.2 Knee Brace Studies.....	18
3.3 Knee Joint Modelling Considerations.....	18
3.4 Computational Models of Human Leg.....	22
3.5 Hypothesis.....	24
Chapter 4 Experimental Methodology.....	25
4.1 Experimental Overview.....	25
4.2 Casting and Dissection.....	28
4.3 Preparation for Testing.....	31
4.4 Moment Arm Measurement.....	36
4.5 Sensor Placement.....	37
4.6 Placing the Knee on the Simulator.....	38
4.7 Jump Landing Testing Procedure.....	40
Chapter 5 Experimental Results.....	43

5.1 Knee Failures .....	43
5.2 ACL Strain Results .....	48
5.2.1 Comparison of Finite Element Model Strain with Experimental Strain .....	48
5.2.2 Comparison of Braced vs. Unbraced Conditions .....	50
Chapter 6 Finite Element Model Setup.....	54
6.1 GHBMC Modifications for Jump Landing Study.....	55
6.2 Background Studies .....	56
6.2.1 Tibial Slope.....	57
6.2.2 ACL Material.....	58
6.2.3 ACL Mesh Convergence.....	60
6.2.4 ACL Element Formulation.....	62
6.2.5 ACL Pre Strain.....	63
6.3 Modelling Considerations .....	63
6.3.1 Coordinate System .....	63
6.3.2 Kinematics Boundary Conditions .....	64
6.3.3 Force Boundary Conditions .....	65
6.3.4 Limb Lengths .....	67
6.3.5 Moment Arms .....	67
6.4 Initialization .....	68
6.5 Jump Landing.....	69
6.6 ACL Strain Measurement .....	69
6.7 Test Matrix for FE Model .....	70
Chapter 7 Computational Results .....	70
7.1 Comparison of Finite Element Model Strain with Experimental Strain .....	71
Chapter 8 Discussion of Results .....	74
8.1 Effect of the Knee Brace.....	74
8.2 Validation of the Finite Element Model .....	74
8.3 Comparison to Literature .....	77
8.4 Limitations of the Study.....	81
Chapter 9 Conclusions and Future Research Directions.....	83
References.....	85
Appendix A: Verification of Experiments and Finite Element Model .....	91

## List of Figures

Figure 2.1 Anatomical directions to describe location on the human body adapted from “Anatomy Language & Histology,” n.d.....	6
Figure 2.2 Anatomy of the human knee adapted from “Knee,” 2018.....	7
Figure 2.3 Valgus and varus motion adapted from “Valgus vs Varus Knee Alignment,” 2017.....	8
Figure 2.4 Patellofemoral and tibofemoral joints of the knee adapted from “Medial Collateral Ligament,” 2011 .....	9
Figure 2.5 The popliteus muscle adapted from Langford, 2018.....	11
Figure 2.6 The anteromedial (AM) and posterolateral (PL) bundles of the ACL adapted from “Single-bundle vs. Double-bundle ACL Surgery,” 2018.....	12
Figure 2.7 Insertion site of the ACL Muneta et al., 1997 .....	12
Figure 3.1 The Michigan Simulator with the added torsion device (T) adapted from Oh et al., 2011 .....	14
Figure 3.2 The original Ohio State Simulator setup. Left: the simulator which applies loads in the sagittal plane. Right: External devices used to apply multi-planar loading adapted from Levine et al., 2013.....	15
Figure 3.3 The Texas Tech Simulator adapted from Hashemi et al., 2007.....	16
Figure 3.4 The University of Waterloo Simulator adapted from Bakker et al., 2016.....	17
Figure 3.5 ACL stress vs. strain curves from Noyes and Grood, 1976 and Chandrashekar, 2005 .....	21
Figure 3.6 ACL force vs. elongation curves from Woo et al., 1991 .....	21
Figure 4.1 Flow chart of previous work done by Bakker, 2014 to create input profiles adapted from Bakker, 2014 .....	25
Figure 4.2 Flow chart of inputs and outputs of experimental and FE modelling adapted from Cassidy et al., 2013 .....	26
Figure 4.3 The Dynamic knee simulator adapted from Cassidy et al., 2013 .....	27
Figure 4.4 A foamed knee wearing a CTi Össur knee brace .....	28



Figure 4.5 Section of the leg received for testing. Photo adapted from “Blank Body Colouring Page,” n.d. .....	29
Figure 4.6 Casted cadaver knee with endplates and locator rod .....	29
Figure 4.7 Dissection procedure flowchart .....	31
Figure 4.8 Anterior frontal plane view of tibia with fibula cut off .....	32
Figure 4.9 Anterior frontal plane view of the cabled knee showing quadriceps muscle cable .....	32
Figure 4.10 Posterior frontal plane view of the cabled knee showing hamstring and gastrocnemius cable setup .....	33
Figure 4.11 Anterior frontal plane view of the knee wrapped in carpet and clear tape with quadriceps muscle tube visible .....	34
Figure 4.12 Posterior frontal plane view of the knee wrapped in carpet and clear tape with hamstring and gastrocnemius muscle tubes visible .....	34
Figure 4.13 The inside of the cast lined with duct tape to prevent it from sticking to the foam mould .....	35
Figure 4.14 The sealed cast oriented using the end plates ready for the foam to be poured.....	35
Figure 4.15 Medial sagittal plane view of a leg covered in foam with the foam and carpet cut away from the knee joint.....	35
Figure 4.16 Left: the moment arm measurement setup. Right: Displacement vs. Angle Plot used to calculate moment arm .....	36
Figure 4.17 Flexion extension procedure during which displacement and knee angle are measured .....	37
Figure 4.18 ACL DVRT (circled) and notchplasty (N) .....	38
Figure 4.19 Hip attachment (A) and ankle attachment (B), adapted from Bakker, 2014. ....	38
Figure 4.20 Connectors attaching cables to the simulator .....	39
Figure 4.21 The foamed knee on the dynamic knee simulator .....	40
Figure 4.22 Muscle force vs. time and velocity vs. time inputs for participant #1 and participant #2 full muscle force jump landing .....	42
Figure 5.1 Medial sagittal plane view of knee 1 in hyperextension after failure .....	44

Figure 5.2 Torn ACL in knee 1 .....	44
Figure 5.3 Crack in the knee brace of knee 1.....	45
Figure 5.4 Cracked patella in knee 3.....	45
Figure 5.5 Patella creating negative mould in block of clay .....	46
Figure 5.6 Patellar tube and reinforcing screws placed inside negative mould .....	46
Figure 5.7 Medial sagittal plane view of knee 3 on the DKS with new moulded patella.....	47
Figure 5.8 Medial sagittal plane view of knee 3 in hyperextension after failure .....	47
Figure 5.9 Torn ACL in knee 3.....	48
Figure 5.10 Experimental relative ACL strain vs. time curves for all loading conditions.....	49
Figure 5.11 Average relative ACL strain vs. time results for unbraced and braced conditions.....	51
Figure 5.12 Comparison of unbraced and braced mean peak relative ACL strains.....	53
Figure 6.1 (a) Full body model (b) Extracted right leg (c) Extracted ACL .....	55
Figure 6.2 Medial, lateral, and coronal tibial slopes of the GHBMC right tibia.....	57
Figure 6.3 Tibial slopes for male subjects compared to GHBMC tibial slope .....	58
Figure 6.4 ACL Stress vs. Strain Curves from Chandrashekar, 2005.....	59
Figure 6.5 Boundary conditions applied to ACL to evaluate realistic force-elongation response.....	59
Figure 6.6 Force vs. elongation curves of original material compared to updated material and literature .	60
Figure 6.7 ACL mesh sizes used in mesh convergence study .....	60
Figure 6.8 Force vs. elongation curves for ACLs of varying mesh size .....	61
Figure 6.9 Force vs. elongation curves for different element formulations .....	62
Figure 6.10 (a) Simulator coordinate system (b) Leg model coordinate system .....	63
Figure 6.11 End caps for application of hip and ankle boundary conditions - anterior frontal plane view	65
Figure 6.12 Application of hip moment-medial sagittal plane view.....	66
Figure 6.13 Muscle forces acting on knee joint-medial sagittal plane view .....	66
Figure 6.14 Scaling of the femur .....	67
Figure 6.15 Moment arm measurement simulation .....	68

Figure 6.16 Flowchart of initialization for participant #1 .....	68
Figure 6.17 ACL DVRT location (left) and ACL strain measurement location in finite element model (right) .....	70
Figure 7.1 Average relative ACL strain results for participant #1 and participant #2.....	71
Figure 8.1 Comparison of experimental and computational relative ACL strains.....	75
Figure 8.2 Comparison of experimental and computational time to peak relative ACL strains.....	76
Figure 8.3 The relative ACL strain profiles of participant # 1 and participant # 2 from the experiments of Bakker, 2014.....	78
Figure 8.4 Comparison of Experimental Results to Literature .....	80
Figure 8.5 Comparison of Computational Results to Literature .....	80
Figure 8.6 Anterior view of the GHBMC knee joint to show coarse mesh .....	82
Figure A.1 Verification of kinetics and kinematics for participant # 1 full muscle force jump .....	91
Figure A.2 Verification of kinetics and kinematics for participant # 1 half muscle force jump.....	92
Figure A.3 Verification of kinetics and kinematics for participant # 2 full muscle force jump .....	93
Figure A.4 Verification of kinetics and kinematics for participant # 2 half muscle force jump.....	94

## List of Tables

Table 2.1 Planes of Human Movement based on Behnke, 2001 .....	4
Table 2.2 Major Muscle Groups affecting knee motion adapted from Behnke, 2001 .....	10
Table 3.1 Literature Review of ACL Material Characterization .....	20
Table 3.2 Finite Element Models of the Human Knee Joint.....	23
Table 4.1 Cadaver Specimen Anthropometrics .....	28
Table 4.2 Participant Information from Bakker, 2014.....	41
Table 4.3 Test Matrix for Experiments.....	41
Table 5.1 Experimental Moment Arm Calculations (in mm) .....	43
Table 5.2 Successful Trials on each Knee Specimen.....	43
Table 5.3 Summary of Experimental and Computational Maximum Relative ACL Strain Results.....	50
Table 5.4 Means and Standard Deviations of Experimental Results .....	50
Table 5.5 Summary of Maximum Relative ACL Strain Values for Unbraced and Braced Conditions .....	52
Table 5.6 Means and Standard Deviations of Braced and Unbraced Relative ACL Strain Results .....	52
Table 5.7 Mean Squared Error of Unbraced vs. Braced Jump Landing Comparison .....	53
Table 6.1 Full 50 <sup>th</sup> Percentile Male GHBMC Model Details.....	54
Table 6.2 Extracted Right Leg of GHBMC Model Details .....	54
Table 6.3 Modifications applied to right leg of GHBMC Model .....	56
Table 6.4 Run Times for Different Mesh Sizes .....	61
Table 6.5 Test Matrix for FE Model.....	70
Table 7.1 GHBMC Moment Arm Calculations (in mm) .....	71
Table 7.2 Summary of Experimental and Computational Maximum Relative ACL Strain Results.....	72
Table 7.3 Mean squared error of ACL strain vs. time curves of experiments and FE model.....	72
Table 7.4 Pearson Correlation Coefficient comparing ACL strain vs. time curves of experiments and FE model .....	73

# Chapter 1 Introduction

## 1.1 Motivation

Anterior cruciate ligament (ACL) injury is very common in sports, and ACL reconstruction is one of the most common sport-related surgical procedures in the U.S (Csintalan et al., 2008). An injured ACL has been shown to cause complications with the knee joint later in life, such as decreased functionality, osteoarthritis, meniscal tears, and other joint abnormalities (Daniel et al., 1993; Hill et al., 2005; Katayama et al., 2004). Understanding ACL behaviour during a potentially injurious activity is an important factor in preventing injury and facilitating recovery. ACL injuries are most commonly non-contact injuries (Boden et al., 2000), meaning that they occur without contact between two athletes. Sudden dynamic movements, such as landing from a jump are often the cause (Boden et al., 2000).

In order to understand ACL injury, different loading mechanisms and their outcomes must be understood (Yu and Garrett, 2007). ACL injury happens when the ligament is subject to a tensile load until failure. Thus ACL strain is a measurable metric to help predict the likelihood of injury (Yu and Garrett, 2007). Determining ACL strain during jump landing can be done *in-vivo*. However, ethics regulations prohibit dynamic *in-vivo* testing since the test subject could experience severe injuries if it experiences loads that approach the magnitude at which failure occurs. Instead of *in-vivo* testing, *in-vitro* studies have been performed, in which a cadaveric specimen is used to model a living human. These studies are expensive and time consuming, and raise the question of how comparable *in-vitro* results are to *in-vivo* results (Bakker et al., 2016). A computational approach can also be used to predict ACL strain. Finite element modelling is a less expensive and less time-consuming alternative to *in-vitro* studies which can be used to simulate the knee joint during dynamic tasks (Beillas et al., 2004). A validated finite element model of the knee joint could be an excellent tool for conducting parametric studies in order to investigate knee injury mechanisms in further detail. A finite element model of the knee could also be used to evaluate the effect of various

knee braces on ACL strain. Since the finite element method is less expensive and less time-consuming than experimental approaches, it is a useful tool for the development of knee brace design.

## **1.2 Research Objectives**

The objective of the current study was to measure relative ACL strain during single leg jump landing using:

1. *In-vitro* cadaver experiments
2. A finite element model of the human knee

The *in-vitro* cadaver experiments were performed using a Dynamic Knee Simulator (DKS) developed by Cassidy et al., 2013. The cadaver knees were first tested without a knee brace, and then tested while wearing a CTi Custom Össur knee brace, in order to determine the effect of the knee brace on relative ACL strain. A FE Model of the human knee was then used to estimate ACL strain, in which a full human body knee model was modified so that it could predict ACL strain during single leg jump landing. The model was validated using experimental data from unbraced trials by comparing computational relative ACL strain to the experimental results.

## **1.3 Thesis Overview**

This thesis will outline two investigations: the experimental study of cadavers performing single leg jump landing *in-vitro* using the University of Waterloo dynamic knee simulator (DKS) in both unbraced and braced conditions, and the application of a FE model of the human knee to perform a single leg jump landing. Chapter 2 will discuss biomechanical background since anatomical orientations, knee anatomy, and more specifically ACL anatomy must be understood in order to fully comprehend the study. Chapter 3 will present a literature review of knee simulators used to perform single leg jump landing experiments, knee brace studies, and finite element modelling considerations for models of the human leg, which will lead to a hypothesis for the current study. Chapter 4 will discuss the experimental methodology for the study in which cadaveric specimens perform a single-leg jump landing at varying intensities in unbraced

and braced conditions. Chapter 5 will present experimental results. Chapter 6 will discuss the preparation of the finite element model. The Global Human Body Models Consortium (GHBMC) right leg was extracted from the full body model and modifications were made to the model in order to make it more biofidelic and numerically stable under jump landing loading conditions, and it was loaded to re-create a single leg jump landing using kinematic and loading boundary conditions. Chapter 7 will present the results of the finite element modelling. Chapter 8 will present a discussion of both experimental and computational results, which will include validation of the finite element model. Finally, conclusions and future research directions will be stated in Chapter 9.

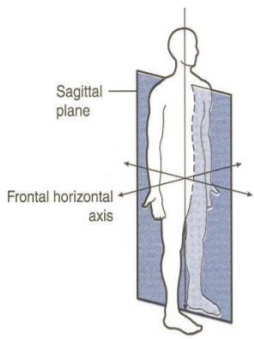
## Chapter 2 Biomechanical Background

Biomechanical terms are often used to describe movements and locations on the human body. This chapter will outline key biomechanical terms needed in order to understand the study of ACL strain during single leg jump landing. The anatomy of the knee, and the structures comprising it will also be discussed, followed by a more in-depth description at the anatomy of the ACL, the main structure being analysed in the study.

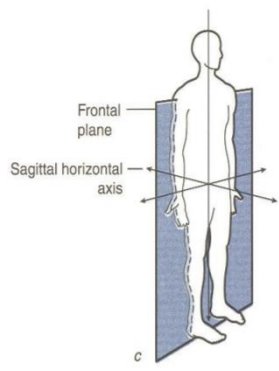
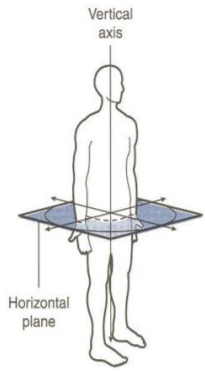
### 2.1 Anatomical Planes and Directions

Human movement has six degrees of freedom and takes place in three anatomical planes. These planes are the sagittal plane, the frontal plane and the transverse plane. The three planes and perpendicular axes used to describe human movement are summarized in Table 2.1. Large movements are often described as occurring in one of these three planes. For example, jumping is a movement which occurs primarily in the sagittal plane, with flexion and extension of the joint occurring about the frontal horizontal axis.

**Table 2.1 Planes of Human Movement based on Behnke, 2001**

Plane	Image	Perpendicular Axis	Rotational Movement
Sagittal Plane		Frontal Horizontal Axis	Flexion/Extension



<p>Frontal/Coronal Plane</p>		<p>Sagittal Horizontal Axis</p>	<p>Abduction/ Adduction</p>
<p>Transverse Plane</p>		<p>Vertical Axis</p>	<p>Rotation</p>

Anatomical directions describe locations on the human body (Figure 2.1). In the sagittal plane, if a structure is toward the front of the body, it is said to be anterior, and if it is toward the back, it is posterior. A structure toward the head is considered superior, and a structure closer to the feet is considered inferior. In the frontal plane, if something is close to the vertical axis, it is medial, but if it is further away from the vertical axis, it is considered lateral. When discussing limbs, if a structure is close to the attachment of the limb, it is considered proximal, but if it is further from the limb attachment, it is considered distal. Finally, structures close to the skin or outside of the body are superficial, while structures inside the body are considered deep.

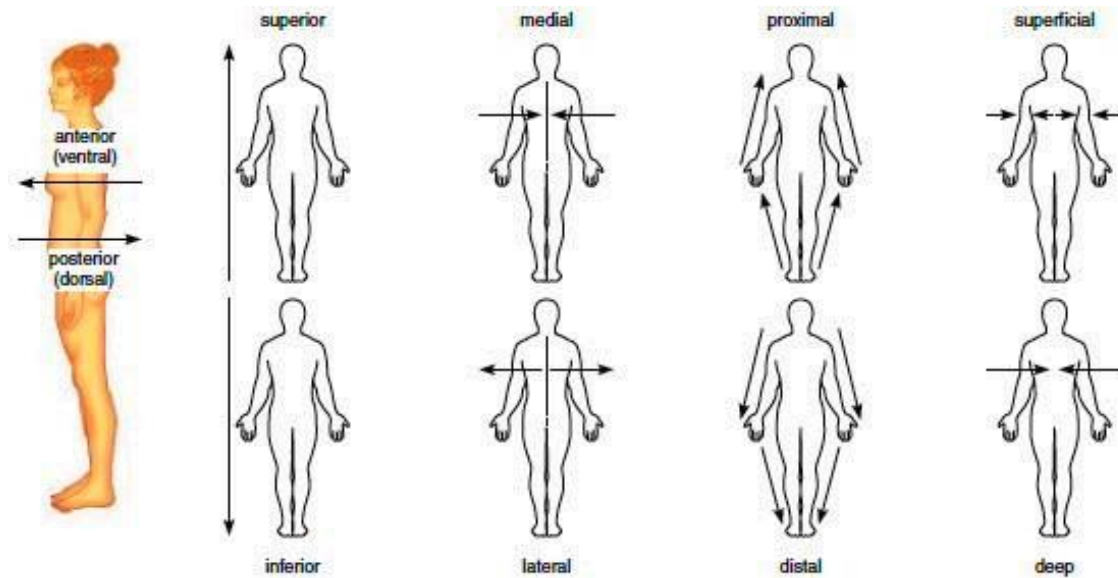


**Figure 2.1 Anatomical directions to describe location on the human body adapted from “Anatomy Language & Histology,” n.d.**

## **2.2 Knee Anatomy**

The main structures in the knee are the ligaments, the meniscus, the articular cartilage, the patellar tendon, the quadriceps tendon, the patella, the femur, and the tibia (Figure 2.2). The knee ligaments connect the femur and tibia bones. The patella, or kneecap, is a bone which is embedded in the quadriceps tendon that connects to the quadriceps muscle. The patellar tendon connects the patella to the tibial tuberosity, an uprising on the anterior tibia. Since the patellar tendon connects bone to bone, it is technically a ligament.

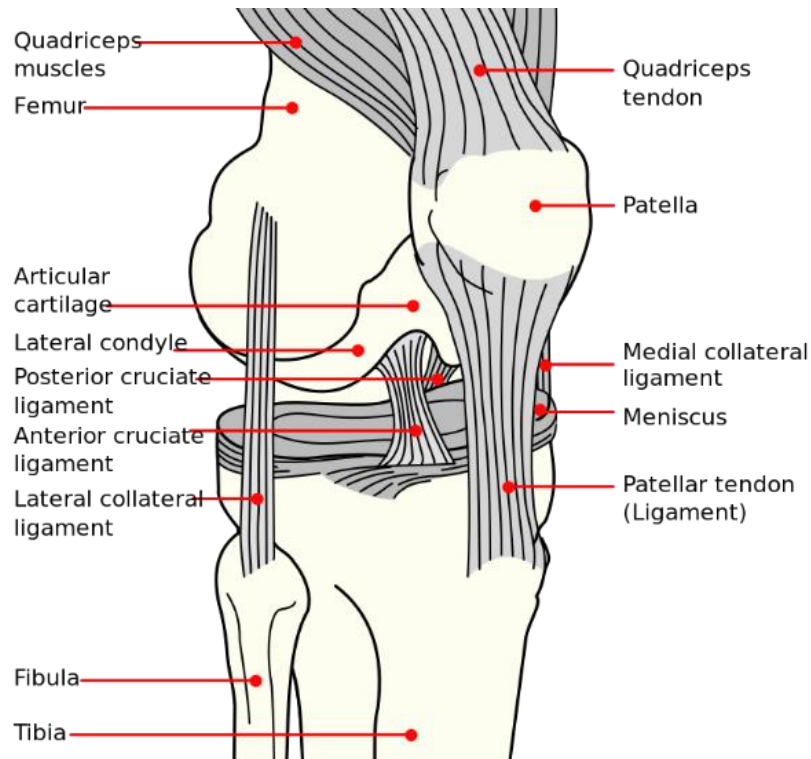


**Figure 2.2 Anatomy of the human knee adapted from “Knee,” 2018**

The tibial plateau (the top of the tibia) is the main loadbearing structure in the knee; however, the articular cartilage is also heavily loaded when the knee joint is in compression. Articular cartilage lines the femur in order to protect it. The meniscus, which is another cartilage structure, helps provide stability by evenly distributing forces on the tibial plateau. In addition, the knee has four ligaments that help stabilize the joint:

1. Anterior cruciate ligament (ACL) which restrains anterior tibial translation (ATT)
2. Posterior cruciate ligament (PCL) which restrains posterior tibial translation
3. Lateral collateral ligament (LCL) which restrains varus angulation (Figure 2.3)
4. Medial collateral ligament (MCL) which restrains valgus angulation (Figure 2.3)

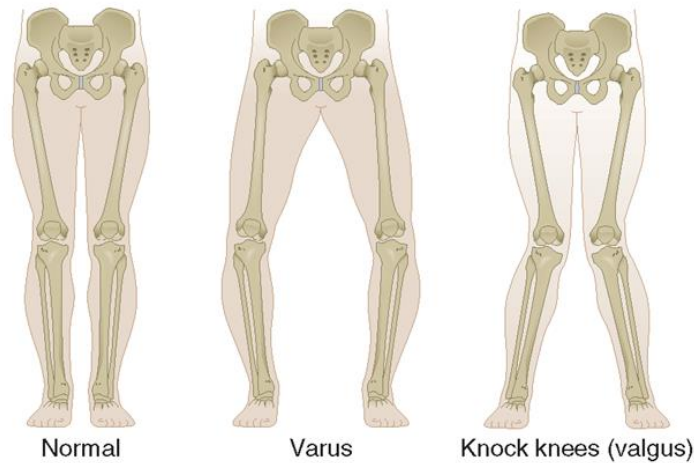
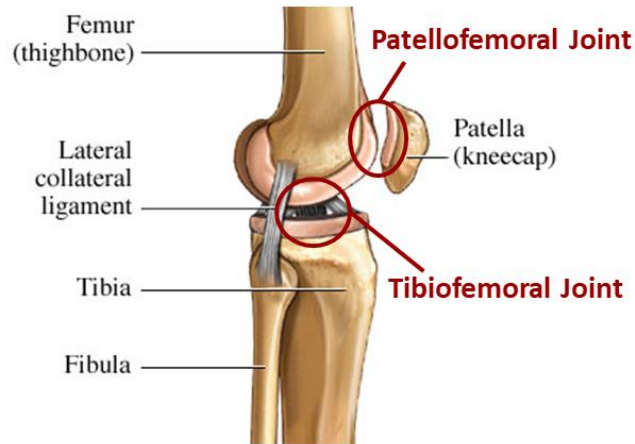


**Figure 2.3 Valgus and varus motion adapted from “Valgus vs Varus Knee Alignment,” 2017**

The iliotibial band, which runs along the lateral side of the knee, also helps stabilize the joint.

The human knee actually consists of two joints: the patellofemoral joint and the tibiofemoral joint (Figure 2.4). As the knee flexes and extends, it also rotates about an axis parallel to the tibial diaphysis, which is the longitudinal axis of the bone.

The patellofemoral joint is the joint created by the patella and the femur. The patella acts as a hinge for the tendon connecting the quadriceps muscle to the tibia. The tibiofemoral joint is the joint between the tibia and the femur responsible for flexion and extension of the knee. The femoral condyles undergo a combination of sliding and rolling motion over the tibial plateau (Frankel et al., 2012).

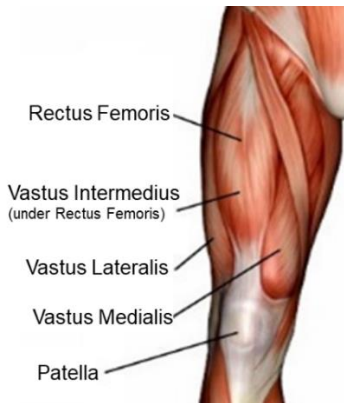
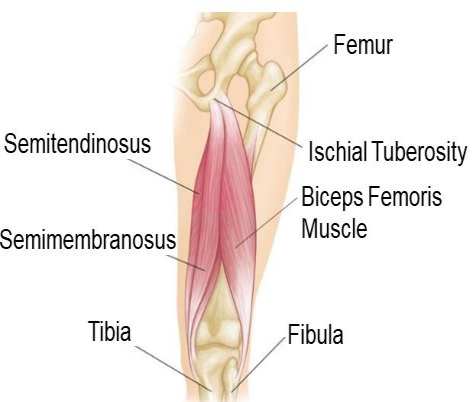
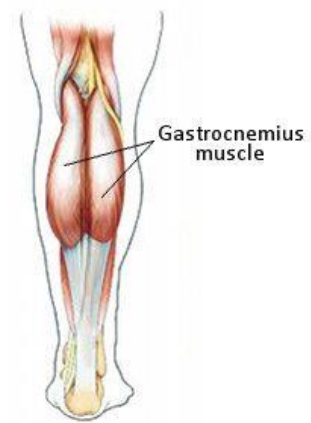


**Figure 2.4 Patellofemoral and tibiofemoral joints of the knee adapted from “Medial Collateral Ligament,” 2011**

Motion of both joints occurs primarily in the sagittal plane. The current study will focus on sagittal plane motion.

There are also many muscles running across the knee joint. The main three muscle groups affecting knee stability are the quadriceps, hamstring and gastrocnemius (calf) muscle groups. These are summarized in Table 2.2. In addition to these main muscle groups, the popliteus muscle (Figure 2.5) spans the knee joint from the lateral femoral condyle to the medial posterior tibia to provide stability (Behnke, 2001).

**Table 2.2 Major Muscle Groups affecting knee motion adapted from Behnke, 2001**

Major Muscle Group	Muscle	Function	Image
Quadriceps	<i>Rectus femoris</i>	<ul style="list-style-type: none"> <li>• Most superficial quad muscle</li> <li>• Inserts on patella base</li> <li>• Extends the knee joint</li> </ul>	 <p>Adapted from “Quadriceps Muscle Diagram,” 2016</p>
	<i>Vastus lateralis</i>	<ul style="list-style-type: none"> <li>• Largest <i>vastus</i> muscle</li> <li>• Inserts on lateral patella</li> <li>• Extends the knee joint</li> </ul>	
	<i>Vastus intermedius</i>	<ul style="list-style-type: none"> <li>• Lies underneath the <i>rectus femoris</i></li> <li>• Inserts on inferior patella</li> <li>• Extends the knee joint</li> </ul>	
	<i>Vastus medialis</i>	<ul style="list-style-type: none"> <li>• Inserts on medial patella</li> <li>• Extends the knee joint</li> </ul>	
Hamstring	<i>Biceps femoris</i>	<ul style="list-style-type: none"> <li>• Inserts on fibula head</li> <li>• Flexes the knee</li> <li>• Externally rotates tibia near full extension</li> </ul>	 <p>Adapted from Hegg, 2018</p>
	<i>Semitendinosus</i>	<ul style="list-style-type: none"> <li>• Inserts on proximal medial tibia</li> <li>• Flexes the knee</li> <li>• Internally rotates tibia</li> </ul>	
	<i>Semimembranosus</i>	<ul style="list-style-type: none"> <li>• Inserts on medial tibial condyle</li> <li>• Flexes the knee</li> <li>• Internally rotates tibia</li> </ul>	
Gastrocnemius	<i>Gastrocnemius</i>	<ul style="list-style-type: none"> <li>• Contains two muscle heads which insert on the medial and lateral femoral condyles</li> <li>• Both muscle heads combine to form one tendon at the ankle</li> <li>• Flexes the knee</li> </ul>	 <p>Adapted from Agarwal, 2017</p>

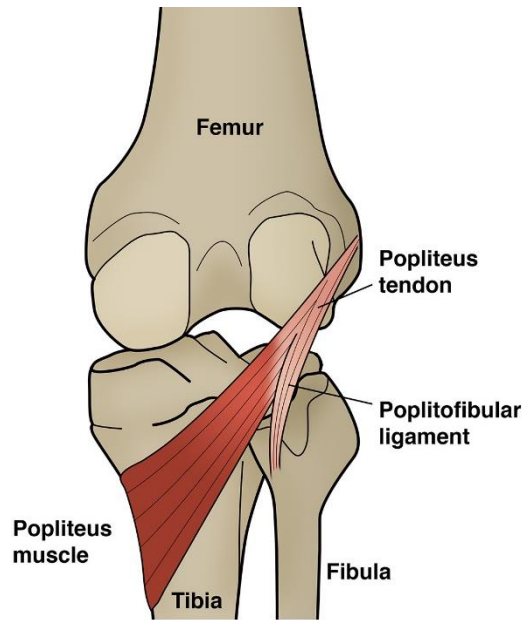


**Figure 2.5 The popliteus muscle adapted from Langford, 2018**

### **2.3 ACL Anatomy**

In the current study, the main structure of interest is the anterior cruciate ligament (ACL). The ACL is composed of collagen fibrils which form fibres. The majority of these fibres run parallel to the long axis of the ligament. A connective tissue called endotenon surrounds the collagen fibre bundles, and a lot of endotenon gives the appearance of bundles. There are two bundles commonly mentioned in the literature: the anteromedial (AM) bundle and the posterolateral (PL) bundle. A diagram of the bundles can be found in Figure 2.6. Sometimes a third intermediate band between the two bundles is also mentioned in the literature (Burks, 1990).

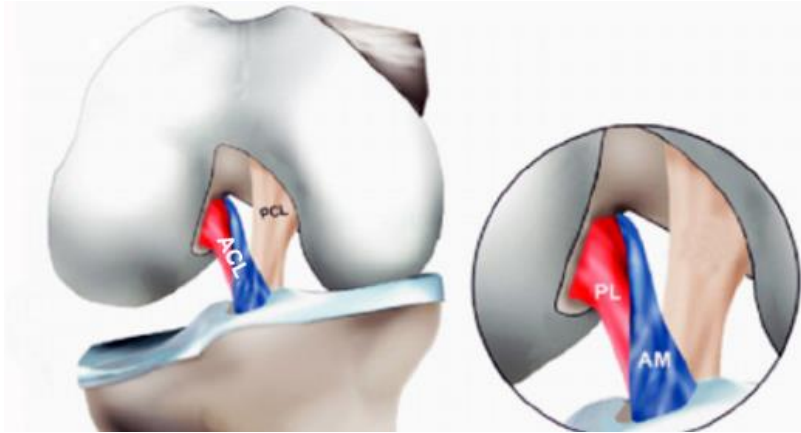


**Figure 2.6 The anteromedial (AM) and posterolateral (PL) bundles of the ACL adapted from “Single-bundle vs. Double-bundle ACL Surgery,” 2018**

Ligaments bind bone to bone. The ACL attaches at the femur along the longitudinal axis and attaches to the tibia along the anteroposterior axis, which leads to a 90 degree twist in the fibres in the coronal plane (Figure 2.7).

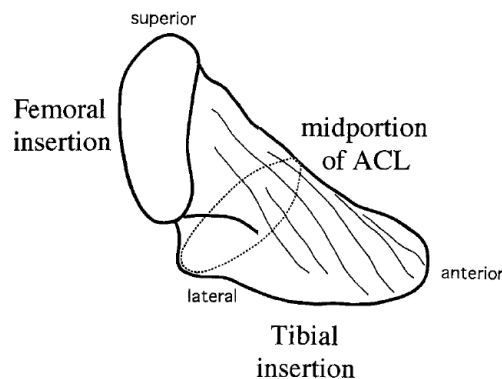


**Figure 2.7 Insertion site of the ACL Muneta et al., 1997**

The cross section of the ACL is wider at the insertion sites. There is a transition zone of fibrocartilage and mineralized cartilage so that the stiffness of the ligament increases gradually. These qualities reduce stress concentrations at insertion sites (Burks, 1990). The cross sectional area of the ACL has been found to be smaller in women than in men (Chandrashekar et al., 2006; Muneta et al., 1997). The primary function of the ACL is to prevent anterior tibial translation. Its secondary functions include preventing hyperextension of the knee and controlling internal rotation of the lower leg. It also prevents valgus and varus motion of the knee (Ellison and Berg, 1985; Shoemaker and Daniel, 1990).



## Chapter 3 Literature Review

The ACL is often injured during sport-related activities, and ACL repair is a very common sport-related surgical procedure in the U. S. (Csintalan et al., 2008). The total incidence of ACL injury is estimated to be 68.6 per 100,000 person years in the U.S. (Sanders et al., 2016), and ACL reconstruction is estimated to have a mean lifetime cost of \$38,121 per patient (Mather et al., 2013). Understanding ACL injury mechanisms is critical in order to prevent ACL injury and to develop effective rehabilitation programs.

### 3.1 Jump Landing Experimental Models

In order to investigate how the ACL behaves under complex loading conditions, such as single-leg jump landing, *in-vitro* studies are often performed (Bakker et al., 2016; Cassidy et al., 2013; Hashemi et al., 2007; Levine et al., 2013; Oh et al., 2011). To apply the boundary conditions required to simulate a jump landing, a type of mechanical device is necessary. Researchers have developed knee simulators, which use data from motion-capture and/or electromyography (EMG) as inputs (Bakker et al., 2016; Cassidy et al., 2013). ACL strain is often measured using a differential variable reluctance transducer (DVRT), a small strain gauge (Cassidy et al., 2013; Hashemi et al., 2007; Levine et al., 2013; Oh et al., 2011). There are dynamic knee simulators at the University of Michigan (Oh et al., 2011), Ohio State University (Levine et al., 2013), Texas Tech University (Hashemi et al., 2007), and the University of Waterloo (Cassidy et al., 2013), were developed for the study of single leg jump landing.

#### 3.1.1 The University of Michigan Simulator

The Michigan simulator (Figure 3.1) is a 2.5 m high loading frame, which holds a cadaveric specimen at a knee flexion angle that simulates a jump, between 20-25 degrees (Oh et al., 2011). Aircraft cables are used to represent the hamstring (H), quadriceps (Q) and gastrocnemius (G), all pretensioned to a predetermined value. A weight (W) is dropped in series with the femur to initiate the dynamic load. In order to measure ACL strain, the AM bundle of the ACL is instrumented with a DVRT ( $\epsilon$ ) (Withrow et al., 2006). The Michigan simulator is often used to quantify the effect of certain inputs on ACL strain, such as whether or

not ACL strain corresponds to impact load, quadriceps force, and change in flexion angle. It was found that ACL strain correlated with quadriceps force and knee flexion angle but not impact force (Withrow et al., 2006). The simulator has also been used to investigate whether an increase or decrease in hamstring tension would affect the peak strain in the ACL (Withrow et al., 2008). A torsion device which adds internal tibial torque was later added to the device in order to investigate the effect of cutting the ACL on internal tibial rotation and anterior tibial translation (Oh et al., 2011). The simulator was also used to study what causes the ACL to fail under repetitive loading (Lipps et al., 2013).

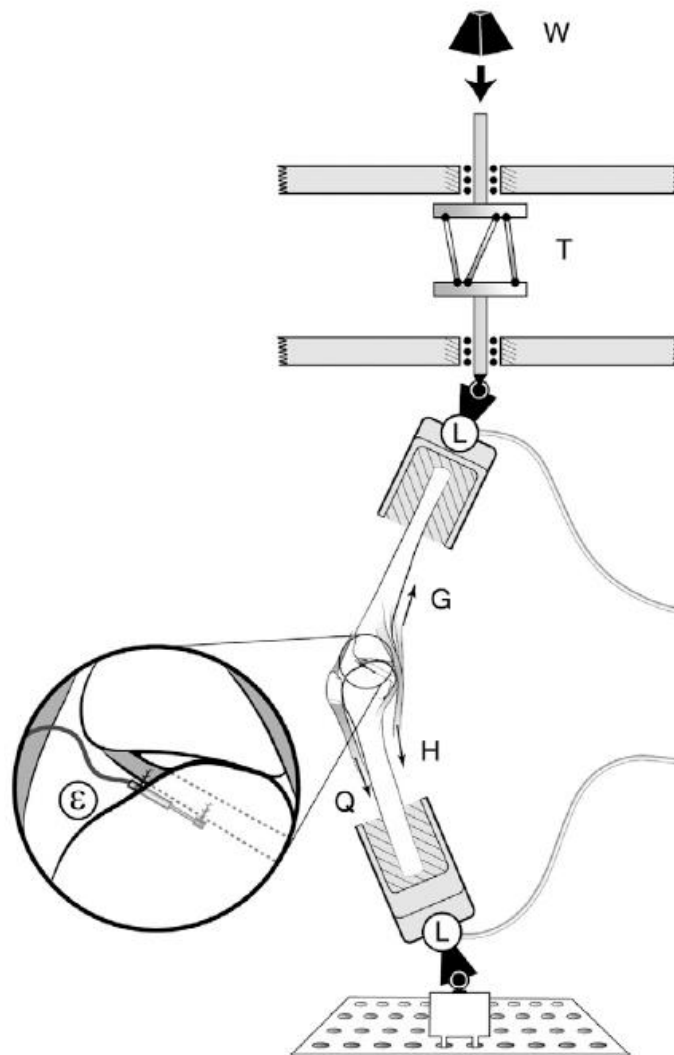


**Figure 3.1 The Michigan Simulator with the added torsion device (T) adapted from Oh et al., 2011**

### 3.1.2 The Ohio State University Simulator

The Ohio State University simulator (Figure 3.2) fixes the femur rigidly, while the tibia is vertical and superior (Levine et al., 2013). The knee is flexed at 25 degrees. Quadriceps and hamstring muscle forces are applied using weighted pulleys along appropriate lines of action. There is a weight dropped on the foot to simulate a ground reaction force. Abduction and internal rotation moments are applied using external apparatus also described in Figure 3.2. The ACL is instrumented with a DVRT to measure strain. (Kiapour et al., 2014; Levine et al., 2013). The simulator is often used to evaluate ACL strain and injury patterns under physiologically relevant loading conditions (Kiapour et al., 2014; Levine et al., 2013; Quatman et al., 2014). The simulator has also been used to investigate the effects of multi-planar loading vs. uni-planar loading effects on ACL strain and injury (Kiapour et al., 2016). The simulator was modified in 2017 in order to consistently recreate failure patterns in ACLs similar to those observed in clinical settings (Bates et al., 2017).

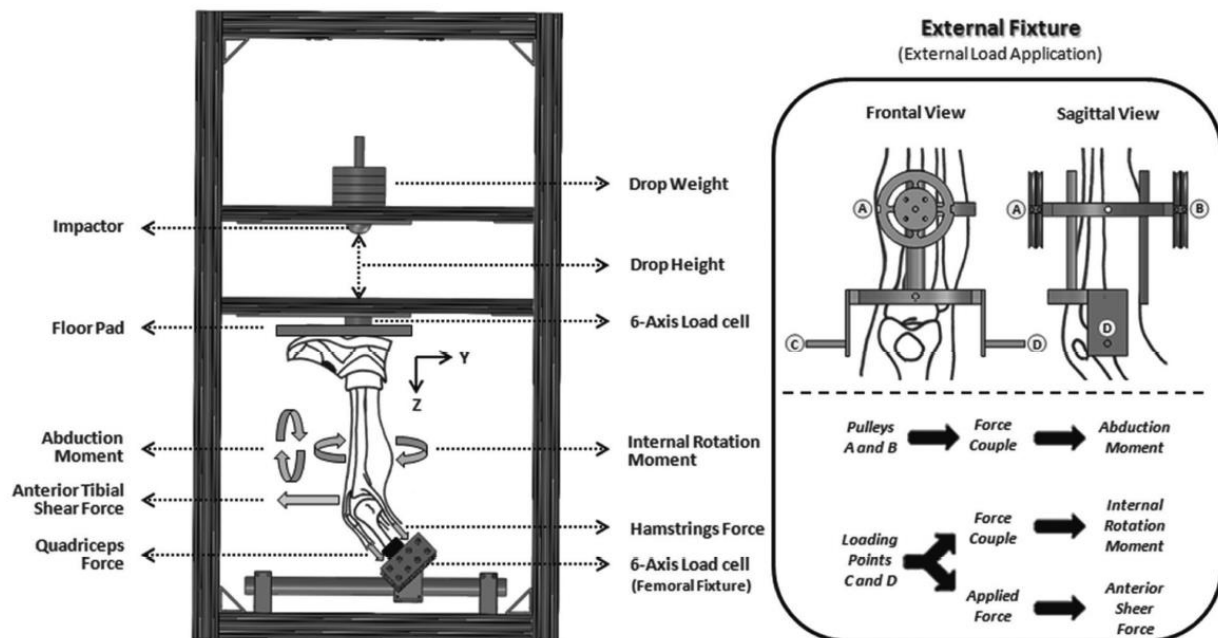


**Figure 3.2** The original Ohio State Simulator setup. Left: the simulator which applies loads in the sagittal plane. Right: External devices used to apply multi-planar loading adapted from Levine et al., 2013.

### 3.1.3 The Texas Tech University Simulator

The Texas Tech simulator (Figure 3.3) is designed to enable dynamic loading of the muscles (Hashemi et al., 2007). Quadriceps and hamstring forces are applied using a pulley system connecting steel cables to actuators. GRF is applied using a lever plate setup: the impactor hits one side of the plate that then hits the ankle, resulting in the “ground” initiating the impact. Hip flexion is allowed to develop naturally. The simulator has been used to successfully recreate jump landing loading conditions which are capable of injuring an ACL; however, the simulator does have limitations in that it does not account for gastrocnemius force or adduction/abduction (Hashemi et al., 2007).

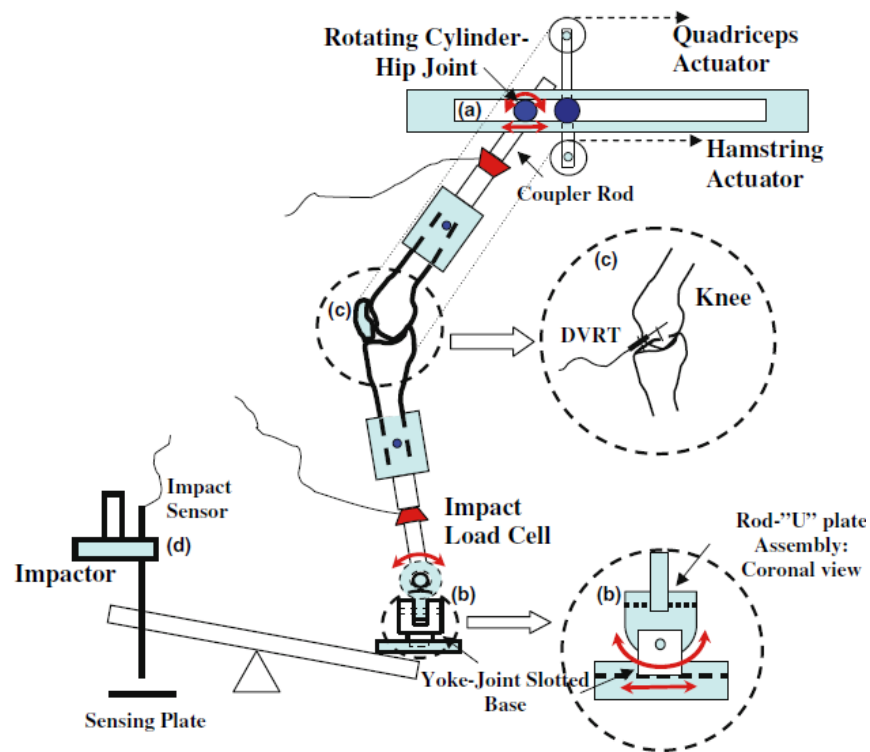
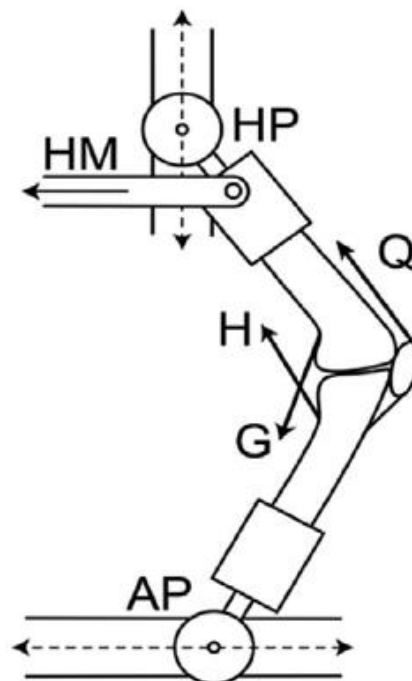


Figure 3.3 The Texas Tech Simulator adapted from Hashemi et al., 2007

### 3.1.4 The University of Waterloo Simulator

The University of Waterloo simulator (Figure 3.4) allows dynamic muscle-force vs. time profiles to be modelled (Cassidy et al., 2013). The simulator has six powerful actuators that provide input: X motion at the ankle (AP), Y motion at the hip (HP), Hip Force (HM), which is applied a distance away from the hip

centre of rotation to induce a moment, hamstring force (H), quadriceps force (Q), and gastrocnemius force (G). Motion capture of a subject performing jump landing on a force plate is performed in order to acquire kinematics and ground reaction force, which can then be input into a lower extremity biomechanical model in order to produce muscle force profiles for the hamstring, quadriceps, and gastrocnemius muscles, as well as a hip moment time profile (Cassidy et al., 2013). The University of Waterloo simulator has been used to study the effect of knee braces of ACL strain (Hangalur et al., 2016). It has also been used in studies to develop an empirical model to estimate maximum strain, which determined that the major factors that affect ACL strain are: increased body weight, increasing ground reaction force, and low knee and hip flexion angles with increasing hip moment (Bakker et al., 2016). The peak relative ACL strain during single leg jump landing investigations tested on the DKS was between 0.03 and 0.20 occurred between 90 and 200ms (Bakker, 2014). The University of Waterloo simulator is currently the only known simulator which can apply dynamic muscle force *vs.* time curves to simulate jump landing (Cassidy et al., 2013).



**Figure 3.4 The University of Waterloo Simulator adapted from Bakker et al., 2016**

### **3.2 Knee Brace Studies**

A few studies have investigated the effect of knee braces on relative ACL strain. Hangalur et al., 2016 tested a cadaver knee on the dynamic knee simulator at the University of Waterloo in unbraced and braced conditions. The inputs for the simulator came from motion capture performed on braced and unbraced participants done by Hangalur et al., 2016, and they concluded that the muscle force profiles from the braced participants resulted in lower relative ACL strain than the muscle force profiles from the unbraced participants. Placing a knee brace on the cadaver specimen did not cause a significant change in relative ACL strain. Thus, Hangalur et al., 2016 concluded that knee braces reduce ACL strain by changing the muscle firing pattern during a dynamic activity. Other studies have attempted to quantify the effect of knee braces *in-vivo*, either by surgically implanting a sensor onto the ACL of participants (Beynnon and Fleming, 1998), or by taking motion capture of participants performing a task while braced and unbraced, and then using a mathematical model to determine ACL strain (Devita and Hortobagyi, 2001). Both Beynnon and Fleming, 1998 and Devita and Hortobagyi, 2001 concluded that the interaction between the soft tissue of the leg and the knee brace contributed to the reduction in ACL strain while the participant was wearing the knee brace. Brandsson and Faxe, 2001 studied the effects of wearing a functional knee brace after ACL repair. They compared two post-op groups: one group wore a knee brace during rehabilitation, while the other group did not wear a knee brace. They found that while the group wearing the knee brace found recovery to be less painful and to have fewer complications, there was no significant difference after two years in knee function and knee laxity between the group wearing the knee brace and the group not wearing the knee brace (Brandsson and Faxe, 2001). Sitler et al., 1990 studied the effect of a prophylactic knee brace on football players, and found that the prophylactic knee brace had no statistically significant effect in decreasing the amount of ACL injuries during the football season.

### **3.3 Knee Joint Modelling Considerations**

Finite element modelling can provide additional insights on loading pattern and timing when simulating loading cases, and allow for deterministic variation of material properties, boundary conditions and

geometry. Since biomechanical movement is very difficult to quantify using *in-vivo* experiments, and is costly and labour intensive *in-vitro*, it is a natural progression to try and develop mathematical models of human subjects in order to perform investigation computationally (Trad et al., 2018). A few researchers have adopted this approach. In order to create a finite element model, the following need to be considered:

1) The geometry:

- Will the model have the same geometry as the cadaver specimens used to validate it? This is known as a subject-specific model. Will the model have a general geometry, such as a 50<sup>th</sup> percentile average-sized male?

2) The mesh:

- Will the mesh size give an appropriate response during the required loading?

3) Material properties:

- Which mechanical material properties will be used in the model and which material model will be used to implement these properties?

4) Loading and boundary conditions (Trad et al., 2018; Weiss et al., 2005)

There are multiple factors which affect the response of a finite element model of the human knee. The main factor considered in the current study was the biological tissue material model of the ACL. The geometry of the model was not subject-specific, since the model used was developed prior to the investigation; however, a mesh convergence study was performed to confirm that the ACL mesh size gave an appropriate tensile response.

Material characterization of the ACL is challenging, since it is difficult to find a stress free state of the ACL that is also physiologically relevant. A few researchers have adopted methods in order to attempt to determine material characteristics of the ACL. Their findings are presented in Table 3.1.

**Table 3.1 Literature Review of ACL Material Characterization**

<b>Author/Year</b>	<b>Noyes and Grood, 1976</b>	<b>Butler et al., 1986</b>	<b>Woo et al., 1991</b>	<b>Chandrashekar et al., 2006</b>
Objective of Paper	<ul style="list-style-type: none"> <li>tested young(6) and old (20) humans and rhesus monkey ACLs in order to determine and compare material properties</li> </ul>	<ul style="list-style-type: none"> <li>measured individual fibre bundles of the human ACL, PCL, LCL, and patellar tendon</li> </ul>	<ul style="list-style-type: none"> <li>tested young, middle-aged, and old human ACL to determine how properties change with age</li> <li>also loaded ACLs in 2 different physiologically meaningful directions to see the effect of loading direction</li> </ul>	<ul style="list-style-type: none"> <li>tested human ACL to determine differences in properties of male and female ACL</li> </ul>
ACL Length (mm)	Young: $26.9 \pm 1.5$ Old: $27.5 \pm 2.8$	Average: 28.7	Not reported	M: $29.61 \pm 2.7$ F: $27.04 \pm 2.9$
ACL Area (mm <sup>2</sup> )	Young: $44.4 \pm 9.7$ Old: $57.5 \pm 16.2$	Average: 1.46	Not reported	M: $72.91 \pm 18.9$ F: $57.32 \pm 15.7$
Strain Rate	100%/s	100%/s	200 mm/min (slow)	100%/s
Knee Flexion Angle of ACL	45 degrees		30 degrees	45 degrees
Direction of Load	Attempted to load along the axis of the ACL; however stated difficulties in doing this consistently	30 degree fibre to grip angle	Anatomical and tibial axes were tested: Anatomical: along direction of ACL fibres Tibial: along tibial diaphysis	Loaded along fibres of ACL
Stiffness (N/mm)	Young: $182 \pm 56$ Old: $129 \pm 24$	Not reported	Middle Age Group Anatomical: $220 \pm 24$ Tibial: $192 \pm 17$	M: $308 \pm 89$ F: $199 \pm 88$
Young's Modulus (MPa)	Young: $111 \pm 26$ Old: $65.3 \pm 24$	$345 \pm 22.4$	Not reported	M: $128 \pm 35$ F: $99 \pm 50$

Noyes and Grood, 1976 and Chandrashekar, 2005 present studies in which entire ACLs were loaded along the direction of the fibres while the knee was flexed at 45°. The results from both studies are similar, as seen in Figure 3.5. Woo et al., 1991 tested full ACLs along the direction of the fibres (anatomical direction) and along the direction of the tibia (tibial direction) when the knee was flexed at 30°. They only reported force vs. elongation, which is depicted in Figure 3.6. Butler et al., 1986 tested individual fibre bundles of



the ACL in tension, as opposed to the entire structure; therefore, the results cannot be compared to the other studies.

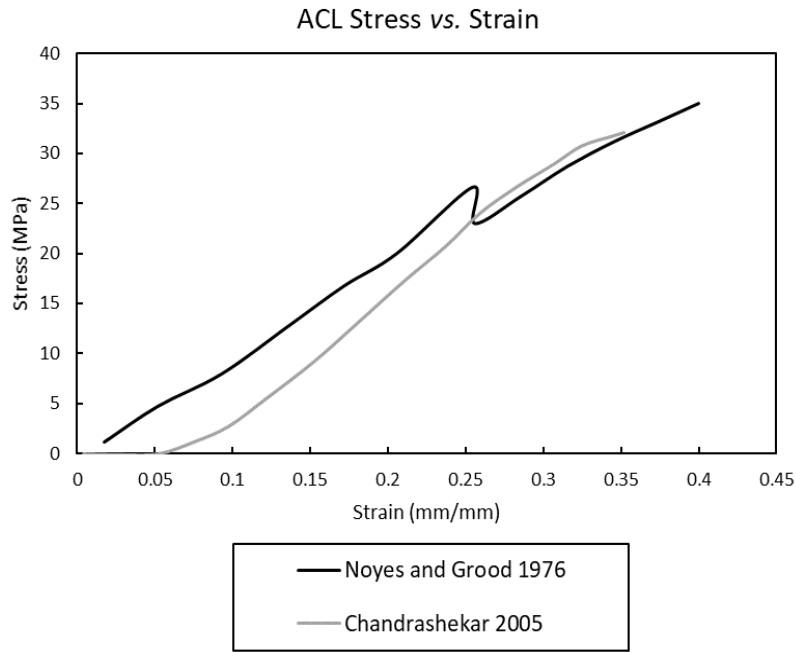


Figure 3.5 ACL stress vs. strain curves from Noyes and Grood, 1976 and Chandrashekar, 2005

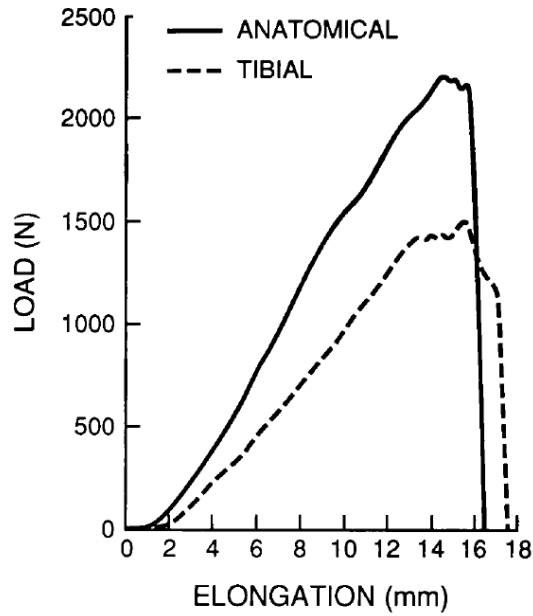


Figure 3.6 ACL force vs. elongation curves from Woo et al., 1991

In addition to determining ACL material properties, there are many studies which have investigated material modelling of the ACL (Kiapour et al., 2013; Peña et al., 2006; Song et al., 2004; Untaroiu et al., 2005). There is no standard procedure for material modelling of ligaments and it can be a challenge to create a model which gives an appropriate response, since ligaments are anisotropic and do not sustain compression (Trad et al., 2018). Many one-dimensional models include non-linear hyperelastic spring elements to represent the bundles composing the ligaments in the knee (Haut Donahue et al., 2003, 2002, Li et al., 2002, 2001, 1999; Peña et al., 2006; Zielinska and Haut Donahue, 2006). Hyperelastic material models are a way of modelling non-linear elasticity by relating strain energy to the deformation of a material in order to get a stress-strain curve independent of strain rate. An isotropic hyperelastic material model can also be used for 3D ligaments (Song et al., 2004; Xie et al., 2009). Isotropic materials exhibit similar behaviour in all three directions of loading. A more complex model, such as a transversely isotropic hyperelastic model, may be more realistic as it partially accounts for the anisotropy of ligaments (Gardiner and Weiss, 2003; Limbert et al., 2004; Peña et al., 2006). Quasi-linear viscoelastic models (Untaroiu et al., 2005, 2013), which are able to replicate both non-linear elastic behaviour and strain rate dependence, and Holzapfel-Gasser Ogden models (Kiapour et al., 2013; Kiapour et al., 2014), which aim to replicate the anisotropic behaviour of crossed fibres embedded in soft tissue (Trad et al., 2018), have also been used.

### **3.4 Computational Models of Human Leg**

Many mathematical models have been developed to study single leg jump landing. There are models to determine the upper bound of quadriceps force during jump landing (Domire et al., 2011), to calculate the injury risk associated with certain kinematic sequences during landing (Leppänen et al., 2017), and even to calculate ligament strain from kinematics acquired from living persons (Taylor and Terry, 2013).

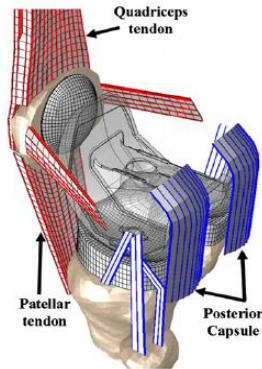
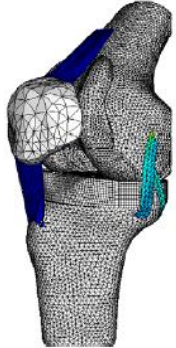
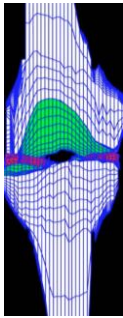
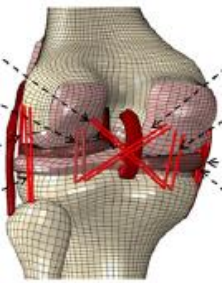
Investigating ACL strain during a single leg jump landing has also been done using finite element modelling by the research group from Ohio State University, who recreated a range of human movement, including jump landing, in a finite element program (Kiapour et al., 2013). They developed a finite element model of a human leg from magnetic resonance imaging (MRI) and validated their model using multiple loading

scenarios, both dynamic and static, on their simulator (Kiapour et al., 2014). The objective of the Kiapour et al., 2013 study was to create a multi-purpose model, which could be used to predict ACL injury in different loading scenarios.

Finite element models need to be validated and compared to experimental data; therefore, it is important to replicate experimental loading conditions, often applied to cadavers on a knee simulator, and to compare experimental and computational results. An example of developing a finite element model and comparing it to experimental data is Baldwin et al., 2012 and Halloran et al., 2005, who both developed finite element models to study kinematics of total knee replacements, and compared their models to experimental data to ensure that they could be used to draw further conclusions. Models are often developed as a tool to study the behaviour of the knee (Haut Donahue et al., 2002; Kiapour et al., 2013; Li et al., 1999).

Table 3.2 depicts some of these finite element models.

**Table 3.2 Finite Element Models of the Human Knee Joint**

Baldwin et al., 2012	Halloran et al., 2005	Haut Donahue et al., 2002	Kiapour et al., 2013
			

The model used in the current study is a model of the lower limb, initially developed as a section model for a full human body model, the GHBMC 50<sup>th</sup> percentile average sized male (Schwartz et al., 2015). The GHBMC model utilizes the lower leg model of a seated occupant developed by Untaroiu et al., 2013. The model was initially developed to study lower limb injury during automotive collision using geometry from

MRI and CT scans of a subject which closely represented a 50<sup>th</sup> percentile male Untaroiu et al., 2013. The material properties were taken from a previous model, developed for the purpose of understanding pedestrian impacts (Untaroiu et al., 2005). The current study will investigate the use of a general model for a modelling objective (measuring ACL strain during jump landing) which is different from the purpose for which the model was developed (impact modelling).

### **3.5 Hypothesis**

For the experimental study of ACL strain during unbraced and braced single leg jump landing, the University of Waterloo DKS was used, and the following hypotheses were examined:

- The maximum ACL strain will fall between 0.03 and 0.20 will occur between 90 and 200ms.
- The two participant input profiles will result in different ACL strains.
- The knee brace will have no effect on ACL strain (MSE between curves <0.001).

For the finite element study of ACL strain during single leg jump landing, the leg model developed by Untaroiu et al., 2005 was used, and the following hypotheses were examined:

- The maximum ACL strain will fall between 0.03 and 0.20 will occur between 90 and 200ms.
- The two participant input profiles will result in different peak relative ACL strains.
- The GHBMCL ACL strain vs. time curve will show a common characteristic for all loading conditions.

# Chapter 4 Experimental Methodology

## 4.1 Experimental Overview

The experimental methodology used for this study was developed by Bakker et al., 2016, Cassidy et al., 2013, and Kalra et al., 2018. Hangalur et al., 2016 applied the same methodology to the testing of cadavers wearing knee braces. Motion capture of a subject performing jump landing on a force plate was performed in the study of Bakker, 2014. Two of the participants with equal limb lengths were considered for this research.

The inputs of the *in-vitro* and finite element simulations was taken from *in-vivo* motion capture performed by Bakker, 2014, in which the ground reaction force and 3-dimensional kinematics from the motion capture were recorded. Bakker, 2014 input the data into a biomechanical OpenSim model, which he used to determine muscle forces and sagittal hip flexor extensor moment throughout time (Figure 4.1). The six resulting inputs were used as the dynamic knee simulator inputs and also the boundary conditions of the finite element model. A flow chart depicting the scope of the work is shown in Figure 4.2.

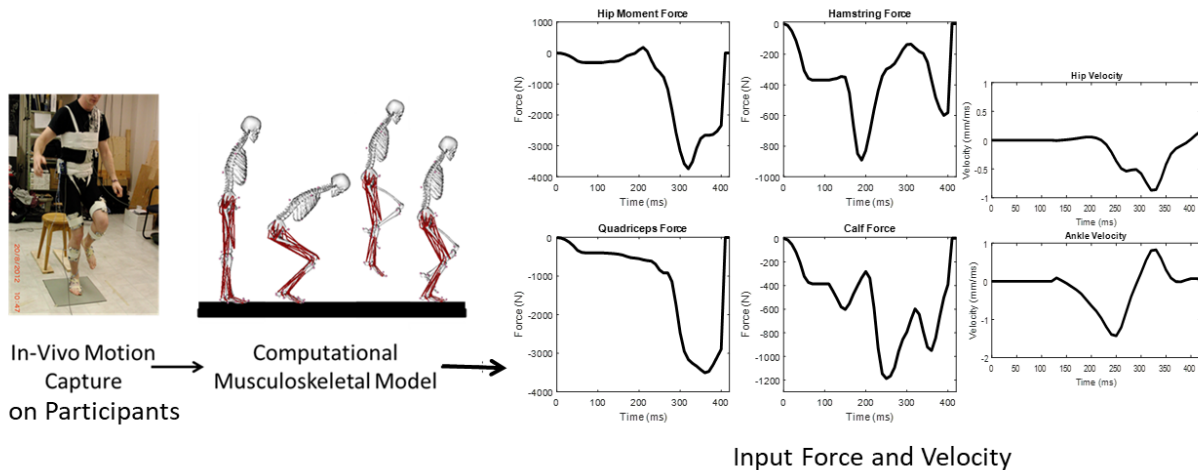


**Figure 4.1** Flow chart of previous work done by Bakker, 2014 to create input profiles adapted from Bakker, 2014

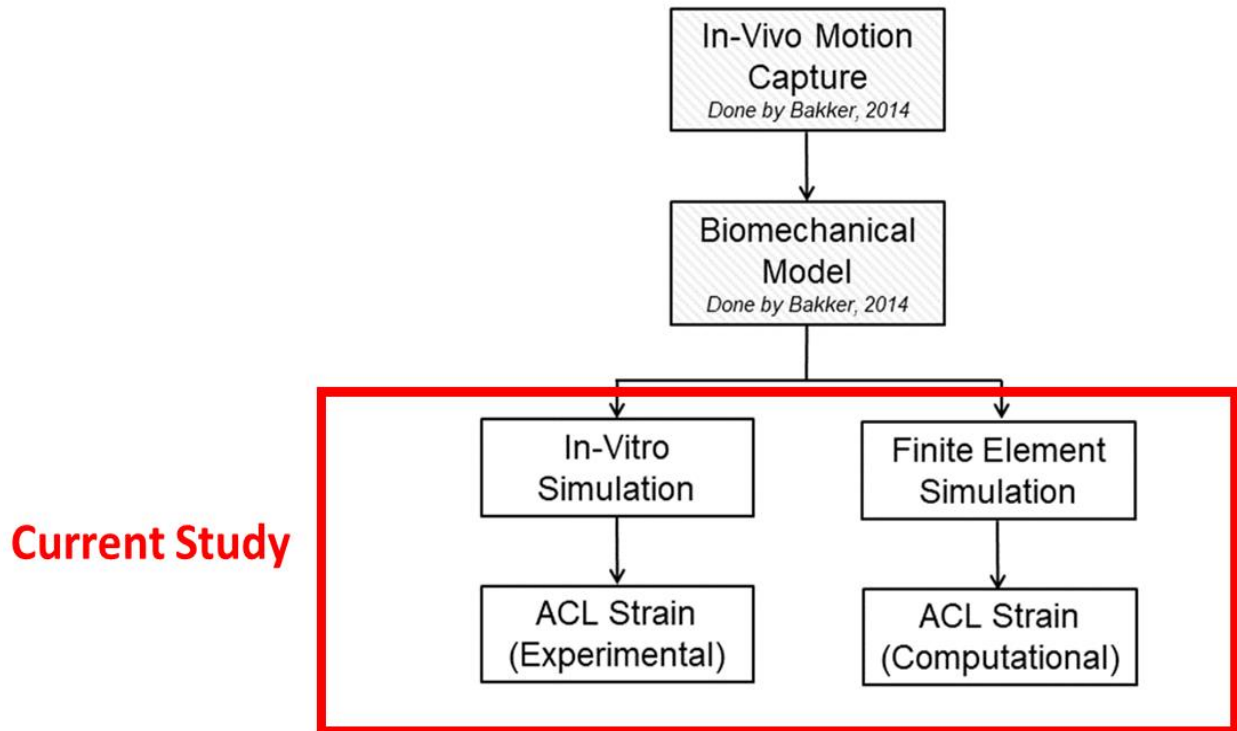


**Figure 4.2** Flow chart of inputs and outputs of experimental and FE modelling adapted from Cassidy et al., 2013

Two different participant profiles were used for the current study. In addition, the cadaver knees were tested wearing a custom Össur CTi knee brace, in order to determine efficacy of the brace in reducing ACL strain. While the effect of the brace was not the main objective of the study, this data could be valuable for future validation of the FE model wearing an identical knee brace.

The test apparatus used in this study was the dynamic knee simulator (DKS) developed by Cassidy et al., 2013, which was discussed in Chapter 3. The simulator has six electromechanical actuators that apply boundary and loading conditions in the sagittal plane, as show in Figure 4.3. The simulator applies three muscle forces representing the quadriceps (Q), the hamstring (H) and the gastrocnemius (G) muscles. A hip moment (HM) is applied as a linear force acting 60 mm away from the centre of rotation of the hip. Finally, hip velocity (HI) and ankle velocity (A) are applied at the hip and ankle, respectively.

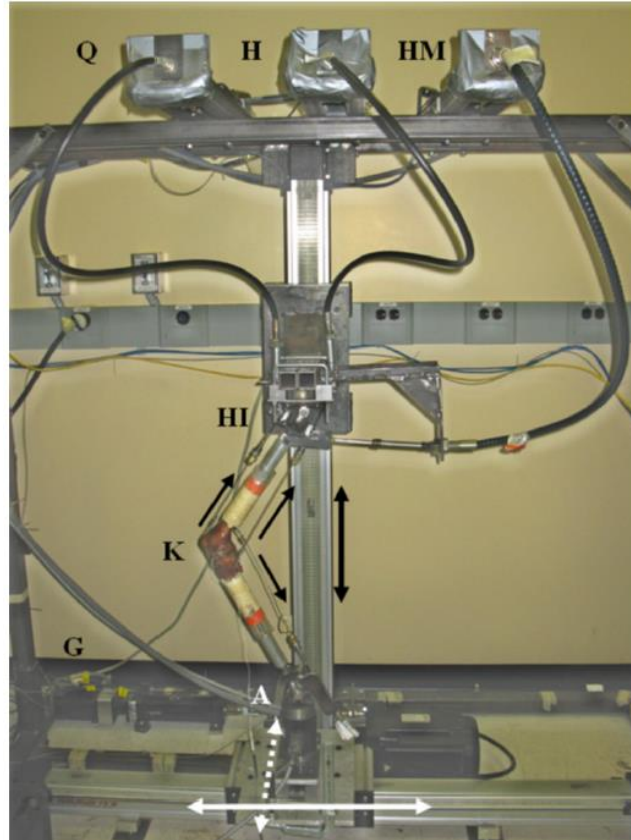


**Figure 4.3 The Dynamic knee simulator adapted from Cassidy et al., 2013**

The DKS was used to test cadaver knee specimens; however, the cadaver knees needed to be prepared to fit onto the simulator before they could be tested. This section will outline the methodology used to prepare the cadavers for testing, the following main points will be discussed:

1. The leg dissection
2. The cabling procedure, in which cables were attached to the dissected cadaver knee at muscle insertion sites. These cables were later attached to the simulator which would apply tension, simulating an actual muscle force acting on the knee.
3. The process of creating a negative mould of the knee before dissection, and then using the mould to create a foam structure on the leg is also discussed. The foam ensured that a knee brace would fit on the dissected knee, as shown in Figure 4.4.
4. The sensor placement procedure



**Figure 4.4 A foamed knee wearing a CTi Össur knee brace**

## **4.2 Casting and Dissection**

Three fresh frozen cadaver knees were received from Innoved Institute (Elk Grove Village, IL).

Anthropometric information about the cadavers tested can be found in Table 4.1. .

**Table 4.1 Cadaver Specimen Anthropometrics**

<b>Knee</b>	<b>Height (in)</b>	<b>Weight (lbs)</b>	<b>Age (years)</b>
<b>1</b>	70	170	49
<b>2</b>	64	155	45
<b>3</b>	65	130	49

The section of the leg necessary for testing included the knee joint and 8 inches above and below the knee joint (Figure 4.5). The legs were kept at -20 degrees Celsius, and were thawed to room temperature when necessary for preparation and testing.



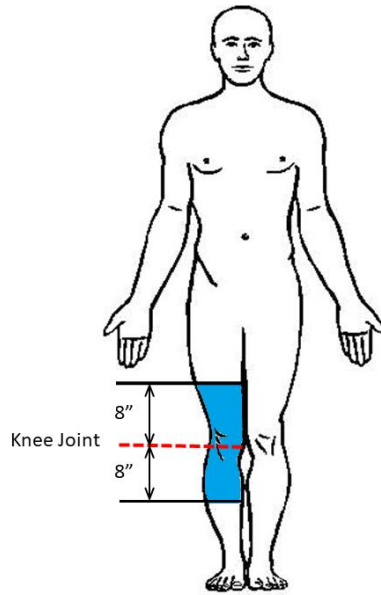


**Figure 4.5 Section of the leg received for testing. Photo adapted from “Blank Body Colouring Page,” n.d.**

The femur and the tibia were located, and a hole was drilled along the axis of each bone. These holes were then tapped so that threaded metal rods could be inserted. The femur tap was 5/8”-11 and the tibia tap was 1/2”-13.

The frozen legs were then cast in fiberglass casting tape in order to create a negative mould. Locator pins were placed in the cast and the leg. Two plastic plates were placed on either end of the leg. Holes were drilled in the plates so locator rods for the femur and tibia could be placed inside. The cast and the plates were used to ensure that the dissected leg was aligned in the cast during the foaming process (Figure 4.6).

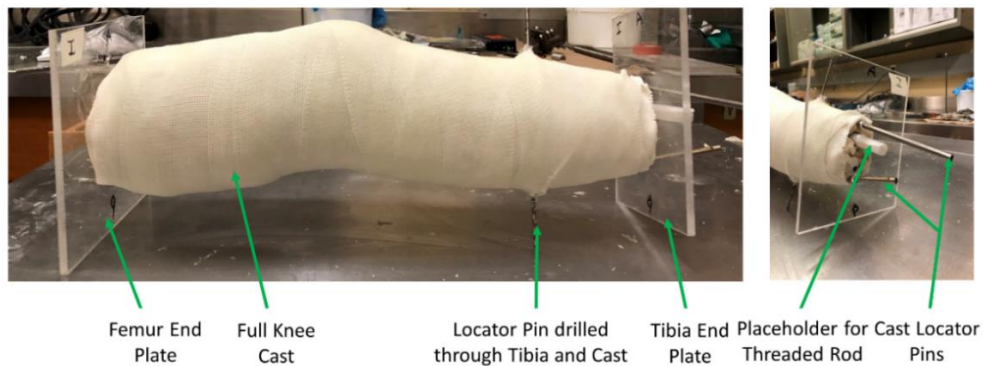


**Figure 4.6 Casted cadaver knee with endplates and locator rod**

The legs were then dissected. Care was taken to ensure that the knee joint was kept intact and that none of the ligaments were damaged in the dissection procedure. The dissection started with a cut made along the leg on the anterior side. The cut was then deepened until the fascia, which are thin fibrous bands of tissue connecting muscles, began to separate on their own. A similar lengthwise cut was then made along the posterior side of the leg. The skin was carefully removed by making light cuts along the fascia connecting the skin to the muscle. Once the skin was removed, the fascia between muscles were separated until the sciatic nerve could be located. Individual muscle groups were then separated and tracked down to the tendons. The muscles groups include the soleus muscle, the hamstring, the gastrocnemius, and the quadriceps. Each muscle head was clipped at the tendon. A summary of the dissection procedure can be found in Figure 4.7. The popliteus muscle was left intact, as it spans the knee joint and is believed to contribute to knee joint stability (Behnke, 2001).

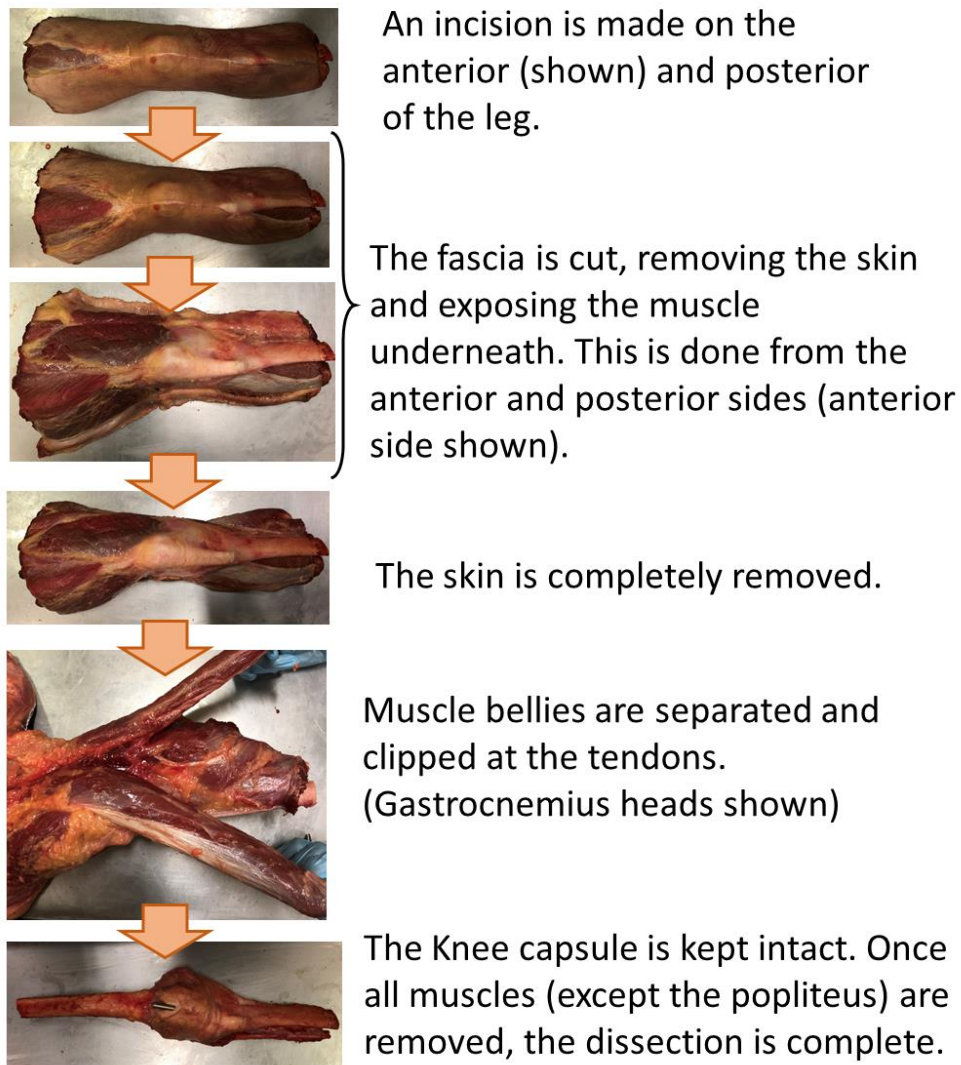


**Figure 4.7 Dissection procedure flowchart**

### **4.3 Preparation for Testing**

After dissection, the leg needed to be prepared to be put on the simulator. Stainless steel cables were attached at muscle insertion sites of the quadriceps, hamstring, and gastrocnemius muscle groups. The other ends of the cables were attached to the actuator and tensed to represent muscles affecting the knee through flexion extension cycles. A 3/32" cable was used to represent the hamstring and gastrocnemius, while the quadriceps cable was 1/8" in diameter.

The fibula was also cut approximately an inch below the tibial plateau, so that the LCL insertion on the fibula was not affected. The remaining segment was kept in place by placing a plastic tube between the fibula and the tibia (Figure 4.8).



**Figure 4.8 Anterior frontal plane view of tibia with fibula cut off**

The quadriceps muscle cable was attached to the tibial tuberosity and crimped, creating the quadriceps muscle insertion site. A hole was drilled in the patella and the tibial tuberosity, a bump on the proximal anterior tibia, allowing the quadriceps cable to be fed through. The cable was also crimped below the patella to ensure that it remained in approximately the correct position along the patellar tendon (Figure 4.9).

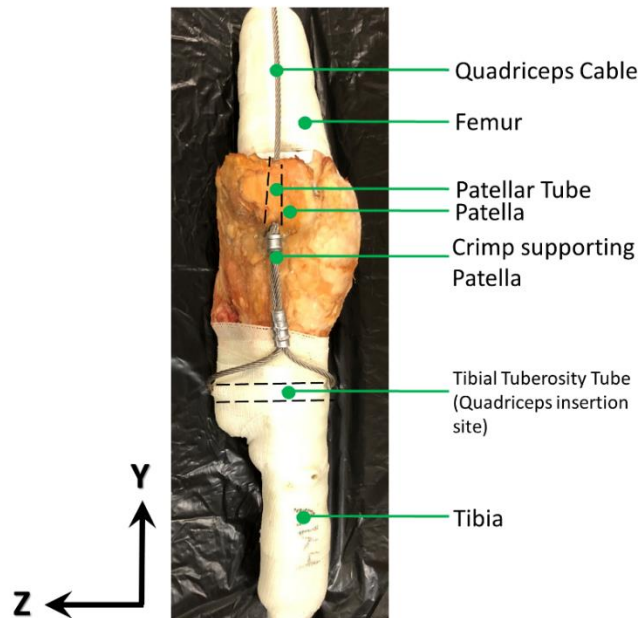


**Figure 4.9 Anterior frontal plane view of the cabled knee showing quadriceps muscle cable**

The hamstring muscle was attached to the bottom of the tibia. The cable was looped around the bottom of the tibia and then clamped. The tibia was then casted, which kept the cable in place, and created an attachment site directly below the back of the knee joint (Figure 4.10).

The gastrocnemius cable was attached on the posterior distal of the femur. A hole perpendicular to the femoral shaft was drilled. A cable was run through the hole and crimped to create the gastrocnemius insertion site. The femur was then casted in fiberglass casting tape to reinforce the bone (Figure 4.10). Finally, a screw was placed in the femur to prevent the femoral threaded rod from rotating.

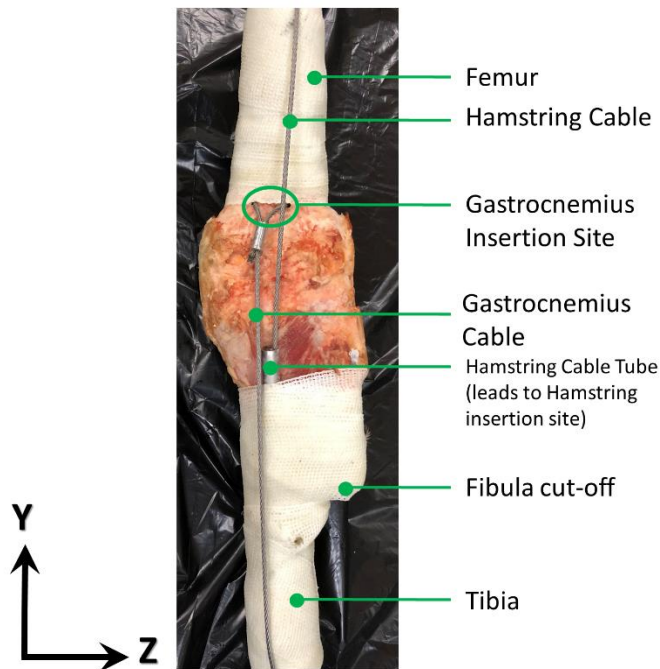


**Figure 4.10 Posterior frontal plane view of the cabled knee showing hamstring and gastrocnemius cable setup**

The knee joint was carefully wrapped in carpet and clear tape in order to ensure that it was not damaged during the foaming process. The muscle cables were placed in steel tubes. The quadriceps muscle tube was parallel to the diaphysis of the femur on the anterior side (Figure 4.11). The hamstring cable tube was parallel to the diaphysis of the femur on the posterior side (Figure 4.12). The gastrocnemius muscle tube was parallel to the diaphysis of the tibia on the posterior side (Figure 4.12).

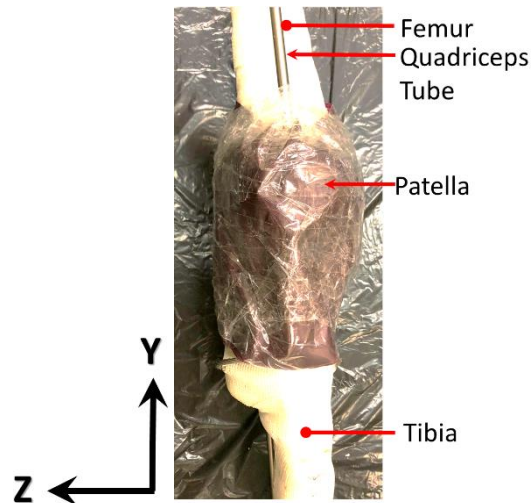


**Figure 4.11 Anterior frontal plane view of the knee wrapped in carpet and clear tape with quadriceps muscle tube visible**

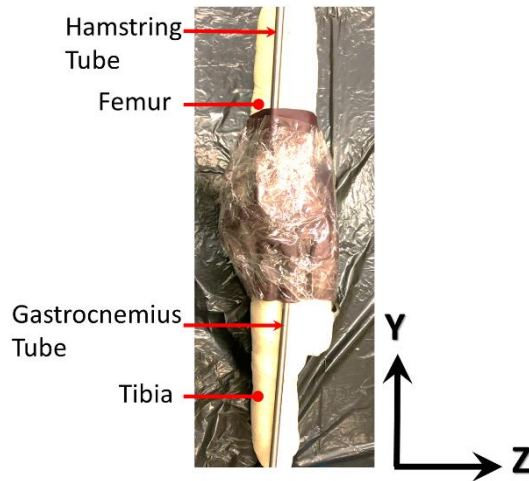


**Figure 4.12 Posterior frontal plane view of the knee wrapped in carpet and clear tape with hamstring and gastrocnemius muscle tubes visible**

Two rectangular holes were cut into the posterior side of the cast in order for the foam to be poured inside. The cast created before dissection was lined with duct tape (Figure 4.13), and the cabled knee was placed inside, using the locator rods to orient the knee. The cast was then taped together with duct tape, forming a tight seal. The ends where the plates are attached were sealed using foam scraps and duct tape. The leg setup for foaming can be seen in Figure 4.14.



**Figure 4.13** The inside of the cast lined with duct tape to prevent it from sticking to the foam mould



**Figure 4.14** The sealed cast oriented using the end plates ready for the foam to be poured

SunMate Liquid Foam (Dynamic Systems Inc., North Carolina) was mixed and poured into the cast. The foam was left for two to four hours to set before the cast was removed. The foam and carpet surrounding the knee joint were also carefully removed, exposing the knee joint, as seen in Figure 4.15.



**Figure 4.15** Medial sagittal plane view of a leg covered in foam with the foam and carpet cut away from the knee joint

## 4.4 Moment Arm Measurement

Moment arms were measured to adjust the muscle force profiles so that the knee moment developed on the cadaver knee would be equal to the knee moment which developed during the actual jump. The tendon excursion method was used, in which moment arms are defined as the slope of the knee flexion angle vs. muscle elongation (An 1984). Knee flexion angle was recorded using a digital goniometer, while muscle force elongation was measured using a linear variable differential transformer (LVDT). The goniometer was taped to the tibia and the femur. The LVDT was attached to a custom-built fixture, which was attached to a sliding shelf. The muscle force cable was rigidly fixed to the same sliding shelf when the muscle cable was the longest (in extension for the quad, and flexed for the gastrocnemius and hamstring). The leg was manually flexed and extended and the change in flexion angle was recorded along with the change in length. A diagram depicting the moment arm measurement setup and output can be seen in Figure 4.16, while the flexion extension procedure is shown in Figure 4.17. Flexion angle vs. length was plotted and an average slope was determined: this was considered to be the moment arm. Each cadaver has three recorded moment arms: one for each muscle cable.

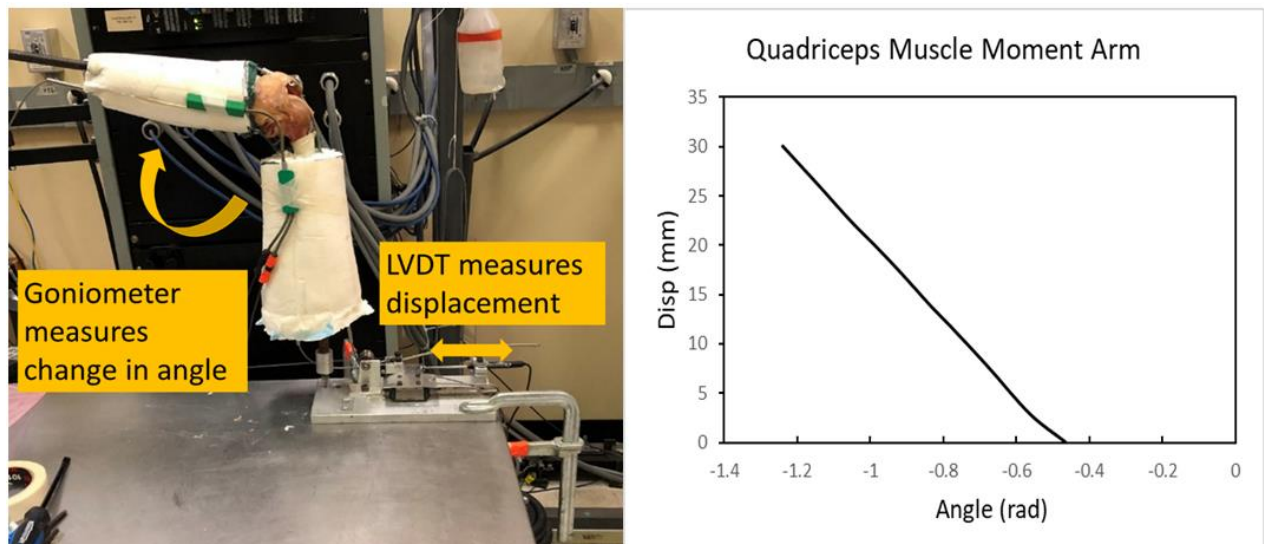


**Figure 4.16 Left: the moment arm measurement setup. Right: Displacement vs. Angle Plot used to calculate moment arm**



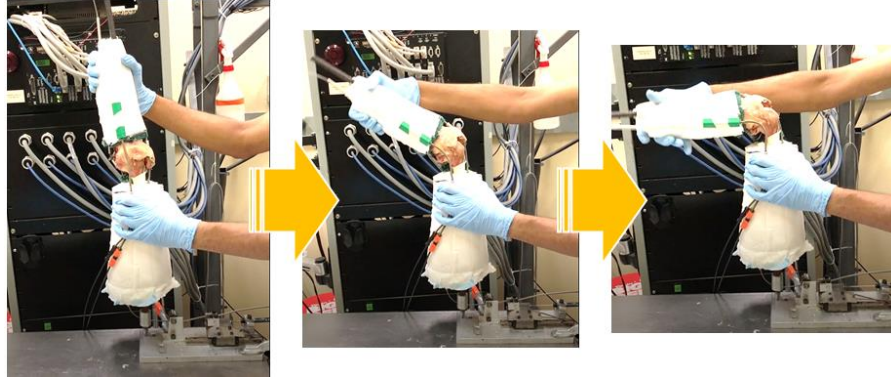


**Figure 4.17 Flexion extension procedure during which displacement and knee angle are measured**

## 4.5 Sensor Placement

A differential variable reluctance transducer (DVRT) was used to measure change in length on both the ACL and the meniscus. A DVRT consists of two pins that slide relative to one another causing a change in voltage. This change in voltage can be converted to a distance. This distance is then used to calculate engineering strain using the following formulas:

$$ACL\ Strain_i = \frac{L_i - L_o}{L_o}$$

where

$$L_i = 5mm + (DVRT\ Voltage - Voltage\ at\ 5mm) \times \left(\frac{mm}{V}\right)$$

$$L_o = 5mm + (DVRT\ Voltage\ at\ 100ms - Voltage\ at\ 5mm) \times \left(\frac{mm}{V}\right)$$

The formulas were adapted from the study of Bakker, 2014. A 50 Hz Butterworth filter was used to filter the strain data (Bakker, 2014).

Prior to DVRT placement, a notchplasty was performed on the lateral femoral condyle, which means that the femoral condyle was grinded down in order to create space for the ACL DVRT, to prevent impingement during knee movement. Care was taken in order not to damage the insertion site of the ACL and the PCL during the notchplasty.

The DVRT was positioned along the axial fibres of the ACL. It was placed on the anteromedial (AM) bundle of the ACL as shown in Figure 4.18. It was confirmed that the output voltage increased during extension and decreased during flexion, since the AM bundle is in tension when the knee joint is extended. The DVRT was then sutured to the ACL.



**Figure 4.18 ACL DVRT (circled) and notchplasty (N)**

#### **4.6 Placing the Knee on the Simulator**

The custom-built hip and ankle fixtures (Figure 4.19) were attached to the hip and ankle. The fixtures allowed the specimen to be mounted on the simulator.

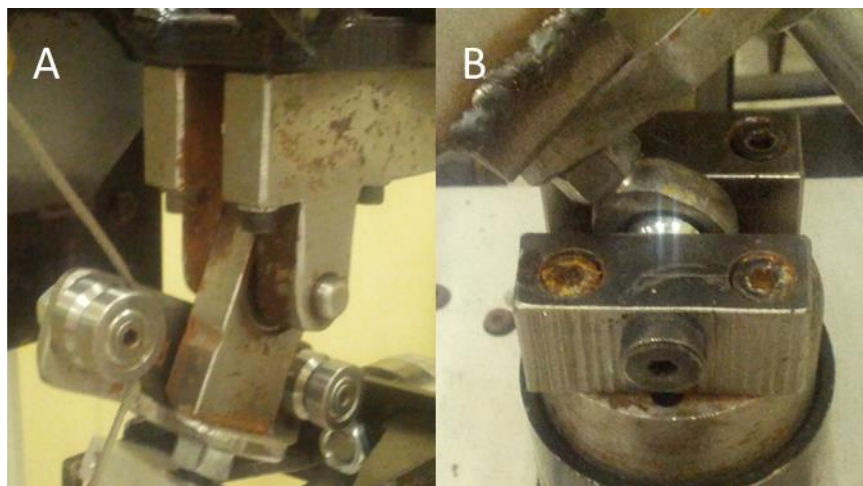


**Figure 4.19 Hip attachment (A) and ankle attachment (B), adapted from Bakker, 2014.**

The muscle cables were also attached to the simulator using screws, so the actuators can apply tension to them. This attachment can be seen in Figure 4.20.

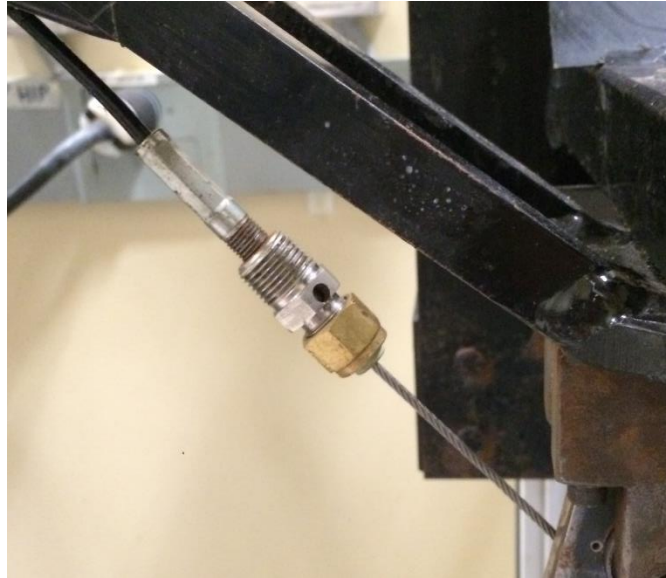


**Figure 4.20 Connectors attaching cables to the simulator**

The hip actuator attached to the hip fixture, 0.6 cm below the center of rotation of the hip.

The Q-angle, the angle which the femur makes with the tibia in the frontal plane, was also adjusted, so that the tibia remained in the sagittal plane during manual flexion extension with the hip held in place.

Finally, when the knee was in the start position for the trial, the ankle was placed in the ankle holder and a pin is inserted to keep it in place. The muscle cables were tightened before each trial. The foamed knee on the simulator can be seen in Figure 4.21.

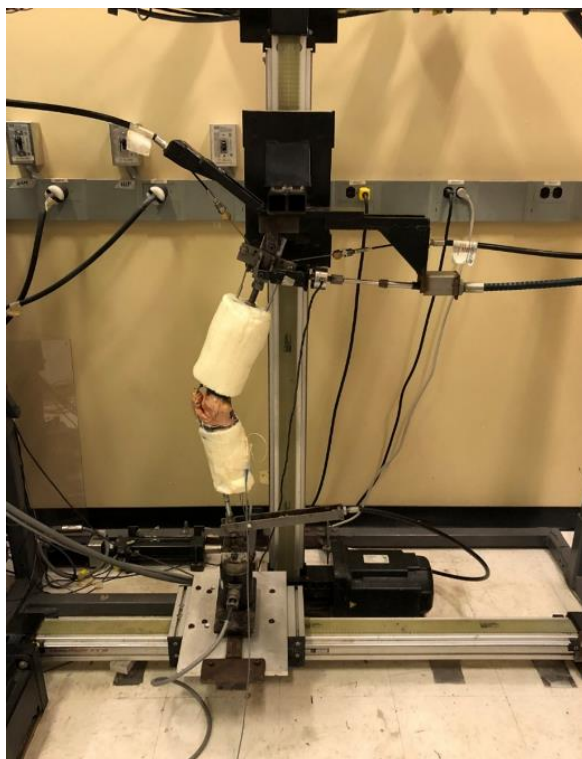


**Figure 4.21 The foamed knee on the dynamic knee simulator**

#### **4.7 Jump Landing Testing Procedure**

The jump landing trials consisted of two separate jump landing profiles from two different participants (Table 4.2), both tested at half muscle force, and full muscle force, unbraced and braced (

Table 4.3). Detailed graphs of all muscle force *vs.* time and velocity *vs.* time inputs for the full muscle force trials for both participants is show in Figure 4.22. Each trial was repeated once. A simple flexion extension was run initially to check that the sensor was placed correctly. The unbraced half muscle force jumps were then tested. After half muscle force jumps, the brace was placed on the knee carefully, ensuring that the sensors were not coming into contact with the brace. The braced half jumps were tested next, followed by braced full jumps. The brace was then carefully removed from knee. A flexion extension trial was run to ensure that the sensors were still in place. Finally, the full unbraced jumps were tested. Due to logistics associated with putting the brace on and taking it off, and to ensure that the brace was placed the same way for all braced trials, this test matrix was not randomized. Trials were run to completion or until the knee

became damaged. Damage was more likely during full force trials; therefore, full force trials were always run last.

**Table 4.2 Participant Information from Bakker, 2014**

Participant	Sex	Body Mass (kg)
1	F	57.5
2	F	67.5

**Table 4.3 Test Matrix for Experiments**

Participant # 1	Half Muscle Force	No Brace
		With Brace
	Full Muscle Force	No Brace
		With Brace
Participant # 2	Half Muscle Force	No Brace
		With Brace
	Full Muscle Force	No Brace
		With Brace

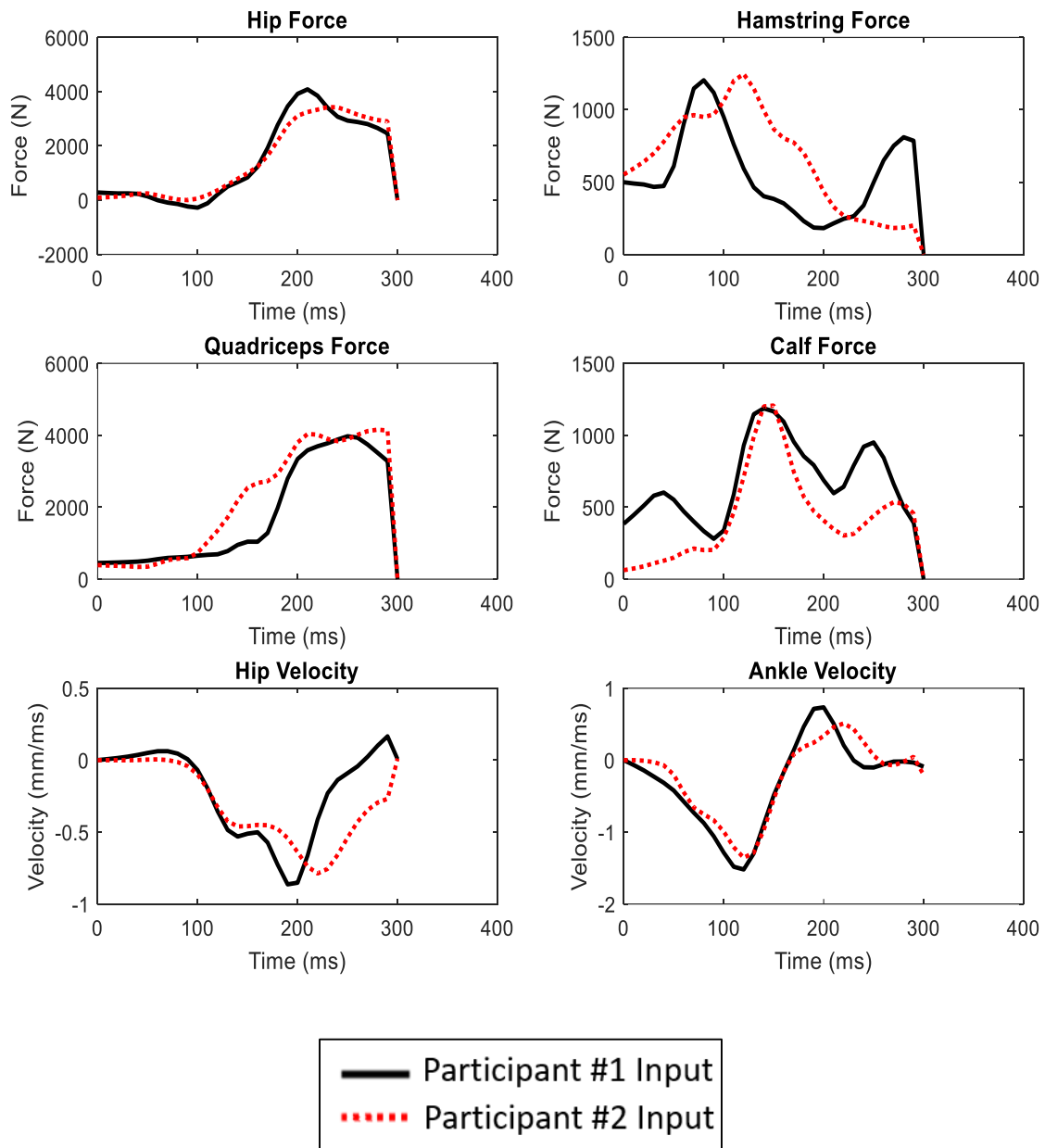


**Figure 4.22 Muscle force vs. time and velocity vs. time inputs for participant #1 and participant #2 full muscle force jump landing**

## Chapter 5 Experimental Results

There were three cadaver knee specimens tested in this study. The moment arms for all cadaver specimens were calculated, and the results are displayed in Table 5.1.

**Table 5.1 Experimental Moment Arm Calculations (in mm)**

<b>Knee</b>	<b>1</b>	<b>2</b>	<b>3</b>
<b>Quadriceps</b>	40.0	38.0	33.0
<b>Hamstring</b>	28.1	31.0	22.8
<b>Gastrocnemius</b>	18.0	16.6	15.4

### 5.1 Knee Failures

During the experiments, some knees broke during full jump landing trials. Table 5.2 summarizes which trials were successfully tested on each knee specimen.

**Table 5.2 Successful Trials on each Knee Specimen**

Loading Condition	Knee 1	Knee 2	Knee 3
Participant #1 Half Force, No Brace	✓	✓	✓
Participant #2 Half Force, No Brace	✓	✓	✓
Participant #1 Half Force, With Brace	✓	✓	✓
Participant #2 Half Force, With Brace	✓	✓	✓
Participant #1 Full Force, With Brace	✓	✓	✗
Participant #2 Full Force, With Brace	✓	✓	✗
Participant #1 Full Force, No Brace	✗	✓	✓
Participant #2 Full Force, No Brace	✗	✓	✗

Knee 1 broke during the first full muscle force trial of participant #2. The knee hyperextended mid trial, and bent backwards (Figure 5.1). This resulted in a torn ACL (Figure 5.2), preventing further testing. The break happened during a braced trial, and the knee brace cracked during the hyperextension as well (Figure 5.3).

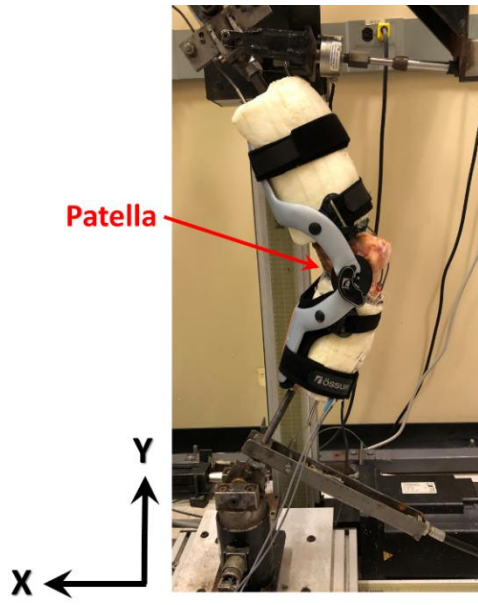


**Figure 5.1 Medial sagittal plane view of knee 1 in hyperextension after failure**



**Figure 5.2 Torn ACL in knee 1**





**Figure 5.3 Crack in the knee brace of knee 1**

Knee 2 did not break during testing, and made it through the full testing matrix.

Knee 3 broke during the first trial. The patella cracked in half (Figure 5.4). The solution was to create a patella mould from the cracked patella and to re cable the quadriceps muscle. The patella was used to create a negative mould in a block of clay (Figure 5.5). A tube and two reinforcing screws were placed in the mould (Figure 5.6). A resin was then poured into the negative mould to create a patella with the same shape as the cracked cadaver patella.

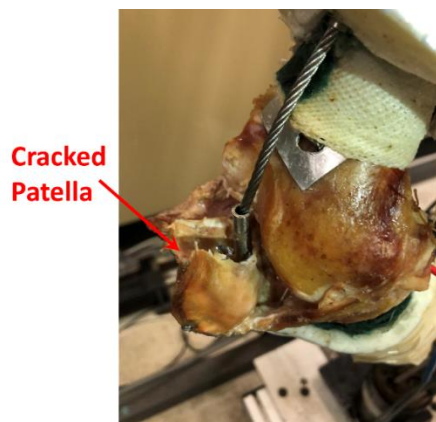


**Figure 5.4 Cracked patella in knee 3**



**Figure 5.5 Patella creating negative mould in block of clay**

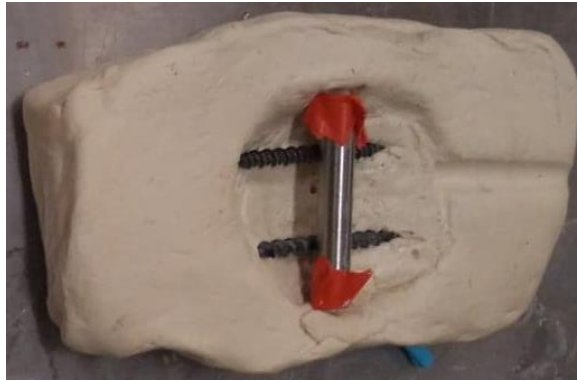


**Figure 5.6 Patellar tube and reinforcing screws placed inside negative mould**

Figure 5.7 shows knee 3 with the moulded patella. A crimp was placed above and below the moulded patella to keep it in place during testing. Knee 3 made it through almost all trials; however, the knee also hyperextended during the first full force trial of participant #2 (Figure 5.8). This resulted in a torn ACL, preventing further testing (Figure 5.9).



**Figure 5.7 Medial sagittal plane view of knee 3 on the DKS with new moulded patella**

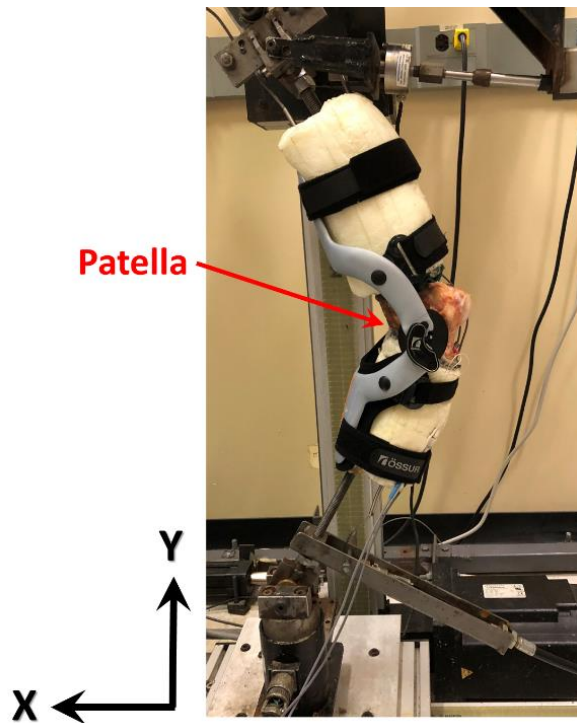


**Figure 5.8 Medial sagittal plane view of knee 3 in hyperextension after failure**

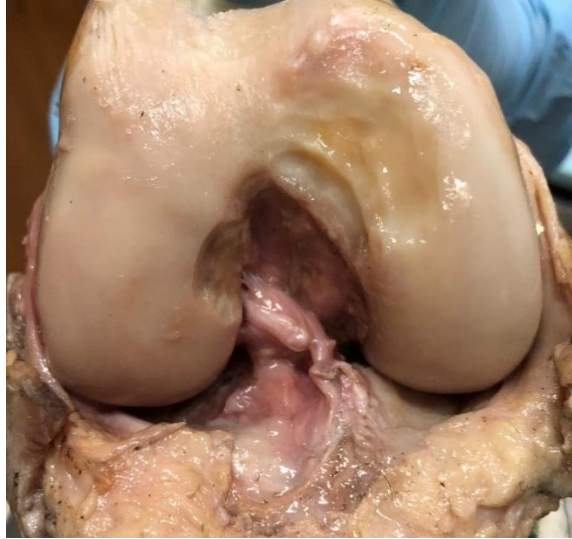


**Figure 5.9 Torn ACL in knee 3**

## **5.2 ACL Strain Results**

### **5.2.1 Comparison of Finite Element Model Strain with Experimental Strain**

Three cadaver knees were tested at the four loading conditions. The graphs used to verify that the DKS was applying the correct kinematic and kinetic boundary conditions are found in Appendix A. Figure 5.10 shows the experimental ACL strain vs. time curves for all four loading conditions.

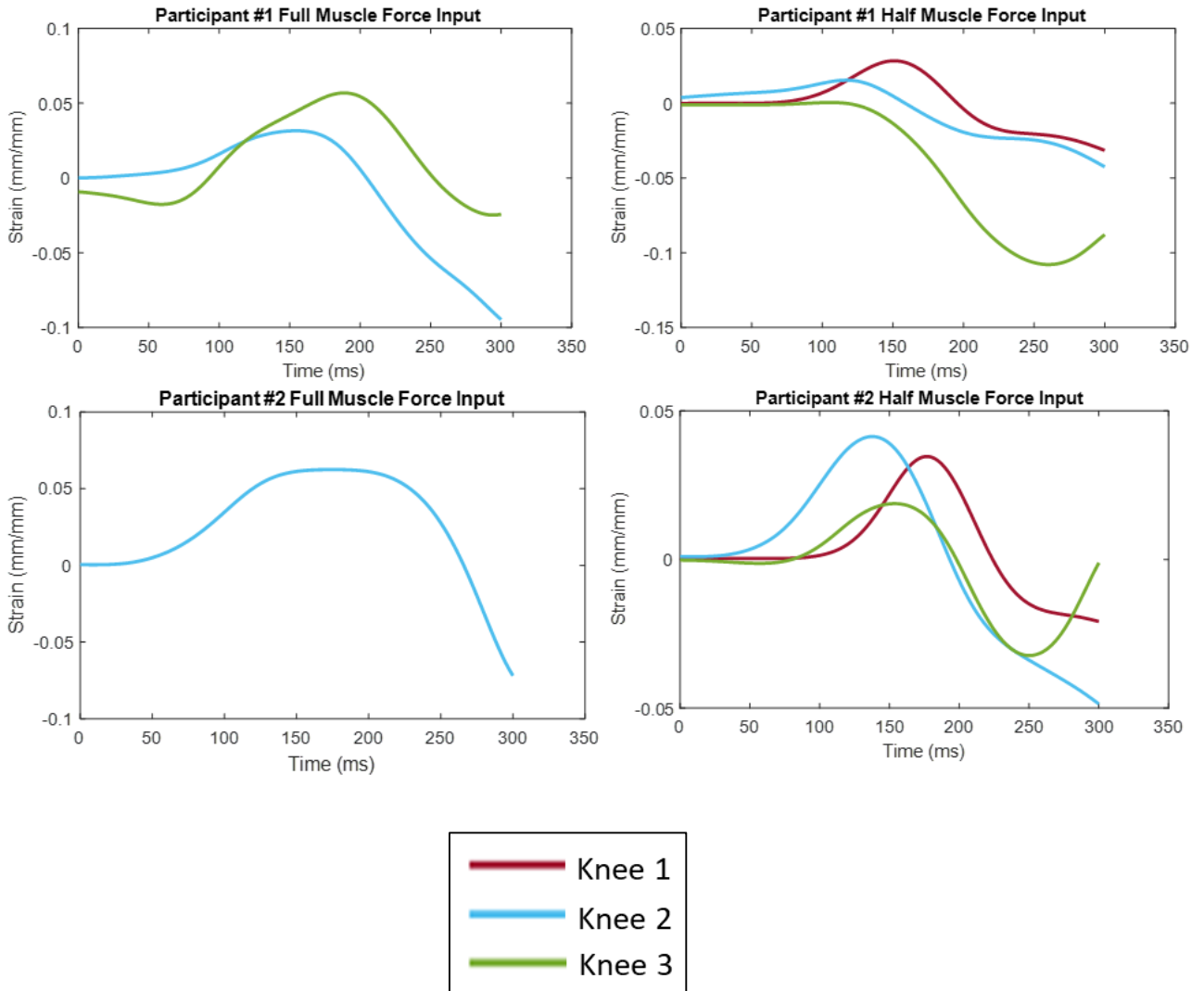


**Figure 5.10 Experimental relative ACL strain vs. time curves for all loading conditions**

The results are summarized in Table 5.3 as well. The main values of interest were the maximum ACL strain and the time at which the maximum strain occurs.

**Table 5.3 Summary of Experimental and Computational Maximum Relative ACL Strain Results**

		Knee 1		Knee2		Knee3	
		Max Strain	T <sub>max</sub> (ms)	Max Strain	T <sub>max</sub> (ms)	Max Strain	T <sub>max</sub> (ms)
<b>Participant #1</b>	<b>Full Force</b>	x	x	0.032	154	0.057	189
	<b>Half Force</b>	0.028	151	0.015	117	0.000	106
<b>Participant #2</b>	<b>Full Force</b>	x	x	0.062	175	x	x
	<b>Half Force</b>	0.035	177	0.041	138	0.019	154

Table 5.4 shows the means and standard deviations of the experimental maximum ACL strain values. It is worth noting that while this table summarizes the experimental results concisely, it is a summary of only three samples and the standard deviations are large. A mean was not calculated for the full force participant #2 jump as only one leg managed to successfully perform the jump on the simulator.

**Table 5.4 Means and Standard Deviations of Experimental Results**

<b>Input Condition</b>	<b>Mean ± Standard Deviation</b>
Participant #1 – Full Force	0.044 ± 0.018
Participant #2 – Full Force	Not Calculated
Participant #1 – Half Force	0.015 ± 0.014
Participant #2 – Half Force	0.032 ± 0.012

### 5.2.2 Comparison of Braced vs. Unbraced Conditions

The cadaver knees were tested in all four loading scenarios while they were unbraced and also while wearing a Össur CTi custom ligament knee brace (Össur, Reykjavik, Iceland). The results for all loading scenarios are presented in Figure 5.11.

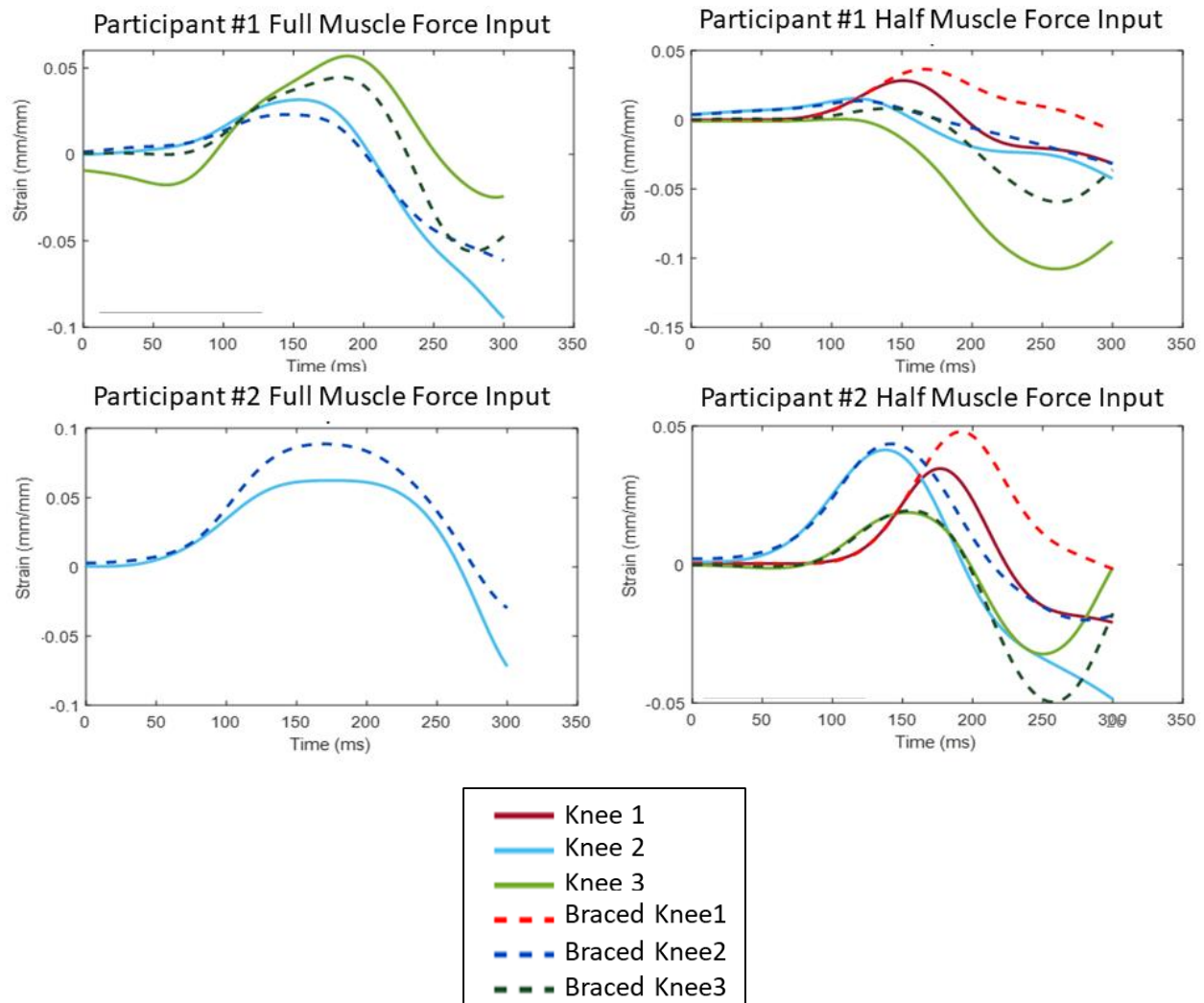


**Figure 5.11 Average relative ACL strain vs. time results for unbraced and braced conditions**

The results are summarized in Table 5.5, while the means and standard deviations of braced and unbraced conditions are summarized in Table 5.6 and Figure 5.12. There were not enough samples of the full muscle force participant #2 jump condition to calculate a mean. The small sample size also made other statistical comparison tests not feasible.

presents mean squared error between unbraced and braced curves for each cadaver knee. The error is very small (less than 0.0011 for all values) when compared with the peak strain values (between 0.00 and 0.09).

**Table 5.5 Summary of Maximum Relative ACL Strain Values for Unbraced and Braced Conditions**

			Knee 1		Knee 2		Knee 3	
			Max Strain	T <sub>max</sub> (ms)	Max Strain	T <sub>max</sub> (ms)	Max Strain	T <sub>max</sub> (ms)
<b>Participant # 1</b>	<b>Full Force</b>	<b>No Brace</b>	x	x	0.032	154	0.057	189
		<b>With Brace</b>	x	x	0.023	146	0.045	184
	<b>Half Force</b>	<b>No Brace</b>	0.028	151	0.015	117	0.000	106
		<b>With Brace</b>	0.036	166	0.014	119	0.008	141
<b>Participant # 2</b>	<b>Full Force</b>	<b>No Brace</b>	x	x	0.062	175	x	x
		<b>With Brace</b>	x	x	0.089	170	x	x
	<b>Half Force</b>	<b>No Brace</b>	0.035	177	0.041	138	0.019	154
		<b>With Brace</b>	0.048	192	0.044	142	0.019	156

**Table 5.6 Means and Standard Deviations of Braced and Unbraced Relative ACL Strain Results**

<b>Input Condition</b>	<b>Mean ± Standard Deviation</b>	<b>Mean ± Standard Deviation</b>
<b>Brace or No Brace?</b>	<b>No Brace</b>	<b>With Brace</b>
Participant #1 – Full Force	0.044 ± 0.018	0.034 ± 0.015
Participant #2 – Full Force	Not Calculated	Not Calculated
Participant #1 – Half Force	0.015 ± 0.014	0.019 ± 0.015
Participant #2 – Half Force	0.032 ± 0.012	0.037 ± 0.015



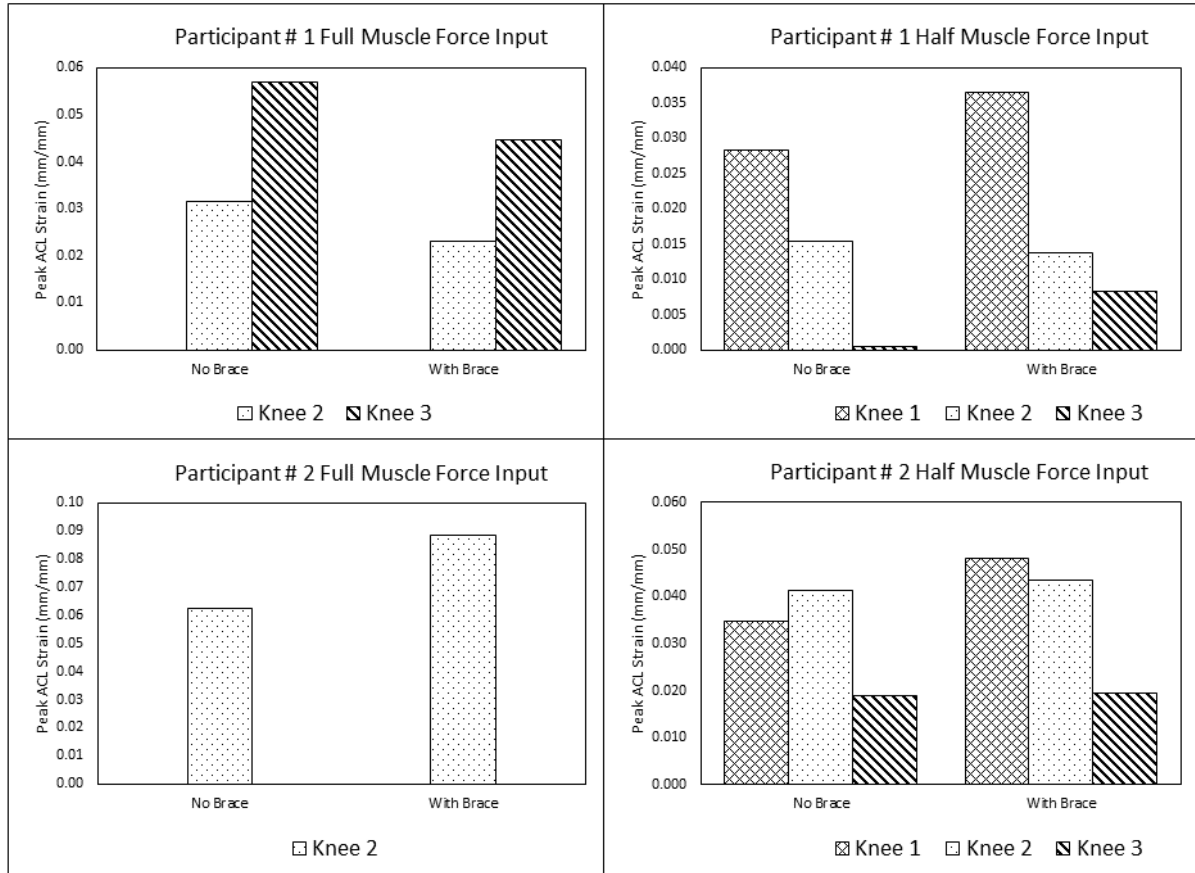


**Figure 5.12 Comparison of unbraced and braced mean peak relative ACL strains**

**Table 5.7 Mean Squared Error of Unbraced vs. Braced Jump Landing Comparison**

		<b>Knee 1</b>	<b>Knee 2</b>	<b>Knee 3</b>
<b>Participant # 1</b>	<b>Full Force</b>	x	0.0001	0.0004
	<b>Half Force</b>	0.0003	0.0000	0.0011
<b>Participant # 2</b>	<b>Full Force</b>	x	0.0003	x
	<b>Half Force</b>	0.0002	0.0002	0.0001

## Chapter 6 Finite Element Model Setup

A finite element model was developed in order to predict relative ACL strain using the same boundary conditions as the dynamic knee simulator. The objective was to take an existing full body finite element model, the Global Human Body Models Consortium 50<sup>th</sup> percentile male v4-4 (GHBMC) and to extract the leg.

The Global Human Body Model Consortium (GHBMC) 50th percentile male model is a detailed full human body model validated for impact testing (Schwartz et al., 2015). Overview details about the finite element model can be found in Table 6.1.

**Table 6.1 Full 50<sup>th</sup> Percentile Male GHBMC Model Details**

<b>Nodes</b>	<b>Elements</b>	<b>Parts</b>	<b>Materials</b>
1259309	2190824	995	662

In the current study, the right leg of the GHBMC model was extracted and evaluated in detail to see if it could be used to reasonably predict ACL strain. The finite element program LS-DYNA was used. Overview details about the right leg are in Table 6.2. The ligaments in the GHBMC leg were all made up of 3D elements, and this chapter will discuss how the material models were modified in order to improve the leg model for the purpose of single leg jump landing.

**Table 6.2 Extracted Right Leg of GHBMC Model Details**

<b>Nodes</b>	<b>Elements</b>	<b>Parts</b>	<b>Materials</b>
55049	52075	27	14

The boundary conditions from the simulator were applied to the extracted leg using the finite element software LS-DYNA (LSTC, Livermore, CA) and the relative strain in the ACL was compared to the experimental relative ACL strain. Figure 6.1 shows the full GHBMC model, the extracted right leg, and the ACL.

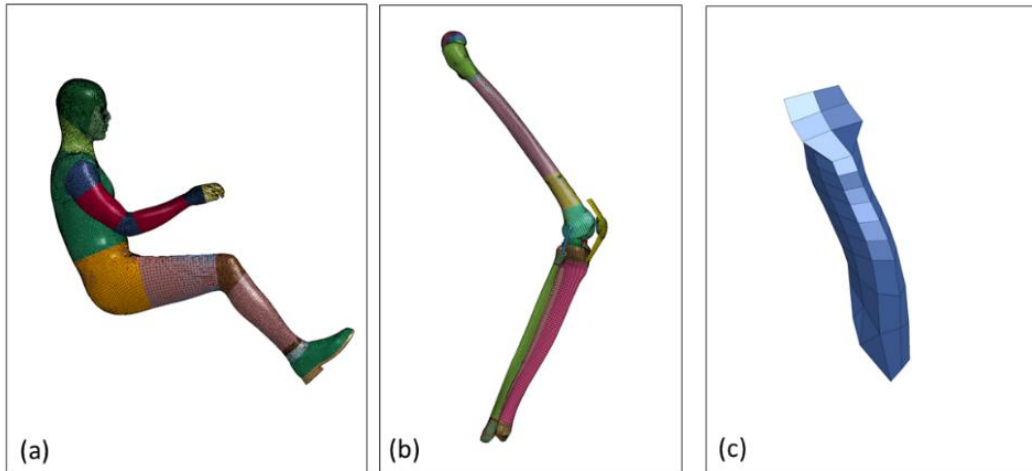


**Figure 6.1 (a) Full body model (b) Extracted right leg (c) Extracted ACL**

It should be noted that the finite element model replicates the *in-vitro* jump landing experiment performed using the DKS. More work is needed to validate the model as an accurate representation of an *in-vivo* jump landing.

### **6.1 GHBMC Modifications for Jump Landing Study**

Modifications were made to the right leg of the GHBMC to improve the biofidelic response and computational stability of the model. The geometry and mesh of the original model were not changed; however, a mesh convergence study was performed on the ACL to confirm the mesh size gave an appropriate tensile response, and some materials were modified. A summary of all modifications can be found in Table 6.3.

**Table 6.3 Modifications applied to right leg of GHBMC Model**

<b>Part affected</b>	<b>Change</b>	<b>Reason for change</b>
<b>Ankle</b>	A new part was created from the geometry of the distal tibia. The material was defined as a linear isotropic material with E = 200 GPa.	The part was created to increase numerical stability when boundary conditions are applied to few nodes on the ankle. The material was chosen to be a very stiff rigid material.
<b>Hip</b>	A new part was created from the geometry of the proximal femur. The material was defined as a linear isotropic material with E = 200 GPa.	The part was created to increase numerical stability when boundary conditions are applied to few nodes on the hip. The material was chosen to be a very stiff rigid material.
<b>Patellar/Quadriceps Tendon</b>	The material was changed to a linear isotropic material with E = 600 MPa (Butler et al., 1986)	The material was defined as an elasto-plastic material with a stress curve defined; however this caused the patella to track too high up on the femur during extension.
<b>Meniscus</b>	The material was changed to a linear isotropic material with E= 59 MPa and Poisson's Ratio =0.49 (LeRoux and Setton, 2002)	The meniscus was defined as an elasto-plastic material; however it showed 0.00 strain during the jump landing and it was decided to use a material model from literature.
<b>ACL</b>	The material was changed to an isotropic hyperelastic material with a stress-strain curve input from Chandrashekar, 2005.	The original material did not provide a sufficiently realistic response. This is described in more detail in the section "ACL Material"
<b>MCL, LCL, PCL</b>	The material of all elements was modelled to be the same as the ACL	Butler et al., 1986 determined that the materials of all the ligaments were similar.

## 6.2 Background Studies

Before the leg could be analyzed in a jump landing, it was important to evaluate how the model predicted metrics associated with ACL injury, and appropriate changes were made in order for the leg model to have a realistic response with regard to non contact ACL injury.

### 6.2.1 Tibial Slope

Tibial slope is defined as “the angle between a line perpendicular to the mid-diaphysis of the tibia and the posterior inclination of the tibial plateau” (Giffin et al., 2004). The tibial plateau affects the distribution of compressive forces acting on the tibiofemoral joint, which affects the amount of anterior tibial translation that occurs in the knee, a key contributor in ACL strain. A higher tibial slope has been shown to be associated with a higher rate of ACL injury (Hashemi et al., 2010). Small increases in tibial slope appear not to affect the anterior tibial translation or forces in ligaments significantly (Giffin et al., 2004). A high medial tibial slope and lateral tibial slope can lead to increased risk of injury, while the coronal slope does not increase risk of injury (Hashemi et al., 2010). Figure 6.2 shows medial, lateral and coronal tibial slopes of the GHBMC.

The tibial slope angles from the existing GHBMC model were plotted against experimentally measured population values from Hashemi et al., 2008. Figure 6.2 shows medial, lateral and coronal tibial slopes of the GHBMC, and Figure 6.3 shows the tibial slope angles of the GHBMC plotted with experimental values from Hashemi et al., 2008. The tibial slopes of the GHBMC were found to be approximately one degree higher than one standard deviation from the mean of the general male population, which may lead to higher ACL strain than anticipated.

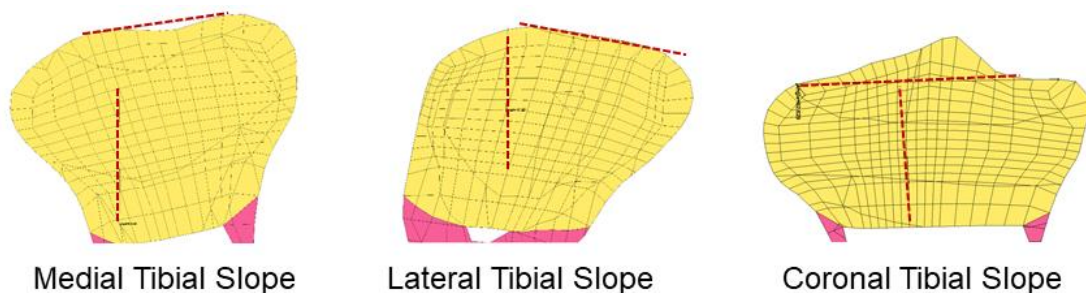


**Figure 6.2 Medial, lateral, and coronal tibial slopes of the GHBMC right tibia**

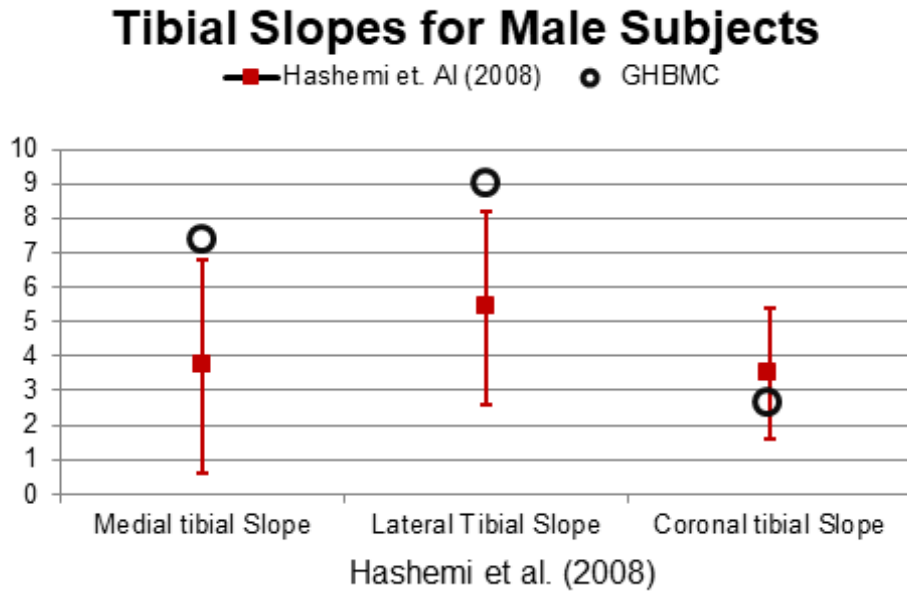


**Figure 6.3 Tibial slopes for male subjects compared to GHBMC tibial slope**

### 6.2.2 ACL Material

The material model of the ACL in the original GHBMC model is a viscoelastic soft tissue model developed by Weiss et al., 1996. The input parameters of the original GHBMC ACL material are based on MCL material testing done by Untaroiu et al., 2005. Since the original GHBMC ACL material model is based on MCL material properties, an isotropic hyperelastic material model developed from ACL material properties found in literature was also developed. The new material model was created using experimental stress vs. strain curves from Chandrashekar, 2005. Ligaments do not provide any structural support in compression, thus the modulus of elasticity in compression was set to zero (Figure 6.4).

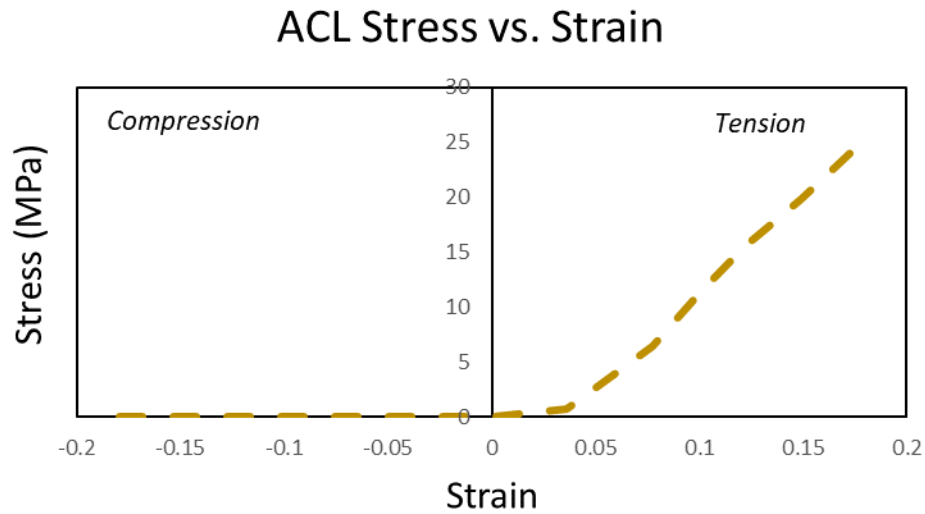


**Figure 6.4 ACL Stress vs. Strain Curves from Chandrashekar, 2005**

The ACL was extracted, and a uniaxial tension test at 200 mm/min was applied to the ACL. The direction of loading was along the longitudinal axis of the ACL (Figure 6.5). The ACL was tested with its original viscoelastic material properties, and then compared to an ACL with updated hyperelastic material properties from Chandrashekar, 2005. Both results were compared to the experimental results from Woo et al., 1991.

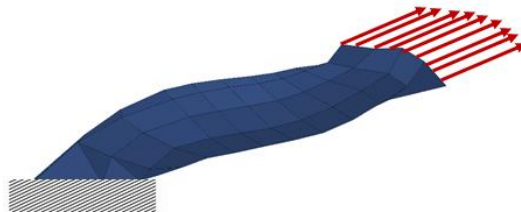


**Figure 6.5 Boundary conditions applied to ACL to evaluate realistic force-elongation response**

The results of the tensile test are shown in Figure 6.6. The response of the updated material is more comparable to the experiments than the original material; therefore, the updated hyperelastic material model based on the curves from Chandrashekar, 2005 was used for the single leg jump landing study.

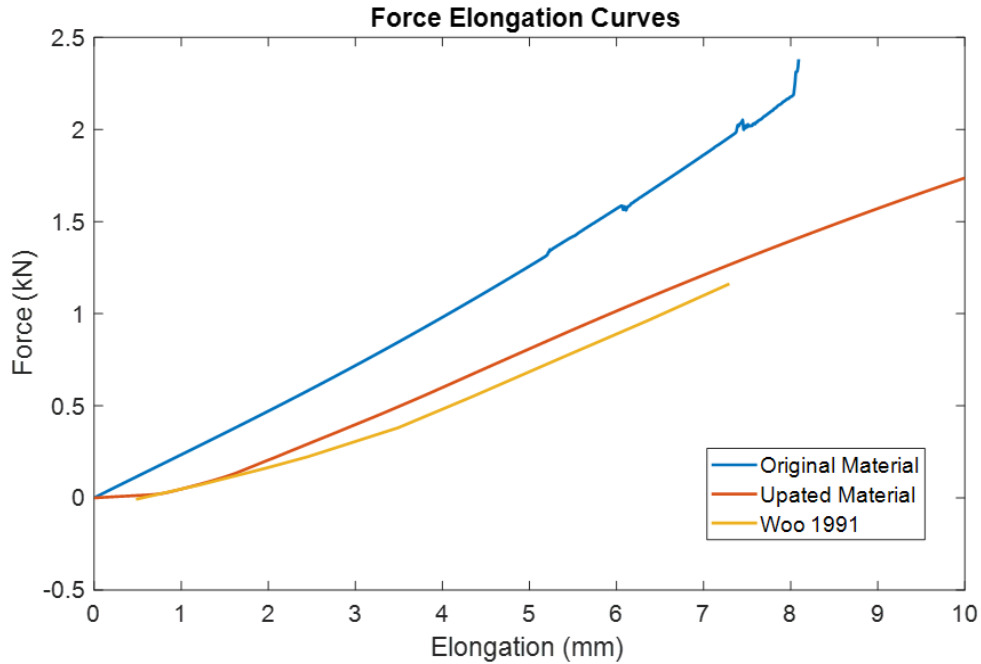


**Figure 6.6 Force vs. elongation curves of original material compared to updated material and literature**

### 6.2.3 ACL Mesh Convergence

Once the material had been modified, a mesh convergence study on the ACL was performed in order to determine whether a finer mesh would impact tensile response of the ACL. The original GHBMC ACL mesh was refined three times to create four different cases (Figure 6.7). The cases were all tested in uniaxial tension along the longitudinal axis of the ACL.

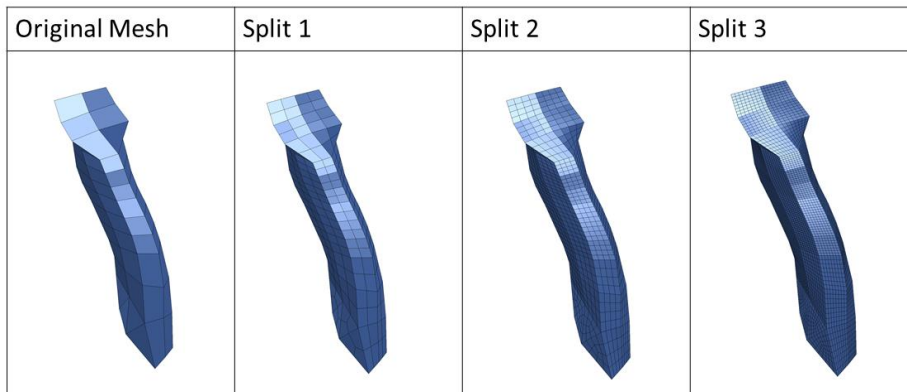


**Figure 6.7 ACL mesh sizes used in mesh convergence study**



The results of each mesh size are illustrated in Figure 6.8, and the run times for each mesh size are listed in Table 6.4. Splitting the mesh resulted in a similar force vs. displacement response; however, it caused a significant increase in run time. Thus the ACL mesh size was not changed.

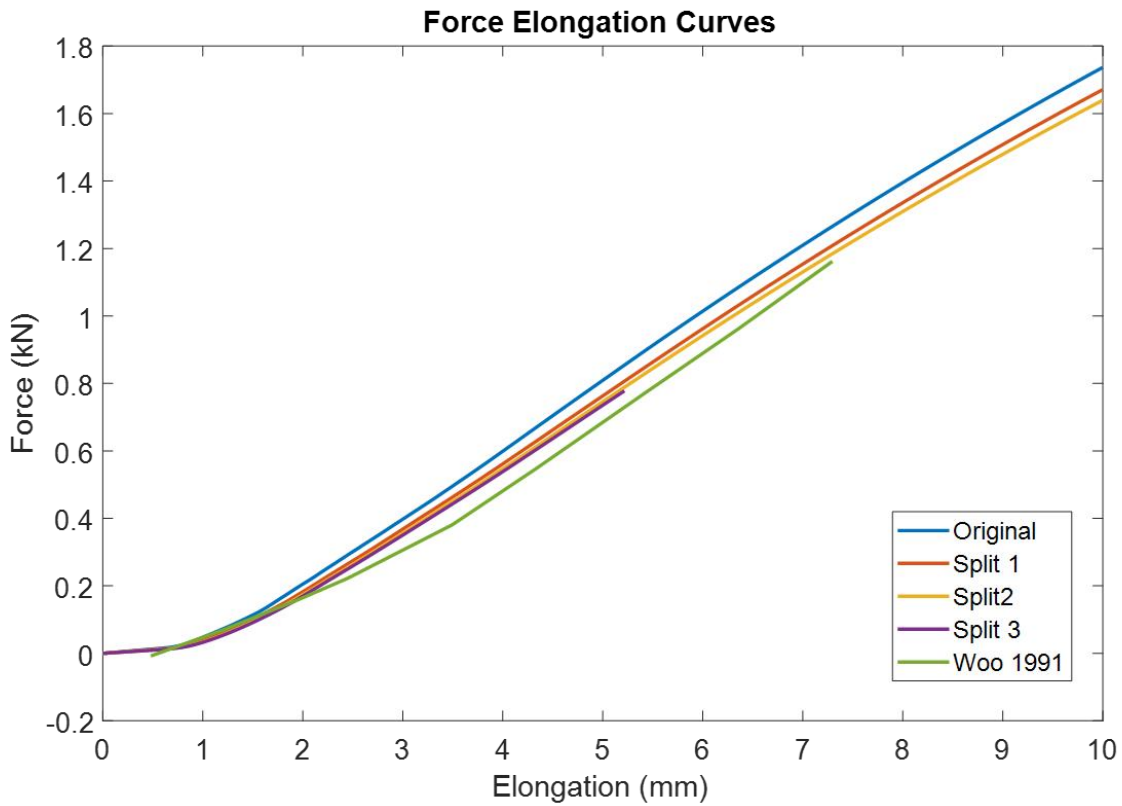


**Figure 6.8 Force vs. elongation curves for ACLs of varying mesh size**

**Table 6.4 Run Times for Different Mesh Sizes**

Original Mesh	1:49
Split 1	3:41
Split 2	11:41
Split 3	114:52 +

## 6.2.4 ACL Element Formulation

The element formulation, or how the software solves the system of equations associated with each element, of the ACL was also evaluated. The original GHBMC ACL uses constant stress elements, known as under-integrated or simply integrated elements. Fully integrated elements, which do not have constant stress, could potentially give a more accurate tensile response; however, using fully integrated elements would increase the run time of the model.

The ACL made up of the original simply integrated was tested in uniaxial tension along the long axis of the ACL, and compared to an ACL made up of fully-integrated elements.

The results of the comparison between the simply integrated ACL and the fully integrated ACL is shown in Figure 6.9. The simplified integration scheme gave a very similar result to the full integration; therefore, the simple integration scheme was not changed for the jump landing simulation.

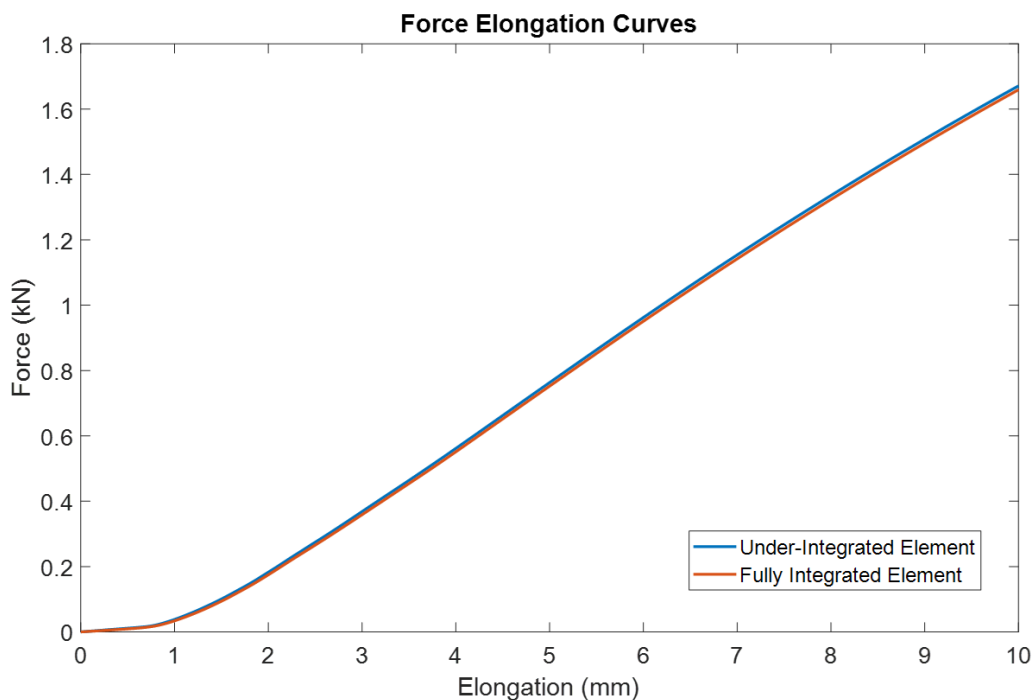


**Figure 6.9 Force vs. elongation curves for different element formulations**

### 6.2.5 ACL Pre Strain

At the beginning of the jump landing simulation, the GHBMC leg was in an extended position. According to the findings of Ellison and Berg, 1985, the ACL can be assumed to be in a zero stress state when the knee flexion angle was 40 degrees, which means that at full extension the ACL would have some strain in it. There was a pre strain applied to the ACL at the starting position of each jump which accounted for the deformation of the ACL from its neutral position, when the knee is flexed at 40 degrees, to the current position of the ACL, when the knee is fully extended.

## 6.3 Modelling Considerations

### 6.3.1 Coordinate System

The origin of the Dynamic Knee Simulator (DKS) coordinate system is defined as the point at which the hip and ankle are aligned. The DKS coordinate system was implemented as a fixed coordinate system in the GHBMC model. The x and y axes define the sagittal plane. Figure 6.10 depicts the axis system on both the DKS and in the FE model.

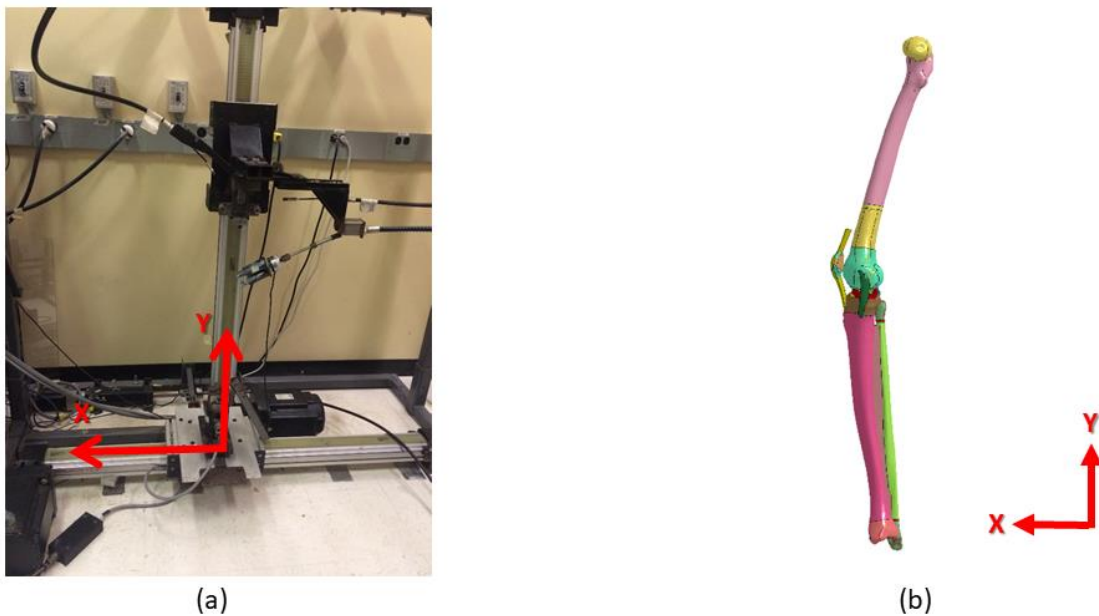


**Figure 6.10 (a) Simulator coordinate system (b) Leg model coordinate system**

### 6.3.2 Kinematics Boundary Conditions

The kinematics are applied only in the sagittal plane. The hip has a motion applied in the y-direction, while the ankle has a force applied in the x direction. In a live jumping human, both the hip and ankle move in x and y; however, for the purpose of simplifying the DKS, the distance between the hip and the ankle is modelled.

The movements along the sagittal plane are input into the simulator as velocities; therefore, they are also input into the finite element model as velocities along the corresponding axes. A node on the hip is defined as the hip centre of rotation, and the boundary condition is applied to this node. Similarly, a node on the ankle is defined as the ankle centre of rotation to which all ankle boundary conditions are applied. The hip and ankle nodes are surrounded by end caps composed of linear elastic material with a high modulus of elasticity (200 GPa) in order to prevent any numerical instability caused by applying boundary conditions to a single node (Figure 6.11). The hip is free to translate up and down along the x-axis, and is constrained along the y and z directions. It is also free to rotate about the z-axis, but rotation is constrained about the x and the y axes. The ankle is free to translate along the y direction and the z direction, in order to allow for medial-lateral movement of the ankle. It is constrained in the x direction. The ankle is also free to rotate about the z-axis only, being constrained about the x and y.



**Figure 6.11 End caps for application of hip and ankle boundary conditions - anterior frontal plane view**

### **6.3.3 Force Boundary Conditions**

There are four main forces acting on the knee joint:

1. Hip Moment: The hip is applied as a linear force acting on six nodes, which are all a distance of 0.06 m away from the centre of rotation of the hip, measured perpendicular to the force applied (Figure 6.12).
2. Hamstring: The hamstring is applied as a force acting on seven nodes. The nodes are located on the posterior proximal tibia and the force is applied along the diaphysis of the femur (Figure 6.13).
3. Quadriceps: The quadriceps muscle is applied as a force to the seven nodes on the top of the patellar tendon. The patella acts as a hinge redirecting the force which is transferred from the end of the patellar tendon, across the patella, and inserts on the leg at the tibial tuberosity. In order to support the transfer of forces from the patellar tendon to the tibia, the material properties of the patellar tendon have also been changed to a stiff linear elastic material, which was described in more detail

in Section 6.1 about changes to the original GHBM. The applied quadriceps force acts parallel to the diaphysis of the femur (Figure 6.13).

4. Gastrocnemius: The gastrocnemius muscle is applied to seven nodes on the posterior distal femur. The applied force acts along the diaphysis of the tibia (Figure 6.13)

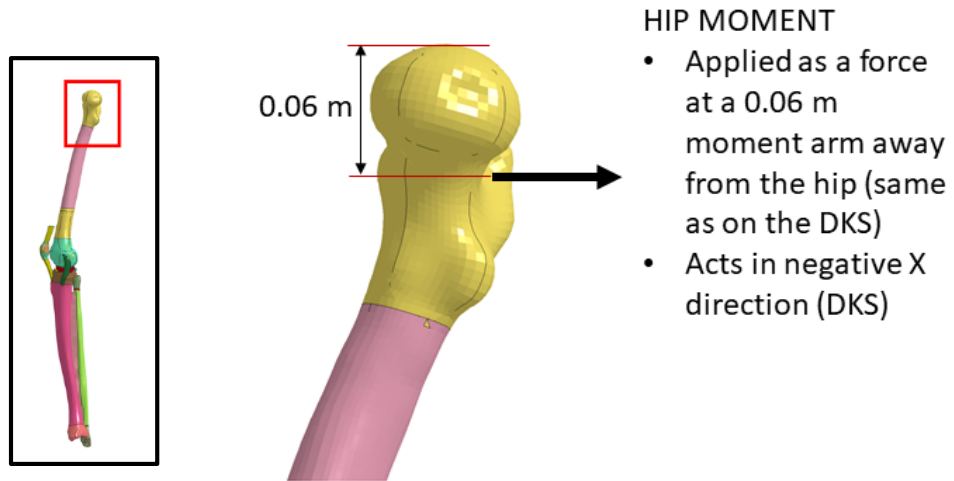


**Figure 6.12 Application of hip moment-medial sagittal plane view**

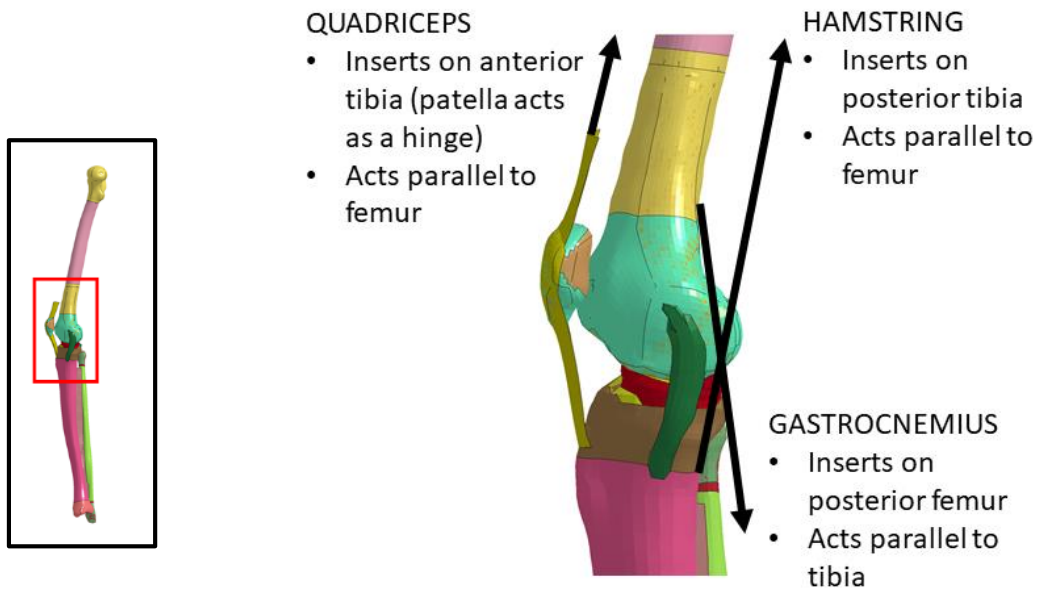


**Figure 6.13 Muscle forces acting on knee joint-medial sagittal plane view**

### 6.3.4 Limb Lengths

The limb lengths of the participants who performed the motion capture study were 381 mm for the tibia and 481 mm for the femur. The GHBMC tibia was within 2% of the desired length so it was left as is. The femur was scaled down to match the desired length of 481 mm (Figure 6.14).



**Figure 6.14 Scaling of the femur**

### 6.3.5 Moment Arms

The muscle moment arms of the GHBMC leg were determined by simulating the experimental moment arm measurement technique. In the case of the quadriceps and hamstring muscles, the femur was held in place using a rigid boundary condition, while the quadriceps or hamstring muscle was pulled with an arbitrary force. The displacement of the nodes comprising the insertion site was then plotted against the knee angle (Figure 6.15). The slope of the node displacement *vs.* the knee angle was taken to be the muscle moment arm. For the gastrocnemius, a similar method was used, except the tibia was held in place. The muscle moment arms were then input into the MATLAB code written by Bakker, 2014 in order to produce muscle force *vs.* time profiles which would create the appropriate external knee moment in the sagittal plane.

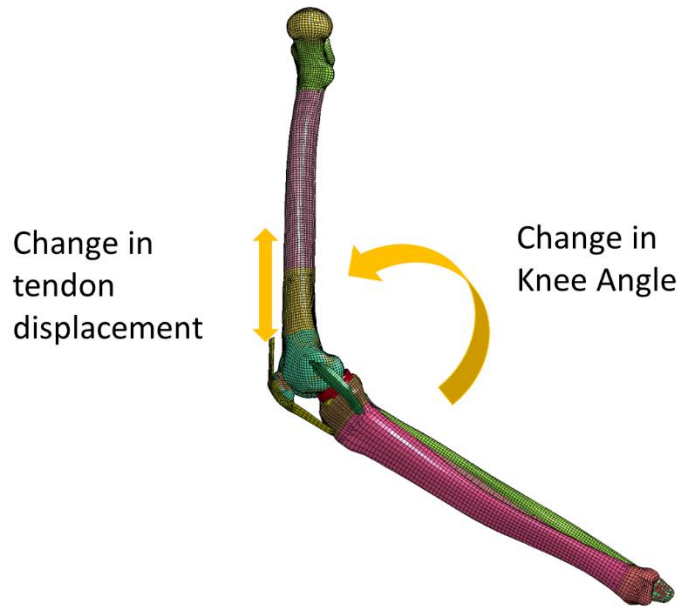


**Figure 6.15 Moment arm measurement simulation**

#### **6.4 Initialization**

Before the jump landing boundary conditions could be applied, the leg had to be taken to the starting position, similarly to how it does on the dynamic knee simulator. Time-displacement boundary conditions were applied to the hip and the ankle along with DKS boundaries, which limit the hip and ankle movement (Figure 6.16). The time-displacement curves were calculated based on the GHBMC positions in the DKS coordinate system and how far they were from the desired starting positions as indicated by the DKS inputs.

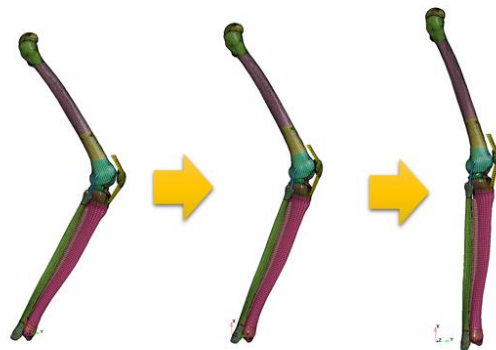


**Figure 6.16 Flowchart of initialization for participant #1**



## 6.5 Jump Landing

The final jump simulation incorporated both the muscle initialization, which is increasing the muscle forces gradually from zero to the starting muscle force value then keeping it steady for a brief period of time in order for the leg to stabilize, and the actual jump landing motion.

For all muscle groups (including the hip), the muscle forces initially ramped up from zero to the starting muscle force and were then held at the starting value for 50 ms in order to stabilize before the jump landing muscle force profiles are applied. It is important to note that the initial length for strain calculations was taken after the muscle forces are initialized.

Once the muscle forces were at a steady state, the jump landing muscle force profile was applied to the knee. Six boundary conditions were applied: hip force, hamstring force, quadriceps force, calf force, and x velocity applied at the ankle, and y velocity applied at the hip.

## 6.6 ACL Strain Measurement

A length between two nodes on the ACL was measured throughout the jump landing timeframe.

Engineering strain was calculated using the formula:  $\epsilon = \frac{l_i - l_0}{l_0}$ , where  $l_i$  is the length at any given time step and  $l_0$  is the initial length of the ACL after the muscle forces are initialized. The strain measured is relative ACL strain, so that results could be compared to the relative strain results from DKS. The two nodes replicated the DVRT placement on the cadaver ACL, as seen in Figure 6.17.

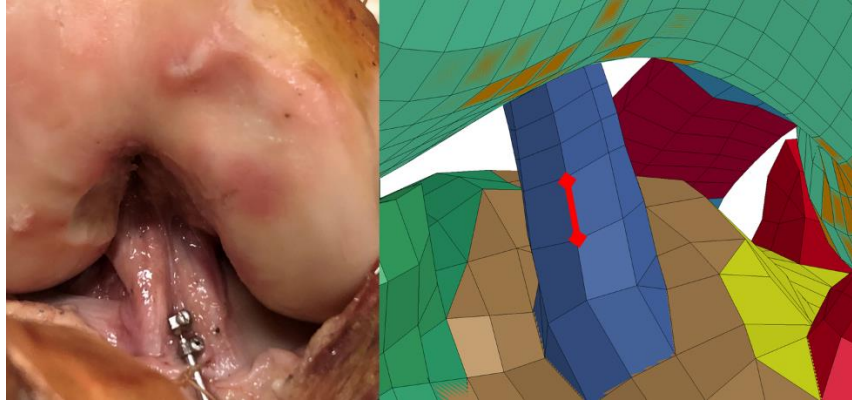


**Figure 6.17 ACL DVRT location (left) and ACL strain measurement location in finite element model (right)**

### 6.7 Test Matrix for FE Model

The FE model was tested using the inputs of two separate jump landing profiles from two different participants, both tested at half muscle force, and full muscle force (Table 6.5). The participant inputs were the same as the inputs used for the experiments.

**Table 6.5 Test Matrix for FE Model**

Participant # 1	Half Muscle Force
	Full Muscle Force
Participant # 2	Half Muscle Force
	Full Muscle Force

## Chapter 7 Computational Results

The finite element model was developed by mirroring the experimental methodology, thus the moment arms of the GHBMC leg had to be calculated first. The moment arms of the GHBMC leg are displayed in Table 7.1.

**Table 7.1 GHBMC Moment Arm Calculations (in mm)**

<b>Knee</b>	<b>GHBMC</b>
<b>Quadriceps</b>	48.0
<b>Hamstring</b>	40.5
<b>Gastrocnemius</b>	18.0

### 7.1 Comparison of Finite Element Model Strain with Experimental Strain

The FE leg model was tested in the four loading conditions. The graphs used to verify that the finite element model was applying the correct kinematic and kinetic boundary conditions are found in Appendix A. Figure 7.1 highlights the results for participant #1 and participant #2 with full and half muscle force. The FE model results are presented overlaying experimental results from the three cadaver specimens tested.

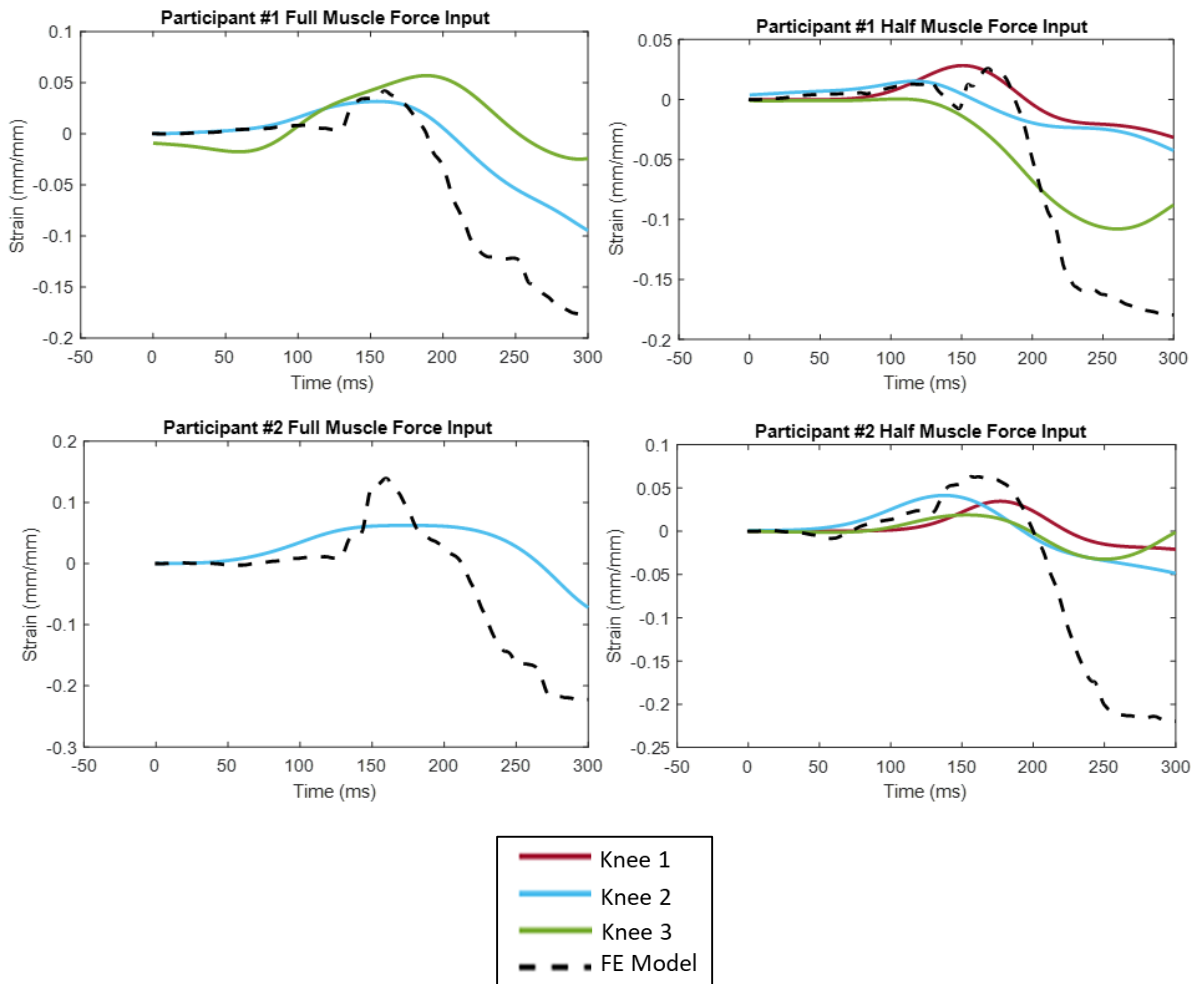


**Figure 7.1 Average relative ACL strain results for participant #1 and participant #2**

The results are summarized in Table 5.3 as well, highlighting maximum ACL strain and the time at which the maximum strain occurs.

**Table 7.2 Summary of Experimental and Computational Maximum Relative ACL Strain Results**

		Knee 1		Knee2		Knee3		Leg Model	
		Max Strain	T <sub>max</sub> (ms)	Max Strain	T <sub>max</sub> (ms)	Max Strain	T <sub>max</sub> (ms)	Max Strain	T <sub>max</sub> (ms)
<b>Participant #1</b>	<b>Full Force</b>	x	x	0.032	154	0.057	189	0.042	160
	<b>Half Force</b>	0.028	151	0.015	117	0.000	106	0.026	168
<b>Participant #2</b>	<b>Full Force</b>	x	x	0.062	175	x	x	0.139	160
	<b>Half Force</b>	0.035	177	0.041	138	0.019	154	0.063	158

The mean squared error comparing the ACL strain *vs.* time curves of the FE model to each cadaver knee were also calculated (Table 7.3). The mean squared error is small relative to the strain values observed (less than 0.01 in all cases). Table 7.4 shows the Pearson correlation coefficient comparing the ACL strain *vs.* time curves of the FE model to the results of each cadaver knee. Most of the correlation coefficients are close to 1.00, indicating a strong positive correlation between the computation and experimental ACL strain *vs.* time curves.

**Table 7.3 Mean squared error of ACL strain *vs.* time curves of experiments and FE model**

		Knee 1/FE Model	Knee 2/FE Model	Knee 3/FE Model
<b>Participant # 1</b>	<b>Full Force</b>	x	0.0022	0.0068
	<b>Half Force</b>	0.0060	0.0055	0.0016
<b>Participant # 2</b>	<b>Full Force</b>	x	0.0087	x
	<b>Half Force</b>	0.0089	0.0069	0.0083

**Table 7.4 Pearson Correlation Coefficient comparing ACL strain vs. time curves of experiments and FE model**

		<b>Knee 1/FE Model</b>	<b>Knee 2/FE Model</b>	<b>Knee 3/FE Model</b>
<b>Participant # 1</b>	<b>Full Force</b>	x	0.9654	0.3385
	<b>Half Force</b>	0.8745	0.8928	0.9335
<b>Participant # 2</b>	<b>Full Force</b>	x	0.6944	x
	<b>Half Force</b>	0.8222	0.9137	0.8773

## Chapter 8 Discussion of Results

### 8.1 Effect of the Knee Brace

The knee brace did not affect the ACL strain. The mean squared error between unbraced and braced ACL strain *vs.* time curves was less than 0.0011 for all loading scenarios. This result is consistent with the results of Hangalur et al., 2016, which stated that the main method in which the knee brace reduces ACL strain is by changing the muscle firing pattern. Since the same muscle firing pattern was used for both the braced and unbraced cadaver specimens in this study, no significant change in ACL peak strain should be observed.

Beynon and Fleming, 1998 and Devita and Hortobagyi, 2001 both found that ACL strain was reduced during knee brace wear; however, both of these studies were performed with *in-vivo* participants wearing and not wearing a knee brace; therefore, it was impossible to separate the effect that the knee brace had on the muscle forces from the purely mechanical effect of the knee brace. The current study only observed the mechanical effect of the knee brace, since the muscle force profile for both participants was determined from participants performing a jump landing not wearing a knee brace.

### 8.2 Validation of the Finite Element Model

There are limited computational studies modelling dynamic movement, specifically jump landing. The dynamic knee simulator developed by Cassidy is unique since it can apply a muscle force *vs.* time profile to the knee joint, and the main objective of this study was to apply the same muscle force *vs.* time profile to an existing finite element model of the human knee joint. The GHBMC right knee was extracted and the boundary conditions from the dynamic knee simulator were applied to the GHBMC right knee using the finite element software LS-DYNA (LSTC, Livermore, CA). The GHBMC model represents a full body 50<sup>th</sup> percentile male, and the cadaver specimens used in the validation experiments had an average age of 48 years.

The GHBMC leg was able to successfully perform a numerically stable jump landing. Figure 8.1 shows the finite element model peak relative ACL strains plotted against the peak relative ACL strain values from the

experiments. The peak relative ACL strains from the FE model are within 0.01 of an experimental result for all loading cases except for the full jump landing profile from participant #2. There was only one cadaver that successfully performed a jump with participant #2 full muscle force inputs; therefore, it was not possible to draw any definite conclusions from the relatively high computational ACL strain.

Figure 8.2 shows the time from the beginning of each trial that it took to reach the maximum ACL strain. These values all fall between the predicted values of 90 – 200ms, and the time to peak relative ACL strain from FE simulation is always within 10ms from an experimental result.

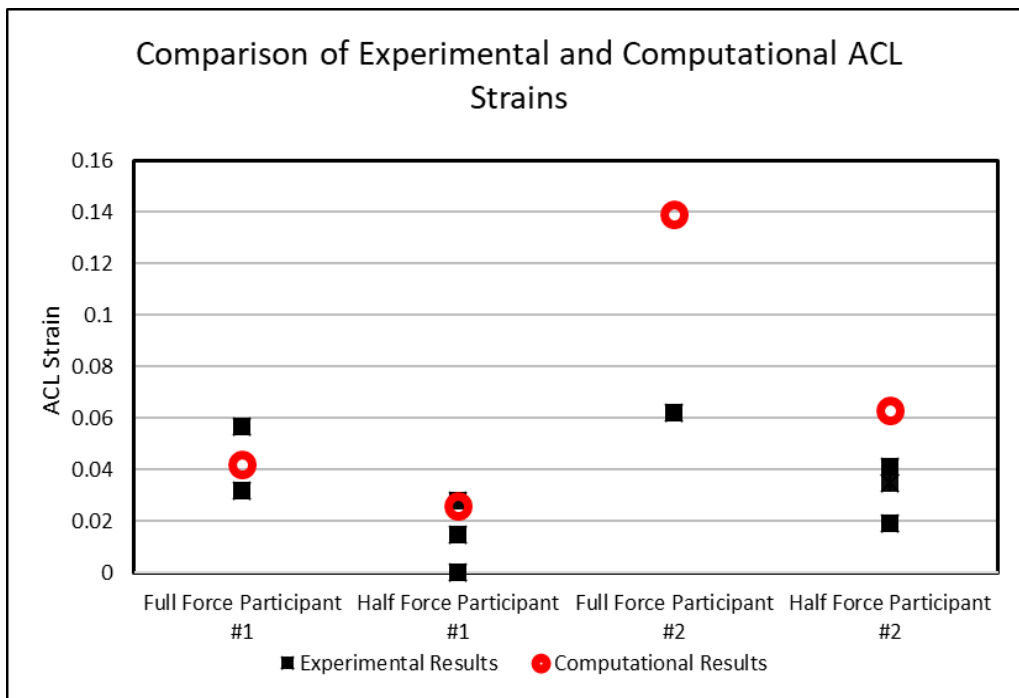


**Figure 8.1 Comparison of experimental and computational relative ACL strains**

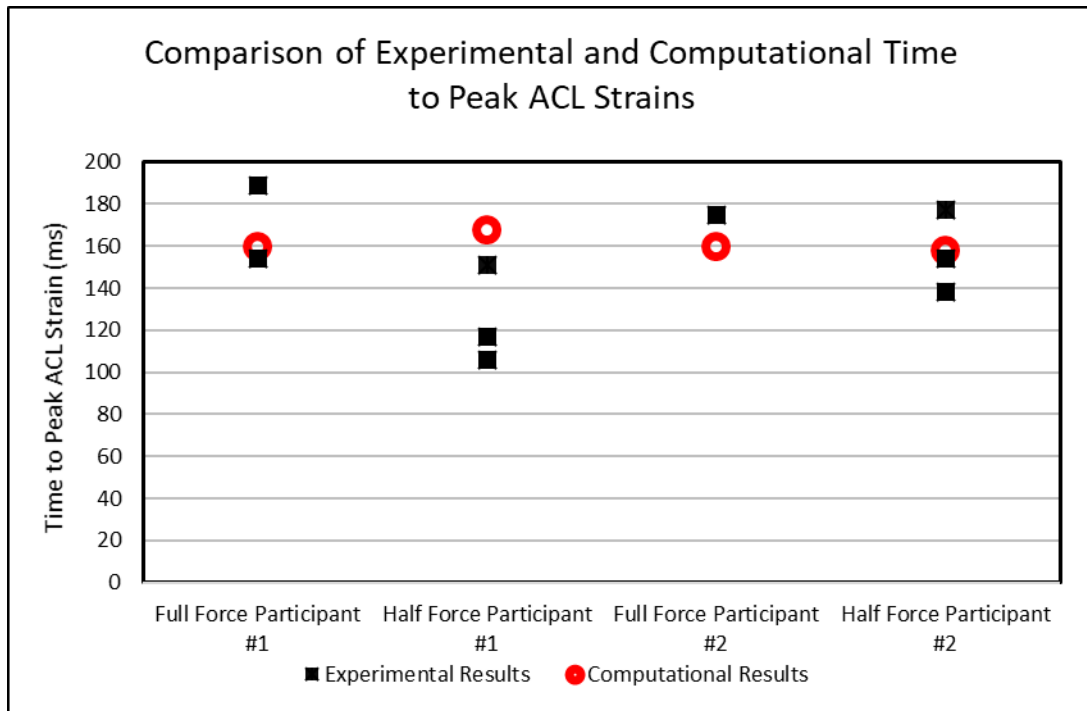


**Figure 8.2 Comparison of experimental and computational time to peak relative ACL strains**

The high peak relative ACL strain for participant #2 may be due to the fact that the knee geometry of the GHBMC did not work well with the boundary condition for participant #2. Bakker et al., 2016 showed that the maximum strains resulting from a particular participant profile will vary when the participant profile is tested on multiple cadaver knees. The GHBMC knee can be considered to be another cadaver knee subject. It also has a unique geometry which will affect how it reacts to a participant muscle force profile.

Although each cadaver knee tends to show trends in the ACL strain vs. time profiles, the peaks strains can vary when different jump landing profiles are tested on the same cadaver knee (Bakker et al., 2016). The GHBMC knee ACL reaches maximum strain between 157-169ms, which fits within the range of 83-200ms during which Bakker, 2014 observed peak relative ACL strain developing; however different participant profiles will result in a different peak value. For the full muscle force jumps, participant # 1 resulted in a peak relative ACL strain of 0.042, while participant #2 had a peak relative ACL strain of 0.139. Similarly, for a half muscle force jump, participant #1 had a maximum relative ACL strain of 0.026, while participant # 2 had a maximum relative ACL strain of 0.063.



The shapes of the ACL strain *vs.* time curves was similar to the experimental ACL strain *vs.* time curves. The ACL strain decreased more near the end of the simulation in comparison to the experimental ACL strain. Compressive material properties of the ACL may need to be examined in further detail; however, this is not critical to this study, since the main point of interest is the peak relative ACL strain and the time at which it occurs.

### **8.3 Comparison to Literature**

Since there are very few computational studies modelling single leg jump landing and reporting ACL strain, it is difficult to compare the results with those of another study. Kiapour et al., 2013 also developed a finite element model which was validated in single leg jump landing. The finite element model of Kiapour et al., 2013 had a maximum relative ACL strain of 0.052. The GHBM right leg model had maximum relative ACL strain values ranging from 0.042 to 0.139. Kiapour et al., 2013 modelled a single leg jump landing using static quadriceps and hamstring muscle forces, and initiated a jump by applying a sudden downward force to the hip which simulated the ground reaction force. The model was validated using the Ohio State University simulator; therefore, it had similar inputs to the simulator (Kiapour et al., 2013). Similarly, the model in the current study aimed to re-create the loading and boundary conditions of the dynamic knee simulator at the University of Waterloo. The dynamic knee simulator is different from the Ohio State University simulator since the inputs required are dynamic muscle force *vs.* time profiles.

Multiple experimental studies have investigated ACL strain during jump landing. Cassidy et al., 2013, Hangalur et al., 2016, and Bakker et al., 2016 tested knees performing single leg jump landing using the University of Waterloo dynamic knee simulator. These studies all used a similar methodology to the current study; therefore, the results should be quite comparable. The two participants were also tested in the study of Bakker, 2014. Figure 8.3 shows the results from participant #1 and participant #2 full muscle force jumps when they were tested by Bakker, 2014.

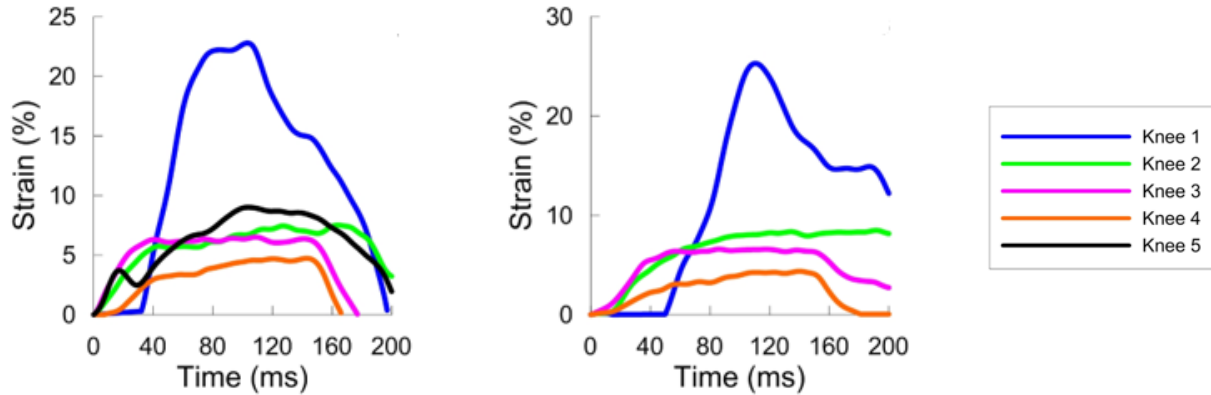


**Figure 8.3 The relative ACL strain profiles of participant # 1 and participant # 2 from the experiments of Bakker, 2014**

The peak relative ACL strains for both the participants cover a large range, from 0.04 to 0.25. In the current study, participant #1 performing a full muscle force jump exhibited an average peak relative ACL strain of 0.0442, while participant #2 only performed one successful full muscle force jump with a peak relative ACL strain of 0.062. The experimental peak relative ACL strains from the current study are in good agreement with the strains from the Bakker et al., 2016. The finite element model peak relative ACL strains are also in good agreement with the strains for both the participants from the study of Bakker, 2014. The GHBMC model exhibits a maximum relative ACL strain of 0.042 for the participant #1 full jump, which is relatively low in comparison to the results of Bakker et al., 2016, while the maximum relative ACL strain of participant #2 performing a full jump was 0.139, which is fairly high in comparison to the results of Bakker et al., 2016, but not unreasonable, since one knee has exhibited a higher peak relative ACL strain without failing.

Taylor and Terry, 2013 tested single leg jump landing *in-vivo* and used a solid 3D model to determine ACL strain. They measured a mean maximum relative ACL strain of  $0.12 \pm 0.07$ . The average peak relative ACL strain for a full muscle force jump in the current study was 0.044 for participant #1 was 0.062 for participant #2. The discrepancy in peak ACL strains may be due to the fact that the methodology of Taylor and Terry, 2013 was very different from the current study, in which the relative ACL strain was determined from the kinematics of the participant performing the jump. The measurement of ACL strain *in-vivo* eliminated the

error which can arise from re-creating the muscle force profile of a participant on a cadaver which may have different knee geometry; however, the study of Taylor and Terry, 2013 had other limitations such as the fact that the ACL strain was determined through the use of a solid 3D model, and not measured directly on the subject.

Hashemi et al., 2007 examined ACL strain experimentally at Texas Tech University using a knee simulator. The study involved pre-tensioning the quadriceps muscle to different values in order to evaluate the effect of the quadriceps force on relative ACL strain. The average maximum relative ACL strain was 0.104, which is high compared to the experimental relative ACL strains from the current study, in which quadriceps force is applied as a dynamic muscle force *vs.* time curve.

Withrow et al., 2006 related quadriceps force to knee flexion and ACL strain at the University of Michigan, by performing simulator experiments. The average relative ACL strain from the study of Withrow et al., 2006 was 0.03, which is a low peak value compared to the current study in which experimental peak relative ACL strains were 0.0442 for participant #1 and 0.063 for participant #2. Withrow et al., 2006 applied a maximum quadriceps force of approximately 1300 N in all of the trials, while the current study applied a maximum quadriceps force of approximately 4000 N for the full muscle force trials, which could be a reason for the ACL strain from the study of Withrow et al., 2006 being lower than the ACL strains from the current study.

The resulting average peak relative ACL strains from Bakker et al., 2016, Hangalur et al., 2016, Cassidy et al., 2013, Kiapour et al., 2013, Taylor and Terry, 2013, Hashemi et al., 2007, and Withrow et al., 2006 are summarized and compared to the experimental results of the current study in Figure 8.4. Figure 8.5 shows the finite element model results compared to the average strains from the literature, including the ACL strain of the finite element model of Kiapour et al., 2013, demonstrating that the peak relative ACL strain for participant #2 of 0.139 is a realistic maximum strain value for a single leg jump landing.

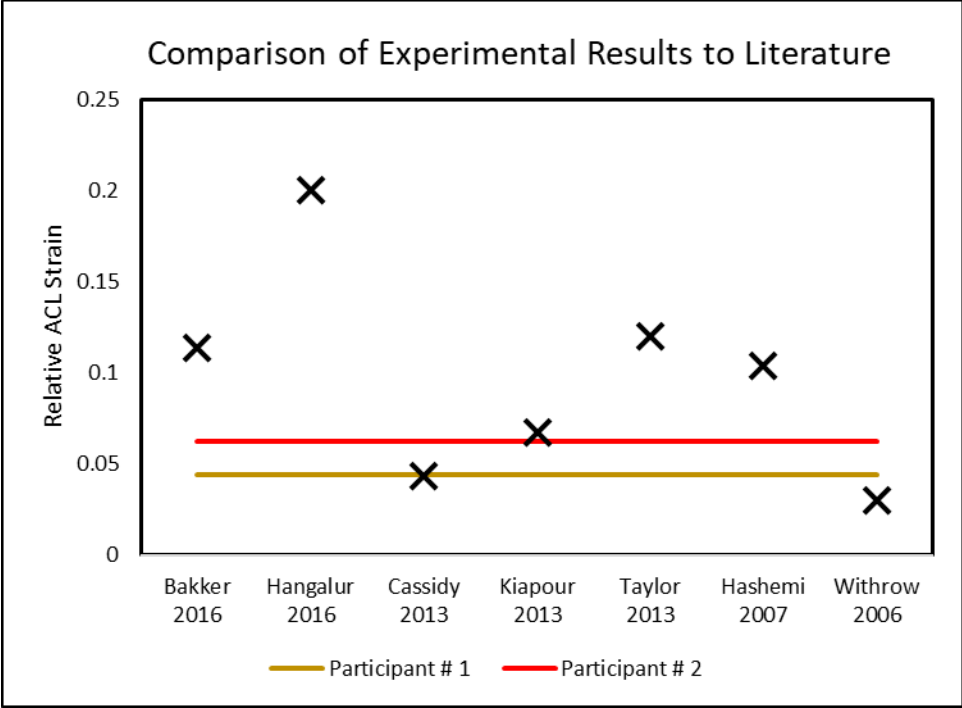


**Figure 8.4 Comparison of Experimental Results to Literature**

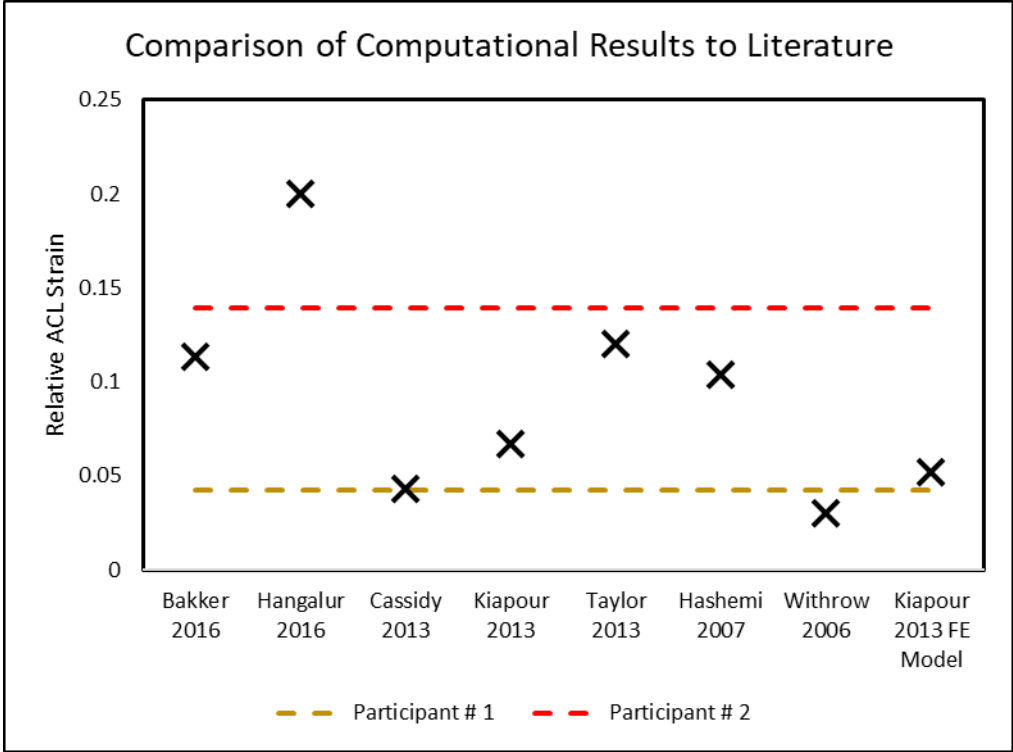


**Figure 8.5 Comparison of Computational Results to Literature**

## 8.4 Limitations of the Study

The current study is interesting, because an existing impact model, the GHBMC model, was taken and reformatted to perform a human movement as if the GHBMC had active firing muscles. The modelling was also based on experiments that were performed in parallel with the modelling, which allowed the exact same methodology and inputs to be applied to both the model and the experiments which were used to validate the model. The model inputs were dynamic muscle force vs. time curves as well as position vs. time curves of the hip and ankle. The dynamic knee simulator allowed for the validation of such a complex finite element model.

There were limitations to both the experimental and computational aspects of this study. Only three samples were tested to develop the experimental data set. There is high variability in the human population, and geometry greatly affects ACL strain (Bakker et al., 2016); therefore the number of samples in a validation study of a generic 50<sup>th</sup> percentile male finite element model performing a single leg jump landing is very important. Three samples are not representative of the entire human population. The model is also not subject-specific. Bakker, 2014 showed that ACL strain for the same jump landing profile applied to cadavers of varying geometries will produce varying results. In order to accurately predict relative ACL strain for a jump landing performed on a specific geometry, a subject-specific model would need to be developed. Finally, the mesh and geometry of the GHBMC knee joint is coarse (Figure 8.6), which may have affected the kinematics of the femur moving over the meniscus during simulation. This motion is critical in jump landing; therefore, a more detailed knee geometry and mesh may provide a more consistent and reliable result. The coarse mesh provided a challenge in the early stages of modelling, when a leg straightening simulation was attempted by holding the femur in place and pulling on the quadriceps tendon. A very high force of 3500 N was not sufficient to straighten the leg, which was likely a result of coarse geometry in the knee joint. A subject-specific model could help fix this issue, since subject-specific models tend to predict kinematics better than generic geometries (Naghbi Beidokhti et al., 2017).

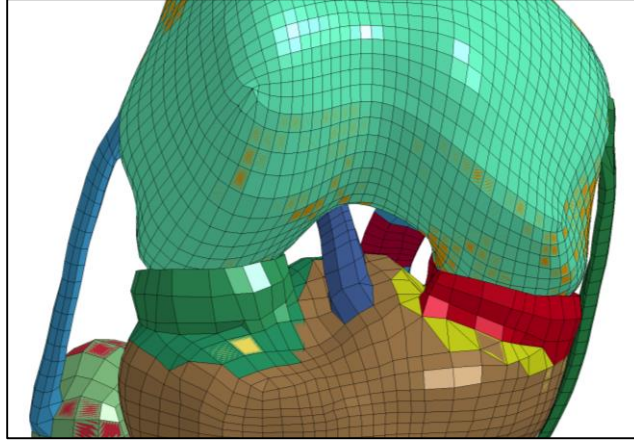


**Figure 8.6 Anterior view of the GHBMC knee joint to show coarse mesh**

## Chapter 9 Conclusions and Future Research Directions

The objective of the study was to ACL strain experimentally and computationally. The experiments included determining the effect of the Össur CTi knee brace on ACL strain, and the computational results were compared to the experiments to validate the FE model. The main conclusions of the experimental study were:

- The experimental peak relative ACL strain was between the predicted values of 0.03 and 0.20 and occurred between 90 and 200ms. The two participant input profiles resulted in varying peak relative ACL strains (0.044 for participant #1 and 0.062 for participant #2).
- The knee brace had minimal effect on ACL strain *vs.* time result (MSE between the curves was less than 0.0011 for all loading conditions)

The conclusions of the finite element study were:

- The computational peak relative ACL strain was between the predicted values of 0.03 and 0.20 and occurred between 90 and 200ms. The two participant profiles resulted in varying peak relative ACL strains (0.042 for participant #1 and 0.139 for participant #2).
- The GHBMC produced a characteristic ACL strain *vs.* time curve that consistently peaked between 170 and 180ms.

Future directions of this research should include adding the knee brace to the GHBMC model to determine if it has the same effect computationally as it does experimentally. The experimental results from this study could be used as a first step in validating a jump landing model wearing a knee brace. A finite element model of a human leg wearing a knee brace is an important first step in developing and evaluating an effective knee brace to protect the ACL during dynamic activities.

The GHBMC model provided reasonable results for single leg jump landing; however, there is still more work that can be done to improve the model and to validate it further. One of the main limitations

of the study was that only three cadaver specimens were tested. A larger data set would be useful in performing a more complete validation of the finite element model. The model could also be tested in a variety of loading conditions to ensure a multi purpose model. Ideally the model would function in static, as well as dynamic, loading scenarios. It may also be wise to validate the model using more parameters than simply ACL strain. While this was enough for the current study, a multipurpose model would be able to predict other factors as well, such as knee flexion angle and strain in other ligaments. The model would also benefit from a subject-specific geometry; since subject-specific models are more accurate in accurately replicating knee kinematics (Naghibi Beidokhti et al., 2017).



## References

- Agarwal, A., 2017. Gastrocnemius [WWW Document]. Hum. Anat. URL <https://www.knowyourbody.net/gastrocnemius.html>
- Anatomy Language & Histology [WWW Document], n.d. . Word Press. URL <https://termandhistology.wordpress.com/anatomy-language/anatomical-positions-planes-directions/> (accessed 10.3.18).
- Bakker, R., 2014. The Effect of Sagittal Plane Mechanics on Anterior Cruciate Ligament Strain During Jump Landing. University of Waterloo.
- Bakker, R., Tomescu, S., Brenneman, E., Hangalur, G., Laing, A., Chandrashekar, N., 2016. Effect of sagittal plane mechanics on ACL strain during jump landing. J. Orthop. Res. 34, 1636–1644. <https://doi.org/10.1002/jor.23164>
- Baldwin, M.A., Clary, C.W., Fitzpatrick, C.K., Deacy, J.S., Maletsky, L.P., Rullkoetter, P.J., 2012. Dynamic finite element knee simulation for evaluation of knee replacement mechanics. J. Biomech. 45, 474–483. <https://doi.org/10.1016/j.jbiomech.2011.11.052>
- Bates, N.A., Schilaty, N.D., Nagelli, C. V., Krych, A.J., Hewett, T.E., 2017. Novel mechanical impact simulator designed to generate clinically relevant anterior cruciate ligament ruptures. Clin. Biomech. 44, 36–44. <https://doi.org/10.1016/j.clinbiomech.2017.03.005>
- Behnke, R.S., 2001. Kinetic Anatomy.
- Beillas, P., Papaioannou, G., Tashman, S., Yang, K.H., 2004. A new method to investigate in vivo knee behavior using a finite element model of the lower limb. J. Biomech. 37, 1019–1030. <https://doi.org/10.1016/j.jbiomech.2003.11.022>
- Beynon, B.B., Fleming, B.C., 1998. Anterior cruciate ligament strain in-vivo: A review of previous work. J. Biomech. 31, 519–525.
- Blank Body Colouring Page [WWW Document], n.d. . homelandsecuritynews. URL <http://homelandsecuritynews.info/blank-body-coloring-page/> (accessed 10.25.15).
- Boden, B.P., Dean, G.S., Feagin, J.A., Garrett, W.E., 2000. Mechanisms of Anterior Cruciate Ligament Injury. Orthopaedics 123, 573–578.
- Brandsson, S., Faxe, E., 2001. Is a knee brace advantageous after anterior cruciate ligament surgery? A prospective , randomised study with a two-year follow-up. Scand J Med Sci Sport. 11, 110–114.
- Burks, R.T., 1990. Gross Anatomy, in: Daniel, D.M., Akeson, W.H., O’Connor, J.J. (Eds.), Knee Ligaments: Structure, Function, Injury and Repair. Raven Press, pp. 77–94.
- Butler, D.L., Kay, M.D., Stouffer, D.C., 1986. Comparison of material properties in fascicle-bone units from human patellar tendon and knee ligaments. J. Biomech. 19, 425–432. [https://doi.org/https://doi.org/10.1016/0021-9290\(86\)90019-9](https://doi.org/https://doi.org/10.1016/0021-9290(86)90019-9)
- Cassidy, K., Hangalur, G., Sabharwal, P., Chandrashekar, N., 2013. Combined in Vivo / in Vitro Method

- to Study Anteromedial Bundle Strain in the Anterior Cruciate Ligament Using a Dynamic Knee Simulator. *J. Biomech. Eng.* 135, 035001. <https://doi.org/10.1115/1.4023520>
- Chandrashekar, N., 2005. Sex-based difference in the morphology, tensile properties and ultrastructure of the human anterior cruciate ligament and patellar tendon. Texas Tech University.
- Chandrashekar, N., Mansouri, H., Slauterbeck, J., Hashemi, J., 2006. Sex-based differences in the tensile properties of the human anterior cruciate ligament. *J. Biomech.* 39, 2943–2950. <https://doi.org/10.1016/j.jbiomech.2005.10.031>
- Csintalan, R.P., Inacio, M.C.S., Funahashi, T.T., 2008. Incidence rate of anterior cruciate ligament reconstructions. *Perm. J.* 12, 17–21.
- Daniel, D.M., Stone, M. Lou, Dobson, B.E., Fithian, D.C., Rossman, D.J., Kaufman, K.R., 1993. Winner of the 1993 O' Donoghue award Fate of the ACL-injured Patient Prospective Outcome Study \*. *Am. J. Sports Med.* 22, 632–644. <https://doi.org/10.1177/036354659402200511>
- Devita, P., Hortobagyi, T., 2001. Functional Knee Brace Alters Predicted Knee Muscle and Joint Forces in People With ACL Reconstruction During Walking. *J. Appl. Biomech.* 17, 297–311.
- Domire, Z.J., Boros, R.L., Hashemi, J., 2011. An examination of possible quadriceps force at the time of anterior cruciate ligament injury during landing: A simulation study. *J. Biomech.* 44, 1630–1632. <https://doi.org/10.1016/j.jbiomech.2011.03.001>
- Ellison, A.E., Berg, E.E., 1985. Embryology, Anatomy, and Function of the Anterior Cruciate Ligament, in: *The Orthopaedic Clinics of North America*. W. B. Saunders Company, pp. 3–14.
- Frankel, V.H., Nordin, M., Walker, P.S., 2012. Biomechanics of the Knee, in: Leger, D. (Ed.), *Basic Biomechanics of the Musculoskeletal System*. Wolters Kluwer, pp. 180–205.
- Gardiner, J.C., Weiss, J.A., 2003. Subject-specific finite element analysis of the human medial collateral ligament during valgus knee loading. *J. Orthop. Res.* 21, 1098–1106. [https://doi.org/10.1016/S0736-0266\(03\)00113-X](https://doi.org/10.1016/S0736-0266(03)00113-X)
- Giffin, J.R., Vogrin, T.M., Zantop, T., Woo, S.L.Y., Harner, C.D., 2004. Effects of increasing tibial slope on the biomechanics of the knee. *Am. J. Sports Med.* 32, 376–82. <https://doi.org/10.1177/0363546503258880>
- Godest, A.C., Beaugonin, M., Haug, E., Taylor, M., Gregson, P.J., 2002. Simulation of a knee joint replacement during a gait cycle using explicit finite element analysis. *J. Biomech.* 35, 267–275. [https://doi.org/10.1016/S0021-9290\(01\)00179-8](https://doi.org/10.1016/S0021-9290(01)00179-8)
- Halloran, J.P., Petrella, A.J., Rullkoetter, P.J., 2005. Explicit finite element modeling of total knee replacement mechanics. *J. Biomech.* 38, 323–331. <https://doi.org/10.1016/j.jbiomech.2004.02.046>
- Hangalur, G., Brenneman, E., Nicholls, M., Bakker, R., Laing, A., Chandrashekar, N., 2016. Can a knee brace reduce the strain in the anterior cruciate ligament? A study using combined in vivo/in vitro method. *Prosthet. Orthot. Int.* 40, 394–399. <https://doi.org/10.1177/0309364615574167>
- Hashemi, J., Chandrashekar, N., Gill, B., Beynon, B.D., Slauterbeck, J.R., Schutt, R.C., Mansouri, H., Dabezies, E., 2008. The geometry of the tibial plateau and its influence on the biomechanics of the

- tibiofemoral joint. *J. Bone Jt. Surg. - Ser. A* 90, 2724–2734. <https://doi.org/10.2106/JBJS.G.01358>
- Hashemi, J., Chandrashekar, N., Jang, T., Karpal, F., Oseto, M., Ekwaro-Osire, S., 2007. An alternative mechanism of non-contact anterior cruciate ligament injury during jump-landing: In-vitro simulation. *Exp. Mech.* 47, 347–354. <https://doi.org/10.1007/s11340-007-9043-y>
- Hashemi, J., Chandrashekar, N., Mansouri, H., Gill, B., Slauterbeck, J.R., Schutt, R.C., Dabezies, E., Beynnon, B.D., 2010. Shallow medial tibial plateau and steep medial and lateral tibial slopes: New risk factors for anterior cruciate ligament injuries. *Am. J. Sports Med.* 38, 54–62. <https://doi.org/10.1177/0363546509349055>
- Haut Donahue, T.L., Hull, M.L., Rashid, M.M., Jacobs, C.R., 2003. How the stiffness of meniscal attachments and meniscal material properties affect tibio-femoral contact pressure computed using a validated finite element model of the human knee joint. *J. Biomech.* 36, 19–34. [https://doi.org/10.1016/S0021-9290\(02\)00305-6](https://doi.org/10.1016/S0021-9290(02)00305-6)
- Haut Donahue, T.L., Hull, M.L., Rashid, M.M., Jacobs, C.R., 2002. A Finite Element Model of the Human Knee Joint for the Study of Tibio-Femoral Contact. *J. Biomech. Eng.* 124, 273. <https://doi.org/10.1115/1.1470171>
- Hegg, J., 2018. Hamstring Tendonitis - The Complete Injury Guide [WWW Document]. Vive Heal. URL <https://www.vivehealth.com/blogs/resources/hamstring-tendonitis>
- Hill, C.L., Seo, G.S., Gale, D., Totterman, S., Gale, M.E., Felson, D.T., 2005. Cruciate Ligament Integrity in Osteoarthritis of the Knee. *Arthritis Rheum.* 52, 794–799.
- Kalra, M., Bakker, R., Tomescu, S.S., Polak, A.M., Nicholls, M., Chandrashekar, N., 2018. The effect of unloader knee braces on medial meniscal strain. *Prosthet. Orthot. Int.* 030936461879817. <https://doi.org/10.1177/0309364618798173>
- Katayama, M., Higuchi, H., Kimura, M., Kobayashi, A., Hatayama, K., Terauchi, M., Takagishi, K., 2004. Proprioception and performance after anterior cruciate ligament rupture. *Int. Orthop.* 28, 278–281.
- Kiapour, A., Kiapour, A.M., Kaul, V., Quatman, C.E., Wordeman, S.C., Hewett, T.E., Demetropoulos, C.K., Goel, V.K., 2013. Finite Element Model of the Knee for Investigation of Injury Mechanisms: Development and Validation. *J. Biomech. Eng.* 136, 011002. <https://doi.org/10.1115/1.4025692>
- Kiapour, A.M., Demetropoulos, C.K., Kiapour, A., Quatman, C.E., Wordeman, S.C., Goel, V.K., Hewett, T.E., 2016. Strain Response of the Anterior Cruciate Ligament to Uniplanar and Multiplanar Loads during Simulated Landings. *Am. J. Sports Med.* 44, 2087–2096. <https://doi.org/10.1177/0363546516640499>
- Kiapour, A.M., Kaul, V., Kiapour, A., Quatman, C.E., Samuel, C., Hewett, T.E., Demetropoulos, C.K., Goel, V.K., 2014. The Effect of Ligament Modeling Technique on Knee Joint Kinematics: A Finite Element Study. *Appl. Math.* 4, 91–97. <https://doi.org/10.4236/am.2013.45A011>
- Kiapour, A.M., Quatman, C.E., Goel, V.K., Wordeman, S.C., Hewett, T.E., Demetropoulos, C.K., 2014. Timing sequence of multi-planar knee kinematics revealed by physiologic cadaveric simulation of landing: Implications for ACL injury mechanism. *Clin. Biomech.* 29, 75–82. <https://doi.org/10.1016/j.clinbiomech.2013.10.017>

- Knee [WWW Document], 2018. . Wikipedia. URL <https://en.wikipedia.org/wiki/Knee> (accessed 10.3.18).
- Langford, T., 2018. Popliteus: Assessment and Rehabilitation [WWW Document]. *Sport. Inj. Bull.* URL <https://www.sportsinjurybulletin.com/popliteus-assessment-and-rehabilitation/> (accessed 10.3.18).
- Leppänen, M., Pasanen, K., Krosshaug, T., Kannus, P., Vasankari, T., Kujala, U.M., Bahr, R., Perttunen, J., Parkkari, J., 2017. Sagittal Plane Hip, Knee, and Ankle Biomechanics and the Risk of Anterior Cruciate Ligament Injury: A Prospective Study. *Orthop. J. Sport. Med.* 5, 1–6. <https://doi.org/10.1177/2325967117745487>
- LeRoux, M.A., Setton, L.A., 2002. Experimental and Biphasic FEM Determinations of the Material Properties and Hydraulic Permeability of the Meniscus in Tension. *J. Biomech. Eng.* 124, 315. <https://doi.org/10.1115/1.1468868>
- Levine, J.W., Kiapour, A.M., Quatman, C.E., Wordeman, S.C., Goel, V.K., Hewett, T.E., Demetropoulos, C.K., 2013. Clinically Relevant Injury Patterns After an Anterior Cruciate Ligament Injury Provide Insight Into Injury Mechanisms. *Am J Sport. Med* 41, 385–395. <https://doi.org/10.1177/0363546512465167>.Clinically
- Li, G., Gil, J., Kanamori, A., Woo, S.L.-Y., 1999. A validated three-dimensional computational model of a human knee joint. *J. Biomech. Eng.* 121, 657–662. <https://doi.org/10.1115/1.2800871>
- Li, G., Lopez, O., Rubash, H., 2001. Variability of a Three-Dimensional Finite Element Model Constructed Using Magnetic Resonance Images of a Knee for Joint Contact Stress Analysis. *J. Biomech. Eng.* 123, 341. <https://doi.org/10.1115/1.1385841>
- Li, G., Suggs, J., Gill, T., 2002. The effect of anterior cruciate ligament injury on knee joint function under a simulated muscle load: A three-dimensional computational simulation. *Ann. Biomed. Eng.* 30, 713–720. <https://doi.org/10.1114/1.1484219>
- Limbert, G., Middleton, J., Taylor, M., 2004. Finite element analysis of the human ACL subjected to passive anterior tibial loads. *Comput. Methods Biomech. Biomed. Engin.* 7, 1–8. <https://doi.org/10.1080/10255840410001658839>
- Lipps, D.B., Wojtys, E.M., Ashton-Miller, J.A., 2013. Anterior cruciate ligament fatigue failures in knees subjected to repeated simulated pivot landings. *Am. J. Sports Med.* 41, 1058–1066. <https://doi.org/10.1177/0363546513477836>
- Mather, R.C., Koenig, L., Kocher, M.S., Dall, T.M., Gallo, P., Scott, D.J., Bach, B.R., Spindler, K.P., 2013. Societal and economic impact of anterior cruciate ligament tears. *J. Bone Joint Surg. Am.* 95, 1751–9. <https://doi.org/10.2106/JBJS.L.01705>
- Medial Collateral Ligament [WWW Document], 2011. . Word Press. <https://doi.org/10.1016/B978-032302588-1.50057-9>
- Muneta, T., Takakuda, K., Yamamoto, H., 1997. Intercondylar notch width and its relation to the configuration and cross-sectional area of the anterior cruciate ligament: A cadaveric knee study. *Am. J. Sports Med.* 25, 69–72. <https://doi.org/10.1177/036354659702500113>
- Naghbi Beidokhti, H., Janssen, D., van de Groes, S., Hazrati, J., Van den Boogaard, T., Verdonshot, N., 2017. The influence of ligament modelling strategies on the predictive capability of finite element

- models of the human knee joint. *J. Biomech.* 65, 1–11.  
<https://doi.org/10.1016/j.jbiomech.2017.08.030>
- Noyes, F.R., Grood, E.S., 1976. The strength of the anterior cruciate ligament in humans and Rhesus monkeys. *J. Bone Joint Surg. Am.* 58, 1074–82. <https://doi.org/10.2106/JBJS.M.00187>
- Oh, Y.K., Kreinbrink, J.L., Ashton-Miller, J.A., Wojtys, E.M., 2011. Effect of ACL transection on internal tibial rotation in an in vitro simulated pivot landing. *J. Bone Jt. Surg. - Ser. A* 93, 372–380. <https://doi.org/10.2106/JBJS.J.00262>
- Peña, E., Calvo, B., Martínez, M.A., Doblaré, M., 2006. A three-dimensional finite element analysis of the combined behavior of ligaments and menisci in the healthy human knee joint. *J. Biomech.* 39, 1686–1701. <https://doi.org/10.1016/j.jbiomech.2005.04.030>
- Quadriceps Muscle Diagram [WWW Document], 2016. . *Anat. Label.* URL <https://humananatomylibrary.co/s/quadriceps-muscle-diagram.asp> (accessed 10.3.18).
- Quatman, C.E., Kiapour, A.M., Demetropoulos, C.K., Kiapour, A., Wordeman, S.C., Levine, J.W., Goel, V.K., Hewett, T.E., 2014. Preferential loading of the ACL compared with the MCL during landing: A novel in sim approach yields the multiplanar mechanism of dynamic Valgus during acl injuries. *Am. J. Sports Med.* 42, 177–186. <https://doi.org/10.1177/0363546513506558>
- Sanders, T.L., Kremers, H.M., Bryan, A.J., Larson, D.R., Dahm, D.L., Levy, B.A., Stuart, M.J., Krych, A.J., 2016. Incidence of Anterior Cruciate Ligament Tears and Reconstruction: A 21-Year Population-Based Study. *Am. J. Sports Med.* 44, 1502–1507. <https://doi.org/10.1177/0363546516629944>
- Schwartz, D., Guleyupoglu, B., Koya, B., Stitzel, J.D., Gayzik, F.S., 2015. Development of a Computationally Efficient Full Human Body Finite Element Model. *Traffic Inj. Prev.* 16, 49–56. <https://doi.org/10.1080/15389588.2015.1021418>
- Shoemaker, S.C., Daniel, D.M., 1990. The Limits of Knee Motion: In Vitro Studies, in: Daniel, D.M., Akeson, W.H., O'Connor, J.J. (Eds.), *Knee Ligaments: Structure, Function, Injury and Repair*. Raven Press, pp. 153–162.
- Single-bundle vs. Double-bundle ACL Surgery [WWW Document], 2018. . *Heal. Clues.* URL <https://www.healthclues.net/blog/en/single-bundle-vs-double-bundle-acl-surgery/>
- Sitler, M., Ryan, C.O.L.J., Hopkinson, L.T.C.W., Wheeler, L.T.C.J., Santomier, J., Polley, C.D., 1990. The efficacy of a prophylactic knee brace to reduce knee injuries in football. *Am. J. Sports Med.* 18, 310–315.
- Song, Y., Debski, R.E., Musahl, V., Thomas, M., Woo, S.L.-Y., 2004. A three dimensional finite element model of the human anterior cruciate ligament: a computational analysis with experimental validation. *J. Biomech.* 37, 383–390.
- Taylor, K.A., Terry, M.E., 2013. Measurement of in vivo anterior cruciate ligament strain during dynamic jump landing. *Magn Reson Imaging* 31, 477–479. <https://doi.org/10.1016/j.immuni.2010.12.017>.Two-stage
- Trad, Z., Barkaoui, A., Chafra, M., Tavares, J.M.R.S., 2018. FEM Analysis of the Human Knee Joint A

Review.

Untaroiu, C., Darvish, K., Crandall, J., 2005. A Finite Element Model of the Lower Limb for Simulating Pedestrian Impacts. *Stapp Car Crash J.* 49, 1–26. <https://doi.org/10.1115/DETC2015-47781>

Untaroiu, C.D., Yue, N., Shin, J., 2013. A finite element model of the lower limb for simulating automotive impacts. *Ann. Biomed. Eng.* 41, 513–526. <https://doi.org/10.1007/s10439-012-0687-0>

Valgus vs Varus Knee Alignment [WWW Document], 2017. . All Heal. Post. URL <https://allhealthpost.com/valgus-vs-varus/> (accessed 10.3.18).

Weiss, J.A., Gardiner, J.C., Ellis, B.J., Lujan, T.J., Phatak, N.S., 2005. Three-dimensional finite element modeling of ligaments: Technical aspects. *Med. Eng. Phys.* 27, 845–861. <https://doi.org/10.1016/j.medengphy.2005.05.006>

Weiss, J.A., Maker, B.N., Govindjee, S., 1996. Finite element implementation of incompressible, transversely isotropic hyperelasticity. *Comput. Methods Appl. Mech. Eng.* 135, 107–128. [https://doi.org/10.1016/0045-7825\(96\)01035-3](https://doi.org/10.1016/0045-7825(96)01035-3)

Withrow, T.J., Huston, L.J., Wojtys, E.M., Ashton-Miller, J. a, 2006. The relationship between quadriceps muscle force, knee flexion, and anterior cruciate ligament strain in an in vitro simulated jump landing. *Am. J. Sports Med.* 34, 269–74. <https://doi.org/10.1177/0363546505280906>

Withrow, T.J., Huston, L.J., Wojtys, E.M., Ashton-Miller, J.A., 2008. Effect of varying hamstring tension on anterior cruciate ligament strain during in vitro impulsive knee flexion and compression loading. *J. Bone Jt. Surg. - Ser. A* 90, 815–823. <https://doi.org/10.2106/JBJS.F.01352>

Withrow, T.J., Huston, L.J., Wojtys, E.M., Ashton-Miller, J.A., 2006. The relationship between quadriceps muscle force, knee flexion, and anterior cruciate ligament strain in an in vitro simulated jump landing. *Am. J. Sports Med.* 34, 269–274. <https://doi.org/10.1177/0363546505280906>

Woo, S.L.Y., Hollis, J.M., Adams, D.J., Lyon, R.M., Takai, S., 1991. Tensile properties of the human femur- anterior cruciate ligament-tibia complex. *Am. J. Sports Med.* 19, 217–225.

Xie, F., Yang, L., Guo, L., Wang, Z., Dai, G., 2009. A Study on Construction Three-Dimensional Nonlinear Finite Element Model and Stress Distribution Analysis of Anterior Cruciate Ligament. *J. Biomech. Eng.* 131, 121007. <https://doi.org/10.1115/1.4000167>

Yu, B., Garrett, W.E., 2007. Mechanisms of non-contact ACL injuries. *Br. J. Sports Med.* 41. <https://doi.org/10.1136/bjism.2007.037192>

Zielinska, B., Haut Donahue, T.L., 2006. 3D Finite Element Model of Meniscectomy: Changes in Joint Contact Behavior. *J. Biomech. Eng.* 128, 115. <https://doi.org/10.1115/1.2132370>

# Appendix A: Verification of Experiments and Finite Element Model

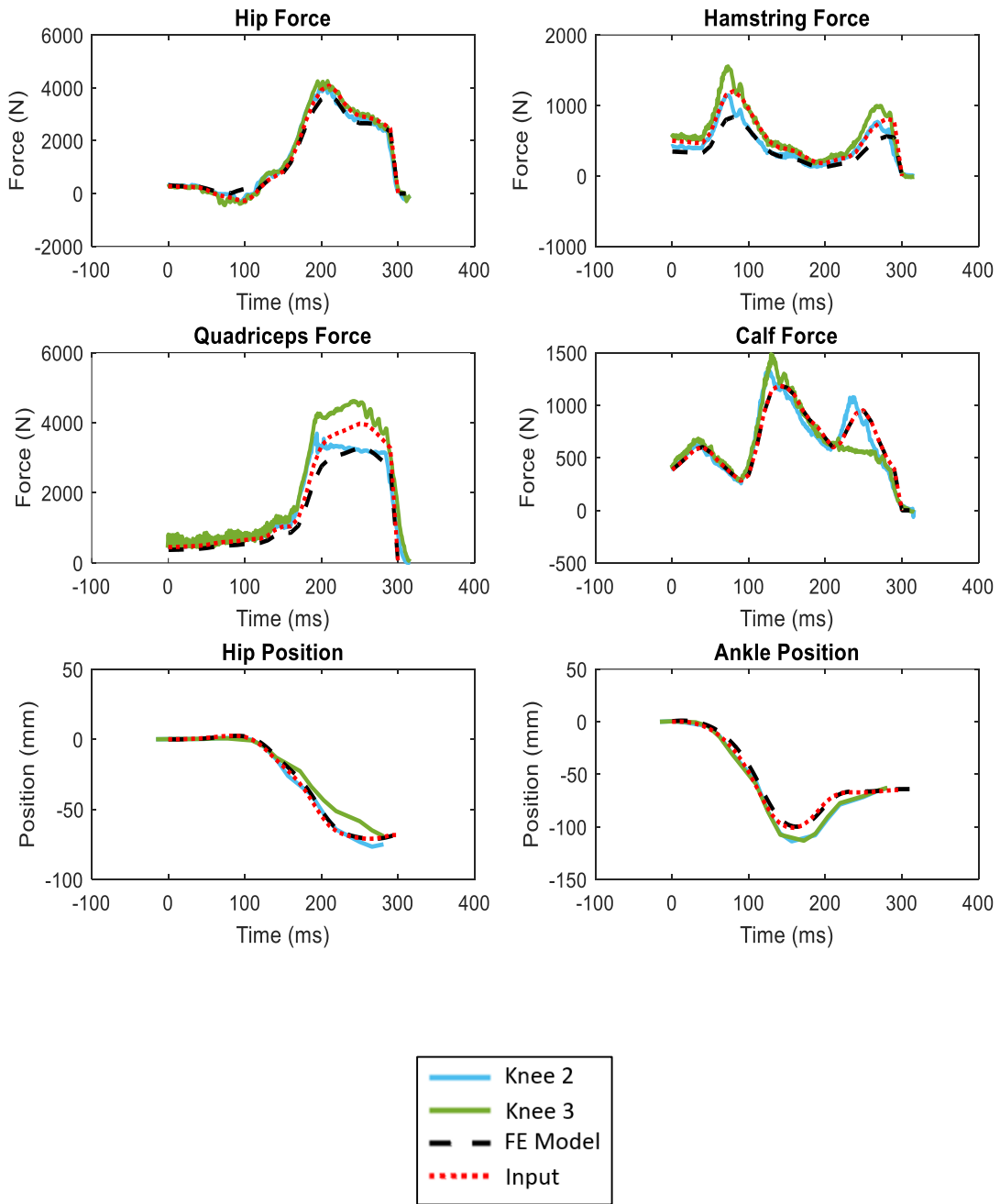
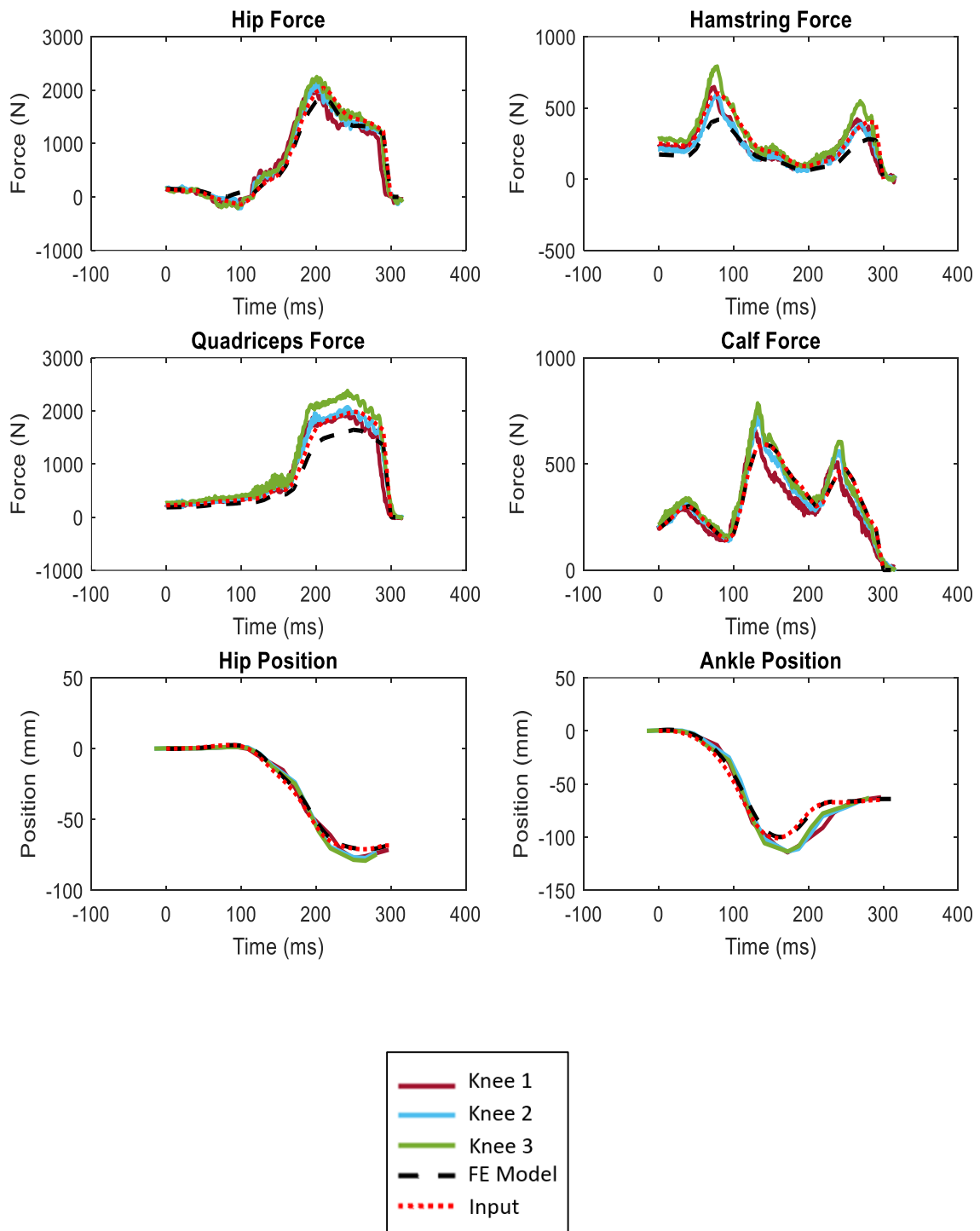
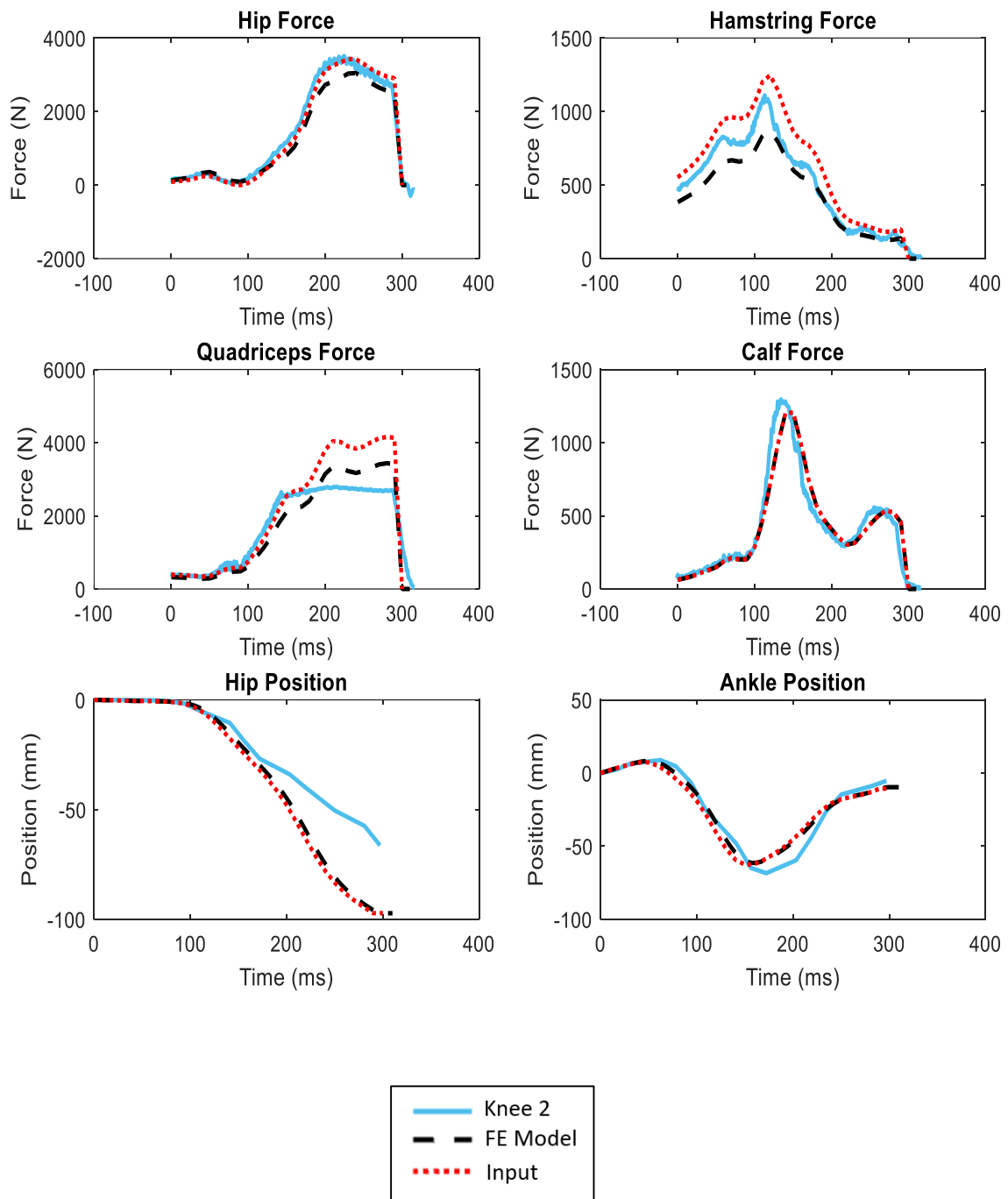


Figure A.1 Verification of kinetics and kinematics for participant # 1 full muscle force jump



**Figure A.2 Verification of kinetics and kinematics for participant # 1 half muscle force jump**





**Figure A.3 Verification of kinetics and kinematics for participant # 2 full muscle force jump**

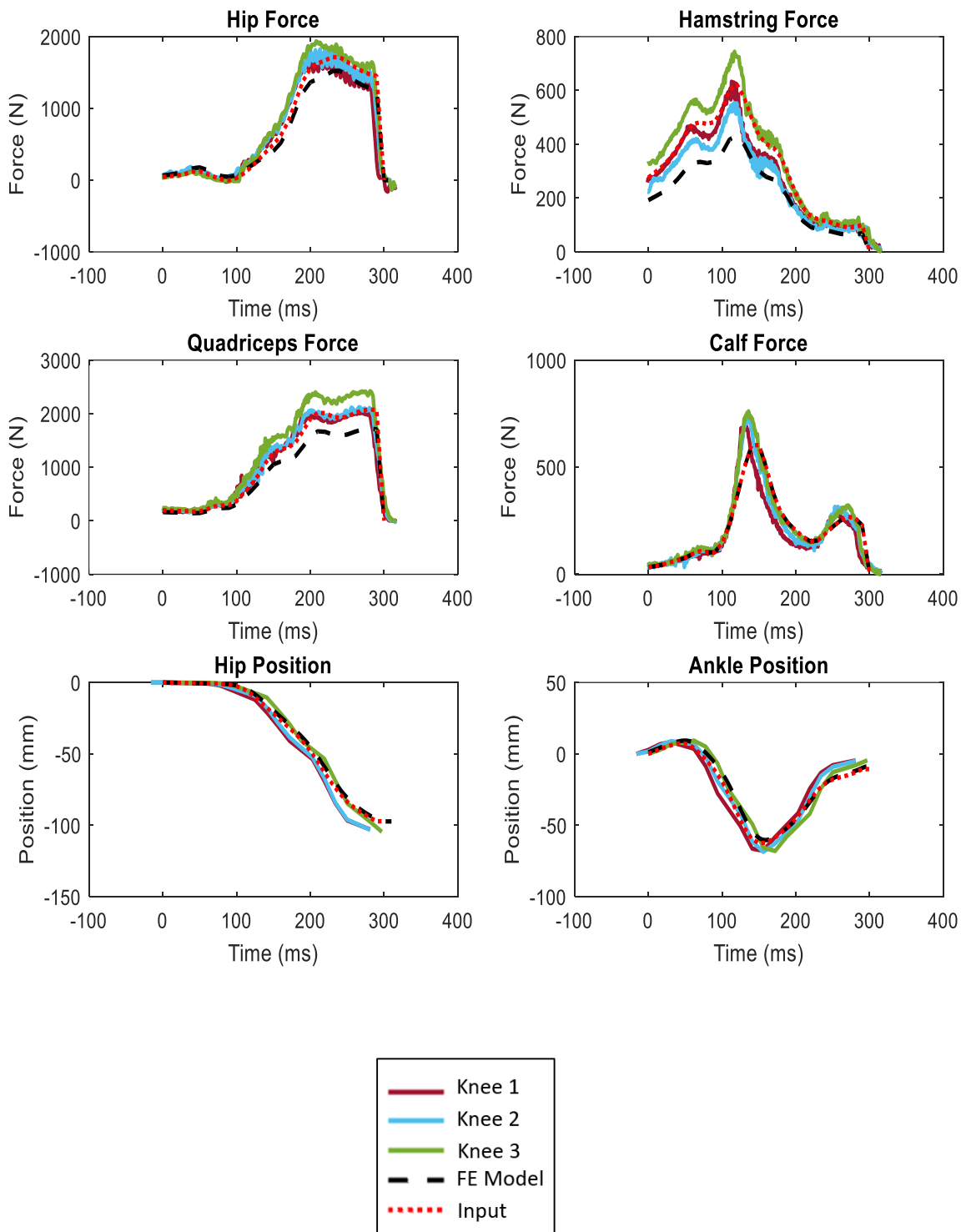


**Figure A.4 Verification of kinetics and kinematics for participant # 2 half muscle force jump**